The Effect of Sagittal Plane Mechanics on Anterior Cruciate Ligament Strain During Jump Landing

by

Ryan Bakker

A thesis

presented to the University of Waterloo

in fulfillment of the

thesis requirement for the degree of

Master of Applied Science

in

Mechanical Engineering

Waterloo, Ontario, Canada, 2014

AUTHOR'S DECLARATION

I hereby declare that I am the sole author of this thesis. This is a true copy of the thesis, including any required final revisions, as accepted by my examiners.

I understand that my thesis may be made electronically available to the public.

Abstract

The Anterior cruciate ligament (ACL) is an important ligament in the knee. Non-contact ACL injuries are a common occurrence among athletes, leading to large financial burdens and long term physical concerns. The underlying biomechanics leading to these non-contact ACL injuries are unknown, in part due to limited experimental studies investigating the mechanics of dynamic activities. Understanding these mechanics is critical for injury prevention and risk analysis.

The primary objective of this study was to investigate the underlying sagittal plane mechanics leading to increasing ACL strain during jump landing. A hybrid in-vivo/computational/in-vitro approach was used to measure ACL strain in relation to these mechanics. Motion capture was performed on ten subjects performing a single leg jump landing and both whole-body kinematics and ground reaction forces were collected. Musculoskeletal models were driven using this data to estimate the lower limb muscle forces from the jump landing. Five cadaver knee specimens were instrumented to measure ACL strain and mounted on a dynamic knee simulator. Muscle forces and sagittal plane kinematics were then applied on the cadaver specimens, dynamically recreating the activity. Strain in the anterior cruciate ligament was measured for each simulation. Bivariate correlation and multivariate linear regression analyses were performed with both maximum ACL strain and time to maximum ACL strain with the sagittal plane mechanics measured during the motion capture.

Correlation analysis found increasing ACL strain was correlated with increasing ground reaction forces, increasing body weight, decreasing hip flexion angles, increasing hip extension moments, and increasing trunk extension moments, among others. Time to max ACL strain was correlated with increasing knee flexion angles and increasing knee angle velocities. The multivariate linear regression revealed anatomical factors account for most of the variance in maximum ACL strain, but suggests landing softly by increasing joint angles and absorbing impact, are important strategies for reducing ACL strain. Time to max ACL strain regression was influenced by anatomic factors and knee velocities.

An athlete may have little or no control over the anatomic factors contributing to ACL strain, but altering their landing strategy to reduce the chance of injury. The empirical relationship developed between increasing joint angles, energy absorption and ACL strain in this study could be used to estimate the relative strain between jumps and to develop training programs designed to reduce an athlete's risk of injury.

Acknowledgements

First, I would like to thank my professor Dr. Naveen Chandrashekar for facilitating this master's thesis and providing guidance throughout the way. Under his guidance, the work I have completed in the Orthopedic Biomechanics Laboratory has been both multidisciplinary and interesting, and has laid the foundation for my future endeavors.

Thanks to Dr. Andrew Liang, who provided guidance in many aspects of this research and facilitated the motion capture. Thanks to Elora Brenneman for performing the motion capture over a number of months. I would like to thank the members of the Orthopedic Biomechanics laboratory, Gajendra Hangalur and Sebastian Tomescu for their contributions and guidance to the project, to whom without this project would not have been completed. In addition, thanks to the co-op students, Amanda Shorter, Kevin Yang, Leo Hee, Nokhez Qazi and Jennifer Dowling-Medley for their individual contributions to the project. Last, I would like to thank my friends and family for their continuous support throughout the process.

Table of Contents

List of Figures

List of Tables

Abbreviations

ACL: Anterior Cruciate Ligament

AMB: Anteromedial Bundle

ATT: Anterior Tibial Translation

CMC: Computed Muscle Control

COM: Center of Mass

DKS: Dynamic Knee Simulator

DOF: Degrees of Freedom

DVRT: Differential Variable Reluctance Transducer

GRF: Ground Reaction Force

IMB: Intermediate Bundle

LCL: Lateral Collateral Ligament

LVDT: Linear Variable Differential Transformer

MCL: Medial Collateral Ligament

OA: Osteoarthritis

PCL: Posterior Cruciate Ligament

PLB: Posterolateral Bundle

RRA: Reduced Residual Algorithm

SD: Standard Deviation

SLJL: Single Leg Jump Landing

Chapter 1

Thesis Overview

There are as many as 250,000 Anterior Cruciate Ligament (ACL) injuries per year in North America (Griffin et al., 2006). Non-contact ACL injuries are a common occurrence among athletes with 58.2% of injuries being non-contact in nature (Gianotti, Marshall, Hume, & Bunt, 2009). Many of these injuries require surgery causing a great demand on North American health care systems. It is estimated that there are 100,000 reconstructions performed per year (Griffin et al., 2006). Each surgery has a mean lifetime cost of $38,000, and costs the United States around $7.6 billion annually (Mather et al., 2013). Due to the large financial burdens and high incidence rates of ACL injury, significant effort has been made to reduce the incidence of injury through determining anatomical risk factors, training programs, and bracing (Shultz et al., 2012).

Despite these efforts, both the total number of ACL injuries and reconstructions has been on the rise (Mall et al., 2014). Between 1994 and 2006, the United States has seen the number of ACL reconstruction surgeries increase by 75% for female athletes and 35% in males. This increase of incidence rate increases the immediate importance for developing comprehensive ACL injury prevention programs.

A major hurdle in the development of comprehensive injury prevention programs is a lack of understanding the underlying biomechanical mechanisms that contribute to these injuries. Although many studies, both experimental and computational, have postulated these mechanisms, the community lacks the ability to validate this research due to the difficulty of measuring ACL strain in-vivo. Although pioneering studies measuring in-vivo strain have been completed, they have limited use in preventing injuries as such measurements are performed on activities unlikely to cause injury (Beynnon & Fleming, 1998). An alternative to in-vivo strain measurement is in-vitro testing of human cadaver specimens. These in-vitro experiments allow for the direct measurement of ACL strain while applying loading conditions on the specimens (Withrow, Huston, Wojtys, & Ashton-Miller, 2008). Relationships can then be created between these loading patterns and ACL strain which can be used to investigate the underlying relationships between the mechanics and injury.

Although there is a vast body of in-vitro research, the critical mechanics leading to injury are still under debate. This is in part due to the substantial limitations of the current in-vitro model of study. The

body kinematics, external forces and internal muscle forces do not replicate the full time history of injury prone activities. Without these full dynamic ranges under realistic conditions, these mechanics of ACL injury will remain unknown.

This study aims to bridge this gap by using an in-vivo/computational/in-vitro approach developed by Cassidy et al (2013) to measure the effect of jump landing technique on ACL strain. In this technique, in-vivo kinematics and kinetics are measured using a motion capture system on subjects performing a single leg jump landing. This information is used to drive a computational musculoskeletal model to predict the muscle forces required to perform the motion. The kinematics and muscle forces are then applied on an instrumented cadaver specimen using the dynamic knee simulator and the resulting ACL strain in measured. The aim of this study is to use this method to develop and empirical model to calculate ACL strain using these kinematics and kinetics as input and thereby identify the risk factors that may be associated with higher ACL strain. Injury prevention and training programs may use this information to develop protocols designed to reduce ACL strain during jump landing.

Chapter 2

Human Body and Anterior Cruciate Ligament Anatomy

2.1 Human Body Definitions

The study of both the human anatomy and biomechanics requires a large quantity anatomic terms and definitions. A set of standard anatomic references are used to reduce the complexity of describing these terms. These terms allow researchers to describe the location and movements of various aspects of the body without having to know exact anatomic definitions.

Universal body directions have been developed and can be seen in Figure 1. *Superior-inferior*: superior means towards the subjects head and inferior is away from the head. *Medial-lateral*: medial is towards the center of the body and lateral is away from the center of the body. *Posterior-Anterior*: posterior being towards the back of body and anterior means towards the front. *Proximal-Distal*: towards and away from the location of interest. *Superficial-Deep*: towards external or internal of the body.

The human body is also divided into three planes of motion; sagittal, frontal and transverse and can be seen in Figure 1. Movements in the sagittal plane consist of flexion extension movements of the joints, movements such as knee, hip and ankle flexion. Frontal plane mechanics consist of abduction-adduction movements such as knee abduction and hip abduction. The transverse plane has movements like tibial rotation, hip rotation and trunk rotation.
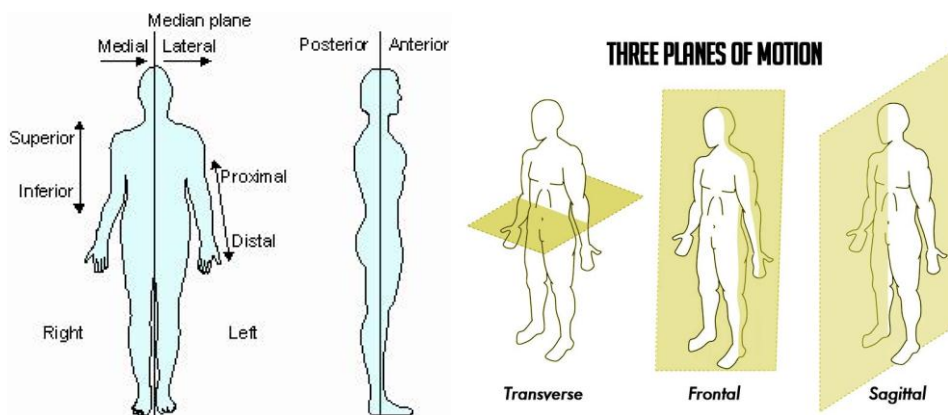
Figure 1 Body Directions and Planes of Motion

2.2 General Knee Anatomy

The knee joint is comprised of three bones; femur, tibia and patella (or knee cap) as seen in Figure 2. These three bones make up the largest joint in the human body. The knee is part of a chain of joints comprised of the ankle, knee and hip joints which are responsible for carrying humans through lower extremity movements such as standing, gait, and cycling.
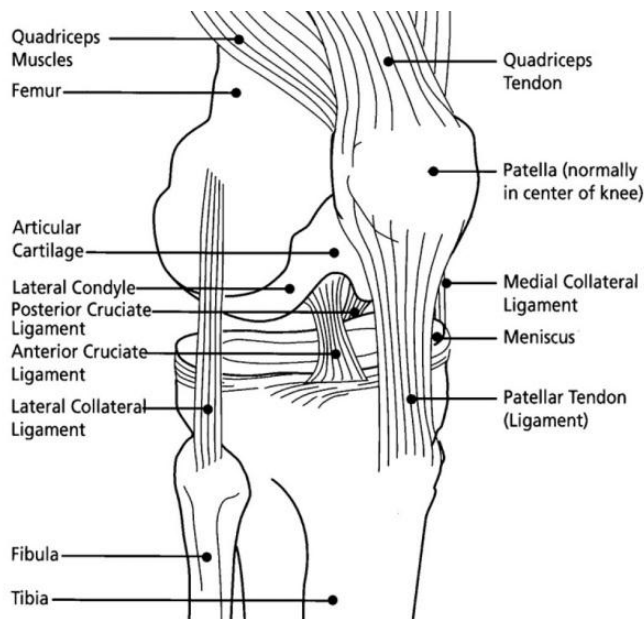
Figure 2 Knee Anatomy

Although generally referred to as a single unit, the knee is comprised of two joints; the patella-femoral and the tibia-femoral joints. The tibia-femoral joint carries the axial loads while the patella-femoral joint acts to increase the moment arm of the quadriceps muscles, reducing the muscle forces necessary to produce knee extension moments. The patella-femoral joint is constrained by the patellar tendon connected between the distal end of the patella and the tibial tuberosity. This tendon transfers the load from the quadriceps onto the tibia while the patella functions as the lever.

The femur and tibia are connected by a series of ligaments, the Anterior Cruciate Ligament (ACL), Posterior Cruciate Ligament (PCL), Medial Collateral Ligament (MCL) and Lateral Collateral Ligament (LCL). The MCL is connected between the femur and the tibia while the LCL is connected between the femur and the fibula. The MCL is a wider fan like structure while the LCL is slender and narrow. These ligaments resist the tibia from translating anteriorly, posteriorly, medially and laterally,

4

while also providing resistance to valgus and varus. The MCL also plays a secondary role in preventing knee rotation.

The ACL and PCL provide restraint to anterior and posterior translation of the tibia with respect to the femur and provides secondary restraint to internal tibial rotation (Noyes, 2009). The ACL connects from the anterior tibial plateau to the lateral posterior femoral notch and prevents anterior tibial translation (ATT). The PCL connects from the posterior tibial plateau to the posterior femur and prevents the tibia from translating posteriorly with respect to the femur.

The femur is protected by articular cartilage which protects the femur and tibia from bone-on-bone contact. The meniscus sits on proximal end of the tibia and is made of cartilaginous tissue. It helps disperse the loads transmitted through the knee joint to reduce the peak contact stresses during articulation and movement. Surrounding these structures is the articular capsule, a fibrous membrane that encompasses the ligaments, patella, meniscus and bursa.

Muscle structures surround the knee provide the forces and torques required for human motion. The quadriceps muscle group consists of the rectus femorus, vastus intermedius, vastus lateralis and vastus medialis (Moore et al., 1999). The rectus femorus connects into the quadriceps tendon while the vastus muscles connect both into the quadriceps tendon and the patella. These four muscles make up the knee extensor muscle group. Knee extensors provide extension torque required to return the knee to a strait position, therefore the quadriceps group is the main load bearing muscle group during gait activities. All three vastus muscles have attachment sites in the femur while the recuts femoris is attached to the pelvis. This means activation of the rectus femoris muscles will create a hip extension torque in addition to the knee extension torque.

The hamstring muscle group consists of the bicep femorus long head, bicep femorus short head, semimembranosus and semitendinosus (Moore et al., 1999). The hamstrings provide flexion torques about the knee and counteract the movement created by the quadriceps. All of the muscles except the bicepfemorus short head are connected to the pelvis creating a biarticular muscle group. When the hamstrings are contracted it will create a flexion movement about the knee and a hip extension moment about the hip. The calf muscles are made up of the medial and lateral gastrocnemius and the soleus muscle. Gastronemuis muscles connect the posterior femur with the calcaneus, also a biarticulate muscle grouping, causing knee flexion and ankle planter flexion. Even though it is considered to be part of the calf the soleus does not span the knee joint, instead connecting the calcaneus with the tibia creating

5

plantar flexion. The popliteus muscle also spans the knee joint and is important in knee flexion, rotation and knee stability. In addition, there are other minor muscles that span the knee joint but do not produce large torques in the sagittal plane including the gracilis, plantaris, and sartoius muscles.
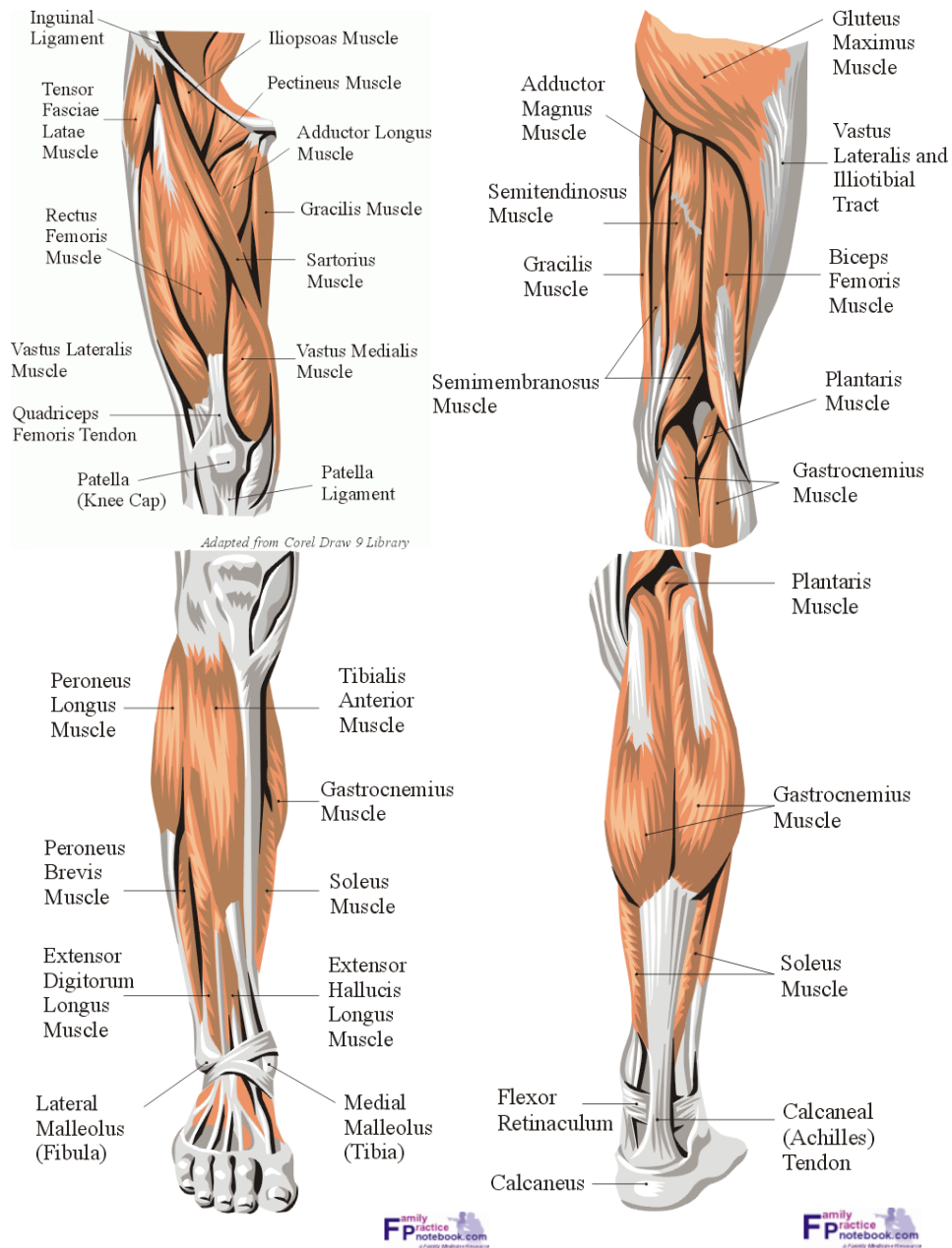
Figure 3 Lower Limb Musculature

While the knee is a major contributor to human lower body movement, the ankle and hip joints are equally important in human propulsion, as they are members of the lower limb chain. The ankle joint is comprised of a number of bones, the fibula, tibia, calcaneus and talus, and connects the foot to the shank. This joint is the first major load bearing joint when analyzing distally from the ground up. The gastrocnemius muscles that cross the knee connect to the calcaneus via the Achilles tendon. Both heads of the gastrocnemius, soleus and plantaris muscles connect into the Achilles tendon making it one of the largest tendons in the body. The soleus is one of the strongest individual muscles in the body connecting the tibia to the calcaneus and can create pure torque about the ankle. The gastrocnemius muscles, due to their biarticulate nature, create both a torque about the ankle and the knee. The Achilles tendon provides the plantar flexion torque (toes down) about the ankle, while the tibialis anterior, peroneus longus, extensor digitorum longus and extensor halluces longus provide dorsiflexion torque (toes up) about the ankle.

The hip carries load from the femur onto the pelvis and can flex/extend, medial/lateral rotate and adduct/abduct, in large rangers of motion. The hip joint is a ball and socket joint that allows for this large range of motion. There is a complex array of 17 muscles that span this joint and is comprised of four groups, the gluteal, adductor, illiposoas, and lateral rotator groups. Gluteal muscles are responsible for hip extension moments and connect the pelvis with the posterior femur. Due to the large number, the remaining muscles will not be discussed in detail.

2.3 ACL anatomy

The anterior cruciate ligament connects from the anterior tibia to the posterior lateral femoral condyle. Although the ACL is described as a fibrous band, the cross sectional area is non-uniform and fans out approaching the femoral and tibial attachment sites (Duthon et al., 2006). The structure is comprised of fibroblasts and collagen fibers, which contribute to the viscoelastic properties of the ligament.

There are three different bundles, the anteromedial, intermediate and posterolateral bundles (AMB, IMB, PLB). Often research categorizes the ACL with only two bundles the AMB and PLB due to the ambiguity where the IMB begins and ends (Duthon et al., 2006). The PLB has a tibial footprint slightly posterior that of the AMB and connects distally/posteriorly on the femur. Each bundle behaves differently throughout knee range of motion. This allows the knee to be able to protect against ATT from

full extension through the range of flexion. At full extension, the PLB is able to provide a stronger ATT restoring force. This is due to its transverse line of action, while the AMB is positioned vertically. As the knee flexes the posterior edge of the femur rotates anteriorly effectively shortening the fiber length and causing slack in the PLB. During knee flexion the tension in the AMB increases as it is pulled posteriorly of the PLB and can provide tension at higher flexion angles. The lengthening of the bundles as a function of a knee angles can be seen in the Figure 4 provided from Amis (Amis, 2012). This ligament lengthening relationship changes the contribution of each bundle to the total ACL force at varying degrees of knee flexion. At 20 degrees flexion, the AMB provides 25%, IB, 30% and PLB 45% of the restoring force where at 90 degrees the AMB provides 60%, IB 35% and PLB 5% (Amis, 2012). This difference in load sharing at different flexion angles can help with the diagnosis of ACL tear. For instance low ATT at low flexion but high ATT at high flexion may imply an AMB tear.
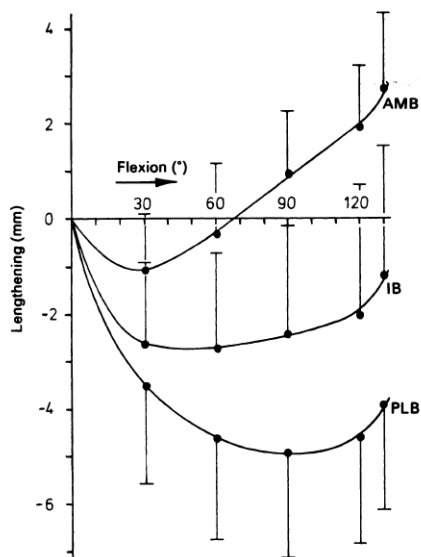
Figure 4 Bundle Lengthening as a Function of Knee Flexion Angle

A number of nerve fibers are present in the ACL, most of which are sensitive to stretching and rapid movements of ACL fibers (Duthon et al., 2006). These fibers are thought to have a proprioceptive effect, where a stretch of the ligament sends a reflex to the surrounding muscles. This is known as the ACL reflex and is thought to play an important role in muscle firing providing important feedback to the muscle controls surrounding the knee. However, this reflex takes a lengthier time than required to prevent injury in a dynamic setting and therefore must have a role in controlling muscle activations during static activities.

8

Chapter 3

Literature Review

3.1 ACL injuries

In addition to the financial costs, discussed in Chapter 1, and the short term pain of an ACL injury, there are long-term physical concerns. The ACL prevents anterior tibial translation, and a lack of constraint in this direction can lead to instability of the knee. The instability can inhibit the ability for the subject to perform in sports and may be uncomfortable. An increased risk of osteoarthritis (OA) is associated with ACL injures. Osteoarthritis damages the load bearing cartilage in the knee, which may result in discomfort, joint stiffness and bone on bone contact. Meniscal damage increases the likelihood of this effect (Mather et al., 2013). Ten years after ACL injury, patients who also suffered meniscal tears had 21-48% risk of OA. ACL injuries with an uninjured meniscus dropped this rate to 0-13%. Unfortunately, there is no cure for OA, and it is common for patients to require total knee replacements in order to reduce pain and increase mobility. This connection between OA and ACL injuries, further cements the need to reduce injury rate.

The rate of ACL injuries is not equivalent between male and female athletes. Female soccer players may be six times more likely to experience an ACL injury (Alentorn-Geli et al., 2009a). This has led a large portion of the literature to focus on the differences between male and female anatomy and mechanics. Despite the increased likelihood of ACL injury the rate of injury is higher among male athletes, due to the increased time males spend performing tasks that have potential to cause injury (Gianotti et al., 2009).

Studying the causal relationships of noncontact ACL injuries is multidisciplinary and requires a large number of techniques. Studies generally investigate two types of variables related to ACL injury, intrinsic and extrinsic variables. Intrinsic factors, factors which cannot be controlled are physical properties of the body. These can be measured with techniques such as tensile tests, x-rays and MRIs. Extrinsic variables include neuromuscular firing patterns, joint angles and external loading conditions. The study of extrinsic variables can use video analysis, in-vivo movement studies, in-vitro simulations and computer simulations.

3.2 Intrinsic Factors

Tensile properties of the ACL are a basic example of intrinsic characteristics. ACL size and structural properties vary widely subject to subject. Chandrashekar et al. (2006) performed tensile tests on 8 male ACLs and 9 female ACLs and found wide variations in the load at failure between the sexes (Chandrashekar, Mansouri, Slauterbeck, & Hashemi, 2006). Male knees failed at 1818($\pm$699) N and female at 1266($\pm$527), and the modulus of elasticity 128($\pm$35) and 99($\pm$50) MPa respectively. Hashemi (2010) created a regression formula to estimate the ACL properties by using the parameters age, body mass, height, BMI, ACL length, minimum area, and ACL volume suggesting that the underlying factors contributing to ACL properties are vast. Injured patients have shown to have smaller ACLs (Neufeld & Liu, 2003) than their non-injured colleagues. ACL's with similar elastic modulus may have vastly different ultimate strengths leaving subjects with weak ACLs at more risk of injury even when experiencing similar loading conditions.

In addition to ACL size, tibial slope is a highly discussed topic during ACL research. Tibial slope is defined as "the angle between a line perpendicular to the mid-diaphysis of the tibia and the posterior inclination of the tibial plateaus" (Giffin, Vogrin, Zantop, Woo, & Harner, 2004) and has been reported to be ten degrees (Dejour & Bonnin, 1994). This angle has been found to be correlated with greater tibial translation during walking (Dejour & Bonnin, 1994). The tibial slope creates an anterior component to the normal force between the tibia and the femur which can both push the tibia forward and prevent the hamstrings from pulling the tibia back.

McLean et al. (2011) tested the importance of tibial slope in an impact scenario. The tibial slope was measured on eleven cadaver knees and placed in knee impact apparatus (McLean et al., 2011). A weight was dropped on the femur and both ACL anteriomedial bundle strain and anterior tibial acceleration were measured. McLean found that ACL strain was proportional to anterior tibial acceleration and significantly correlated with posterior tibial slope (p=0.007) and found for every one degree of posterior tibial slope the anteromedial bundle was subject to 0.6% greater strain (Bennett et al., 2008).

Giffin et al. (2004) used a robotic loading system to test the importance of tibial slope. Three loading conditions were tested with varying axial and anterior-posterior loads on the tibia. An osteotomy was performed to increase the average tibial slope from 8.8 to 13.2 degrees and the loading conditions were repeated. Axial compression increased ATT with the osteotomy while direct anterior – posterior

forces did not see an increase in ATT. This suggests that increasing tibial slope can be detrimental under increasing axial forces.

In addition to in-vitro studies, Marouane et al. (2014) applied a finite element approach for measuring the effect of tibial slope on ACL strain. This FEM model was added to a musculoskeletal model in order to determine the effect on active gait and under knee joint compression. The posterior tibial slope was altered by ± five degrees and it was found that increasing the posterior slope by 5 degrees increased ACL force by 75% (Marouane, Shirazi-Adl, Adouni, & Hashemi, 2014).

Q-angle or the angle between the quadriceps femoris and the tibia is also a known predictor of ACL strain. Q-angle is disproportionately greater in females. It changes the lower limb kinematics putting the knee in more abduction moment prone kinematic positions (Shultz et al., 2012).

The association between the femoral notch width and ACL injury has been studied by a number of researchers (Ireland, Ballantyne, Little, & McClay, 2001; Shultz et al., 2012) . Ireland et al performed a radiographic analysis to determine the correlation of intercondylar notch width with ACL injury. The width was measured at the level of the popliteal groove. 186 non-injured and 108 injured participants were measured. Significant correlation between smaller notch width and injuries were found (p<.001). A similar study was conducted by Domzalski et all (2010) among young underdeveloped athletes using magnetic resonant imaging. Statistically smaller notches were found in the injury group then the control.

Other factors such as collagen fiber percentage, femoral notch height, notch angle, ACL laxity, joint laxity have all been proposed to be correlated with increasing ACL injury rates (Shultz et al., 2012). Intrinsic factors associated with ACL injury include many factors that can be studied post injury, such as ACL size and notch width. Researching these factors post injury, allows for large sample sizes due to the availability of research techniques such as X-rays and MRI's. Extrinsic factors do not share this luxury.

3.3 Extrinsic Factors

Despite the large quantity of research available on non-contact injuries, the specific extrinsic conditions that contribute to ACL injuries is unknown (Shultz et al., 2012). Pioneering studies by Beynnon (1998) have measured ACL strain in-vitro. A differential variable transducer (DVRT) is arthroscopically mounted in the ACL of a patient. This allows for direct measurement of ACL strain during different movements and forces to determine the effect. This method has been used to measure ACL strain during ACL reconstruction rehabilitation exercises such as static quadriceps contraction, stair

climbing and cycling (Beynnon & Fleming, 1998; Fleming et al., 1998, 1999). These studies can help reduce the strain on the ACL during low impact activities, but have not been tested during activities that may injure the ACL in the first place. Due to the complications with in-vivo methods this technique is not commonly used to study ACL strain.

Video analysis provides valuable insights into the kinematic conditions present during ACL injury. These studies typically analyze video post ACL injury to determine the kinematics of the subject during the injury sequence. The general lack of videotaping at the recreational level increases the difficulty of finding data for these analyses. Video analysis allows researchers to recreate and calculate the kinematics that occurred during the motion of injury.

Boden et al (2009) analyzed the video tapings of 29 ACL injuries and compared the kinematics to videos of subjects performing the same motion but where no injury occurred. It was found that injured subjects landed flatfooted, had less plantar-flexed ankles and larger hip flexion angles when compared to the uninjured control (Boden, Torg, Knowles, & Hewett, 2009). A similar study of 10 video analyses of injuries during handball and basketball, concluded that ACL tears occurred 40 milliseconds after initial contact with the ground, and found evidence of a valgus collapse mechanism in nearly all cases (Koga et al., 2010).

Sagittal plane mechanics have been a large point of discussion. A key factor in sagittal plane mechanics is the trunk flexion angle. Increased trunk flexion or "leaning forward" when landing has been shown to increase knee and hip flexion angles, decreased ground reaction force (GRF), decreased quadriceps load when landing which are suggested to reduce the load on the ACL (Blackburn & Padua, 2009; Shimokochi, Ambegaonkar, Meyer, Lee, & Shultz, 2013). Increasing the knee flexion angle decreases the GRF and potentially reduces the load on the quadriceps muscles (Podraza & White, 2010). Podraza found significant correlation between decreasing ground reaction forces and co-contraction indices of the quad-hamstrings with increasing knee flexion, and increasing knee extension moments with increasing knee angle. Conversely, a training study from Hewett (1996) found that plyometric training in female athletes for six weeks was able to increase jump height, and decrease ground reaction forces, without significantly altering knee or hip flexion angles (T E Hewett, Stroupe, Nance, & Noyes, n.d.). This training program was speculated to have potential effect for prevention of knee injuries.

In addition to the relationship between knee flexion angle and ground reaction forces, knee flexion angle also changes the ACL elevation angle. As the knee flexes the elevation angle of the ACL

relative to the tibial axis decreases (Herzog & Read, 1993) increasing the tension in the ACL to produce equivalent posterior restoring force. This additional force is shear force exerted on the ACL, and has been shown to decrease the ultimate load and energy absorption of the ACL (Lyon, Woo, Hollis, Marcin, & Lee, 1989).

Hewett (2005) performed a female cohort study with 205 female basketball, soccer, and volleyball participants over a 13 month period (Timothy E Hewett et al., 2005). At the onset of the study, motion capture was performed on each athlete performing a jump-landing task to calculate the kinematics and kinetics. Nine ACL injuries were observed. Hewett performed correlation analysis and predicative regression using the motion capture data with the injured participants. Decreasing peak knee angles and increasing peak hip extension moments were found to be correlated with injury ($p<.01$). No correlation was found with knee extension moments. Although hip extension moment and knee angles were significantly correlated with injury, they were not helpful for the injury prediction model created by Hewett, while non-sagittal mechanics knee abduction angles and moments were. It has been suggested that this increase in hip extension moment is supported by increased gluteus maximum activation (Alentorn-Geli et al., 2009b).

The role of quadriceps force on ACL injury is a debated topic. Both (Myers et al., 2012; Withrow, Huston, Wojtys, & Ashton-Miller, 2006) showed increased risk of ACL injury and anterior tibial translation (ATT) with increasing quadriceps force, while (J. Hashemi et al., 2007) found that increasing the quad force prevented injury by increasing the contact forces within the knee. Increasing the compressive joint force will also increase the frictional force inside the knee preventing slip. This issue is further convoluted due to the patellar line of action, which changes from anterior to posterior at low knee flexion angle (Herzog & Read, 1993).

Quadriceps/Hamstring contraction ratio has been shown to be a deterrent to ACL injuries (Withrow et al., 2008). The Quad/Ham ratio provides extension/flexion torques about the knee, so a large hamstring force would increase the necessary force needed from the quadriceps, increasing the tibial-femoral contact force which may cause increased ATT. Increasing the hamstring force without increasing quadriceps force will decrease ATT. This scenario is not possible because the net knee joint torque must be preserved. This relationship should be studied under dynamic loading conditions that reflect realistic torques about the knee. In addition, Hashemi et al. (2011) suggests that a delayed or slow co-activation may increase the chance of ACL injury.

Hashemi et al. (2011) proposed the hip flexion knee extension paradox as a sagittal plane injury mechanism when a number of factors converge. "1. Delayed activation of Quad and Ham muscles 2. Ground reaction force applied when knee is near full extension 3. Shallow medial plateau and 4. A stiff landing due to incompatible hip and knee flexion velocities." This theory combines both intrinsic and extrinsic factors of the ACL strain.

In addition to increasing ACL strain values, the timing of peak ACL strain and strain rate has been variables of interest. Hashemi (2007) used a custom built knee injury simulator to measure ACL strain on nine cadavers during jump landing simulations. It was found that during safe landing conditions strain rates were as low as 60-80%/s, while during damaging simulations the strain rate increased to 250%/s. Due to the viscoelastic properties of the ACL increasing the strain rate increases the force experienced by the ligament for a given elongation (Pioletti, Rakotomanana, & Leyvraz, 1999). Pioletti el al. (1999) showed that that a strain rate of 40% per second, over 70% of the stress in the ligament was caused by strain rate effects when compared to the strain rate of 1% per second. This increase means that the ACL becomes very stiff at high strain rates and may cause failure at lower strain values.

A number of studies have investigated the difference between male and female biomechanics in attempt to clarify the increased likelihood of ACL injuries among women. A study from Krosshaug (2007) studied the kinematics from the videotapes of 39 injuries during basketball and studies the differences between male and female injury mechanisms. It was found that females had both higher knee flexion angles and a higher occurrence of valgus collapse than their male counterparts. Due to the higher occurrence of ACL injuries in women than men, the study suggested training programs should focus on the reducing valgus movement (Krosshaug et al., 2007). Alternatively it has been suggested that females perform tasks with a more upright posture. Yu (2005) found that females land from stop-jump tasks had smaller knee and hip angles at ground contact and decreased range of joint motions indicating stiffer landings (Yu et al., 2005). Chappell (2007) found similar results. Females performing vertical stop-jumps were observed to have a decrease in knee and hip flexion in addition to increases quadriceps activation over their male counterparts (Chappell, Creighton, Giuliani, Yu, & Garrett, 2007). Although these studies have been aimed at determining biomechanical differences that cause an increased injury incidence among women, a causal relationship has not been found due to the lack of direct ACL measurements available through these techniques.

3.4 Computational Musculoskeletal Models

In the field of biomechanics, often situations arise where the variables of interest such as joint moments and muscle forces are not directly observable. These variables need to be computed using specialized computer models. Motion capture labs are limited to collecting displacement measurements and external forces. Displacement measurements can be in the form of individual markers placed on the body or angles measured using angle goniometers among others. They are not able to track the center of mass (COM) displacement over time because the COM is unknown for body segments and may change over time with respect to the body due to soft tissue deformation. Forces can be directly measured using load cells in all but very specific cases, such as an instrumented total knee replacement, measured externally to the body. In live subjects, muscles forces cannot be measured directly, but can be estimated using buckle transducers. Buckle transducers are invasive requiring the muscle to be string through the buckle and can cause discomfort to the patient. Each buckle transducer measures the force in one individual muscle or tendon, so complications increase with the number of muscle force needed. These complexities in measuring internal forces and torques in the body lead to the requirement for computational musculoskeletal models to predict these values.

There are three multibody dynamics modeling programs that can be used to help estimate many of these variables; *Visual 3D* (C-motion), *AnyBody* (AnyBody Technology), and *OpenSim* (Stanford University). Visual 3D is a program designed to integrate easily into the motion capture lab, and can be used to compute joint angles, and moments. Visual 3D human body models are made by creating individual body segments, which are able to free float in space. If prescribed each body can apply force to other body segments such as the foot can apply force to the tibia and are computed by inverse dynamics algorithms. Visual 3D cannot compute muscle forces.

AnyBody modeling software can be used to also compute inverse kinematics and dynamics and in addition can compute muscle forces (Damsgaard, Rasmussen, Christensen, Surma, & de Zee, 2006). These muscle forces are calculated using an inverse dynamics algorithm that uses and optimization routine because the number of muscles (forces) outnumbers the degrees of freedom of the model. Biomechanists can study muscle forces to determine the stress and metabolic load different activities have on the body. Unfortunately, ACL strain cannot be directly computed in *AnyBody* because the ligament has not been modeled. However, muscle force calculations may be used to determine the loading conditions

for physical testing of cadaveric tissue where ACL strain can be measured in-vitro (Cassidy, Hangalur, Sabharwal, & Chandrashekar, 2013).

Opensim has many of the same features as Anybody, but is available in an open source package (S L Delp et al., 1990). This package can compute muscle forces using a number of different optimization schemes and can also compute forward dynamic simulations. Due to the wide acceptance of the optimization algorithms, Opensim was chosen to be the software of choice for this study. Opensim also has a unique reduced residual reduction algorithm. A number of studies have used this software as the main computational model for their studies. Hamner et al. (2013) computed the muscle force contributions to body accelerations over a number of running speeds (Hamner & Delp, 2013). Mokhtarzadeh (2013) (Mokhtarzadeh et al., 2013) used Opensim to quantify the protective effect the soleus has on ACL strain during drop landing, and Kar 2012 (Kar & Quesada, 2012) implemented an ACL into an Opensim model and calculated the ACL strain during different dynamic activities.

Studying the ACL directly in Opensim can be problematic for a number of reasons. The tibia and the knee are connected by a custom joint. The joint has translation in both the Anterior-Posterior and Proximal-Distal directions and are prescribed as a function of the knee angle. In-vivo the knee translates in these directions as both a function of knee angle and force applied. This relationship is not applied in Opensim. An increase in AP force does not cause an increase in ACL strain, because displacement is a function of the joint angle only. Therefore this type of study is limited to low force applications where the translation due to this force is minimal.

3.5 Knee Simulators

The in-vitro study of the underlying biomechanical mechanisms that lead to ACL injury often require mechanical testing of cadaver specimens. Mechanical testing requires a testing rig that allows for specific biomechanical factors to be tested under controlled conditions. The testing apparatus that are aimed at determining the biomechanical influence on ACL strain during impact activities are discussed here. Simulators designed by research groups at University of Michigan, Ohio State University, Texas Tech University, and the University of Waterloo all test anterior cruciate ligament strain on cadaveric tissue with impact loading conditions.

The simulator built in Michigan has taken aim primarily at understanding the sagittal and pivot shift mechanisms (Lipps, Oh, Ashton-Miller, & Wojtys, 2014; Lipps, Wojtys, & Ashton-Miller, 2013;

Oh, Lipps, Ashton-Miller, & Wojtys, 2012; Withrow et al., 2006, 2008). A cadaver knee is dissected removing the muscle tissue, while leaving the hamstring, gastrocnemius, and quadriceps tendon in-tact. The tibia and femur are potted into 3D load cells and placed in an apparatus secures the translations of the tibia in all directions and the femur both in the anterior-posterior direction and the medial lateral direction. Both load cells allow flexion and extension moments while preventing axial torsion and adduction/abduction movements. The quadriceps, hamstring and gastrocnemius cables are pretentioned to mimic the muscle forces during the activity of interested, primarily jump landing. A weight is dropped onto the femoral attachment creating an impact force with the same magnitude as the activity of interest and force is naturally developed in the cables. The flexion angles, joint reaction forces, and ACL strain are measured.
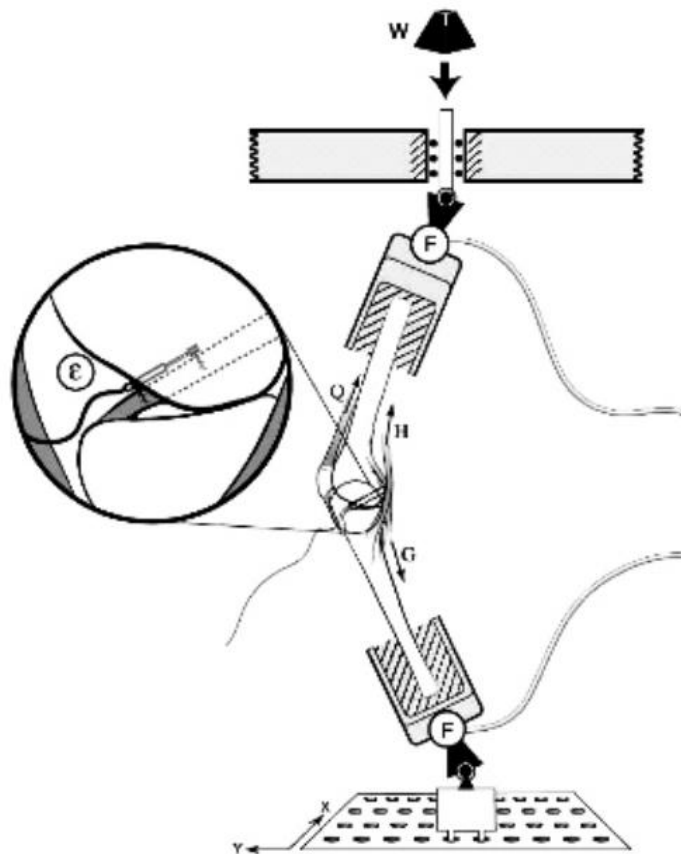
Figure 5 Michigan Simulator

The simulator from Ohio has a similar setup with a few key differences. The cadaver tissue remains intact with the foot and the femur is cut midway and attached to a 3D load cell. The quadriceps and hamstring force are provided with a system of pulleys and an attached mass to simulate muscle force. A weight it dropped from a tower onto the platform attached to the foot. This weight it to simulate the ground reaction force directly instead of onto the tibia. The research conducted in this lab is concerned with adduction/abduction modes of failure, timing sequence and comparing ACL and MCL injuries (Kiapour, Quatman, et al., 2014; Kiapour, Wordeman, et al., 2014; Levine et al., 2013; Quatman et al., 2014).
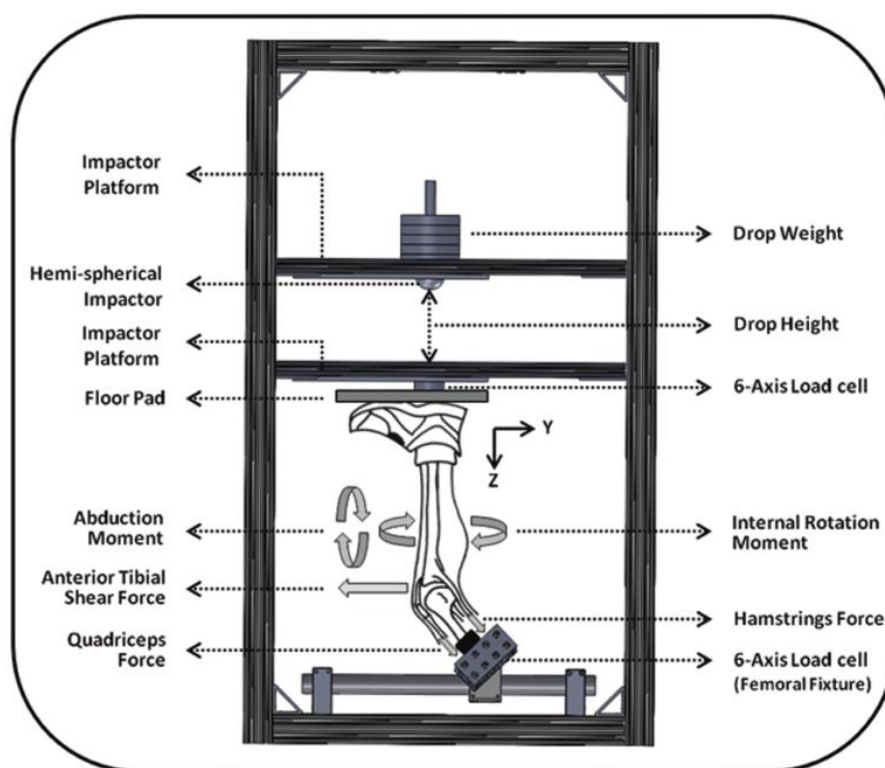
Figure 6 Ohio Simulator

Hashemi (2007) used a similar drop weight simulator to investigate the effects of sagittal plane mechanics during jump landing. A cadaver specimen was loaded in similar fashion to that of Ashton Miller with load cells at the femur and tibia. The Quad and Hamstring cables were connected to muscle actuators that apply a constant force or apply a prescribed displacement. The research group has found that elevated levels of quadriceps are protagonist to ACL strain and that restricting the hip flexion while

applying small quadriceps force is agonist to strain. This relationship between the quadriceps force and ACL strain is opposed to the findings from Ashton-Miller.
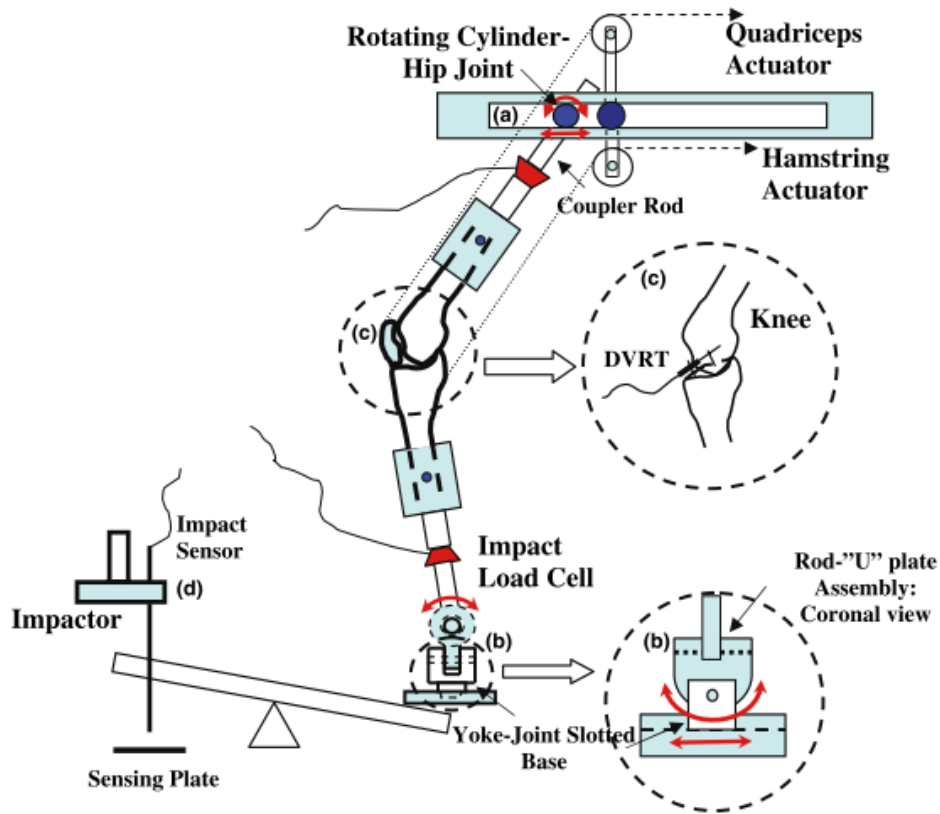
Figure 7 Texas Tech Simulator

These three simulators have produced many important findings related to ACL injury throughout the last decade, but have a number of limitations. First, although the knee is usually positioned in the approximate flexion angles experiences during jump landing they lack the ability to dynamically mimic the knee kinematics. Therefore, the effect of dynamic changes in the hip, knee and ankle kinematics, such as range of motions and flexion velocities are difficult to study. Second, these simulators lack the ability to apply dynamic muscle forces to the specimens. The muscle cables are pretentioned with weights or actuators, and although the cable forces change after impact may not reflect the physiologic muscle forces and in turn, joint torques seen during these activities. Third, the application of the impact force is applied by dropping a weight. This weight drop increases the GRF faster than seen in the motion capture lab.

Peak forces experiences in Withrow (2006) were experiences within a few milliseconds of impact, where motion capture studies from Laughlin (2011) have shown the development of vertical GRFs over 60ms. Due to these limitations it is unknown if the finding from these studies still hold under physiologic conditions.

To address these limitations, a new simulator has been developed by Cassidy (2013) at the University of Waterloo. The simulator was built to recreate sagittal plane loading mechanisms, calculated using musculoskeletal models, throughout time on cadaveric tissue. A cadaver knee specimen is mounted onto hip and ankle actuators, able to replicate hip and ankle positions and produce realistic knee flexion angles throughout time. Cables are attached to the cadaver specimen at the quadriceps, hamstring and gastrocnemius muscle force insertion sites. The cables are able to replicate desired force-time profiles using closed loop feedback with electromechanical actuators. Hip extension moments are applied by a cable pulling posteriorly on the femur, just under the hip attachment.
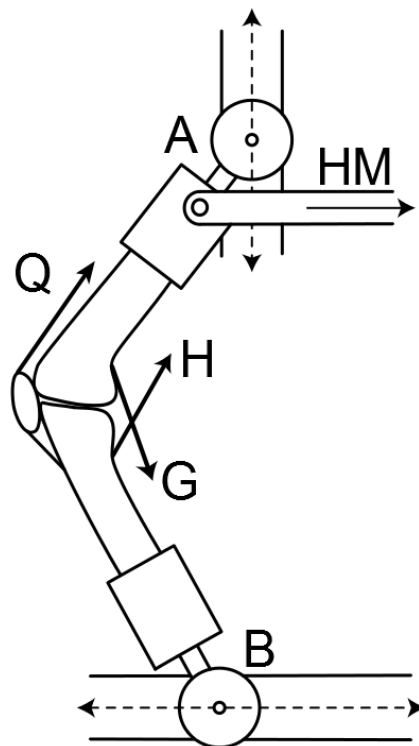
Figure 8 University of Waterloo Simulator: hip actuator (A), ankle actuator (B), quadriceps force (Q), hamstring force (H), gastrocnemius force (G), and hip moment actuator (HM)

Chapter 4 Methods

The methodology employed in the current study used the procedure pioneered in Cassidy (2013). An in-vivo/computational/in-vitro approach was used to measure ACL strain on cadaver specimens. Motion capture was collected on ten subjects performing a single leg jump landing. The motion capture results were fed into a computational musculoskeletal model to estimate the lower limb muscle forces required for this motion. These muscle forces, along with the kinematics, were applied on five cadaver knee specimens and the resultant ACL strain was measured. Correlation analysis and multivariate linear regression was completed on the resultant ACL strain and the sagittal plane variables comprising the simulations. A diagram depicting this methodology is shown in Figure 9.
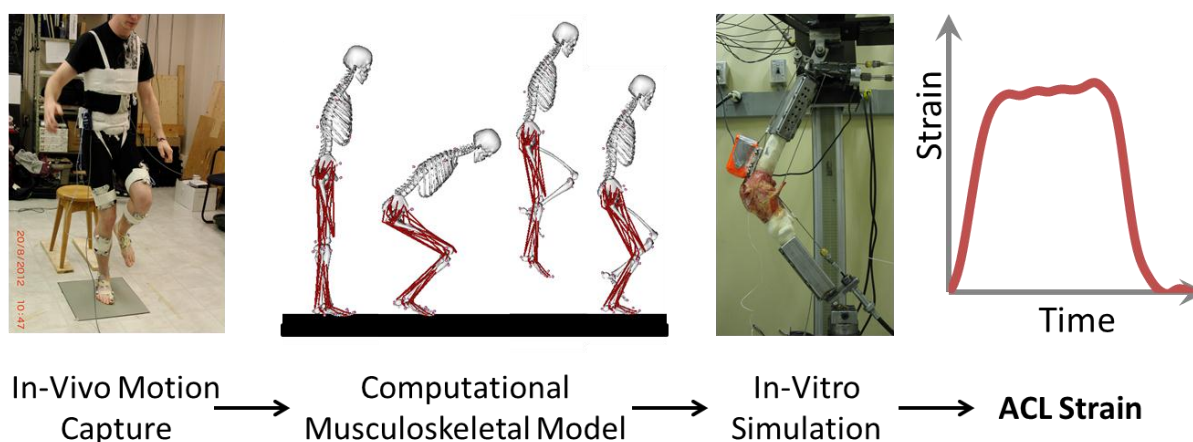
Figure 9 Procedural Overview: in-vivo motion capture, computational musculoskeletal model, in-vivo simulation and resulting ACL strain

4.1 Motion Capture

Ten subjects were recruited from the University population (5 male, mean (SD) body mass of 67 (7) kg age of 24.5 (4) years). The participants were recreational athletes, who participated in sport at least twice a week, and had no previous lower body injuries. Lower body injuries were defined as any injury requiring surgery, known damage to a knee ligament, or any broken bones within the last two years. The athletes were recruited from acquaintances and recruitment flyers.

The motion capture session required the participants to perform a maximum voluntary single leg jump landing (SLJL), on their right leg. Marker data was collected using an *OptoTrack* (Northern Digital,

Inc., Waterloo ON) camera system, using 35 infrared markers, with 8 marker clusters and 3 redundant markers on the right foot. The clusters were placed on the right and left thigh, shank and foot, in addition to the trunk and pelvis. Three additional markers were placed on the right big toe, metatarsal one, and metatarsal five. Thirty-nine individual marker positions were digitized off these clusters. Detailed information of the palpations can be found in Appendix A. Marker data was captured during SLJL using Optotrack motion capture system (Northern Digitals, Waterloo, ON) at a frequency of 80HZ. Kinetic data was collected using an AMTI force plate (OR6-7-2000, AMTI, Watertown, MA) with a capture frequency of 1600Hz.

At the start of each session, the subject was required to stand in anatomic position, seen in Figure 10, for five seconds while a static calibration trial was collected. Instructions were given for the SLJL; jump as high as possible, launch vertically with both legs, and land on the right leg in a natural posture. The subjects usually requested three to five practice trials before they felt comfortable with the task. Ten SLJLs were collected for each subject. Often, participants would land imbalanced, and would need to place their left foot down to regain stability. The jump landing trials were considered to be acceptable if the subject balanced after landing for at least two seconds without placing their left foot down. The capture was performed using *NDI First Principles* software and the data was saved in *C3D* format.

Figure 10 Motion Capture of Participant Standing in Anatomic Position

4.2 Data processing

Although ten SLJLs were collected for each participant, only one was selected for simulation. During every recording, there were short periods of time where the camera system was not able to detect individual markers, leading to marker dropout. Marker dropout can be viewed in *C3D,* and the trial with the least percentage of marker dropout was selected as for each participant.

Raw forceplate data was transformed from a voltage to a force vector using the type 2 forceplate calibration matrix provided from the manufacturer. The subject was oriented on the lab forceplate with the X axis – participant anterior, Y axis – participant left and Z axis - participant vertical. This is not the orientation of the coordinate system (+X anterior, +Y vertical, +Z to the right of model) that is used by the musculoskeletal modeling software *OpenSim* used in this research. Therefore, a coordinate transform needed to be applied. In addition, the center of pressure location and the free moment were calculated (Winter, 2009).

The marker and analog forceplate data were exported from *C3D* and run through a *Matlab* processing function, where both were filtered using a 15Hz, 4th order dual pass Butterworth filter

(Hamner & Delp, 2013; Kristianslund, Krosshaug, & van den Bogert, 2012). After processing, *OpenSim* compatible marker files (.trc) and forceplate files (.mot) were created using templates provided by *OpenSim*.

The musculoskeletal modeling software *OpenSim* (S L Delp et al., 1990) was used to simulate the SLJLs. *OpenSim* uses the kinematics and kinetics collected during the motion capture to determine the muscle forces required to reproduce the movement. There are two musculoskeletal models provided from *OpenSim* that can calculate muscle forces required for lower body movement - Gait2354 and Gait2392. Gait2354 and Gait2392 include both legs and a torso, have 23 degrees of freedom and 54 or 92 muscles respectively. Gait2392 is considered to be more anatomically correct because it includes more of the known lower body musculature, but it can take longer to simulate muscle forces due to the increase in the number of variables. In this project, muscle forces were simulated for short periods of time (300ms), requiring 15 minutes to simulate with the 2392 model; it was not necessary to use the simplified 2354 model.

A number of changes were made to Gait2392 model. The maximum isometric contraction of each muscle was increased twofold. Maximum isometric contraction was calculated using various cadaver and in-vivo studies (Friederich & Brand, 1990). These forces work during low impact gait maneuvers, but a number of studies have reported that during high-force high-impact maneuvers, the model is not able to generate the necessary torque about the joints. These studies, which include studies from the *OpenSim* team, have increased the maximum isometric contraction twofold for all muscles (Hamner & Delp, 2013; Laughlin et al., 2011; Mokhtarzadeh et al., 2013). Further investigation is necessary to validate this force increase, but is beyond the scope of the current project.

The model was stripped of all left leg and trunk musculature, replaced with torque actuators. The Gait2392 model was built for gait simulations with knee flexion angles less than 90 degrees. When a subject performs a SLJL, they naturally curl their left leg for balance, increasing the knee angle up to 150 degrees. This flexion angle in the Gait2392 model causes irregularities in the hamstring muscle line of action, providing a knee extension moment instead of a flexion moment, which is non-anatomical. In addition, the trunk was also stripped of musculature to decrease simulation time. Stripping this musculature does not affect the right leg muscle forces because the joints and body segments still provide the same net torque and therefore do not alter the inverse dynamics chain.
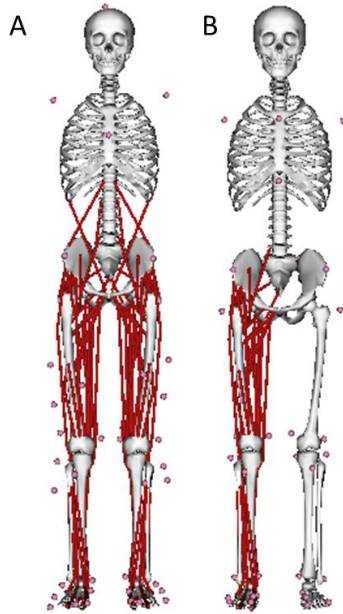
Figure 11 A. Original Gait2392 Model B. Modified Gait2392 Model

The first step in simulating muscle forces was to scale the generic model. The Gait2392 has the height, weight and size of a 50th percentile male. The participants were not the same size as this generic model; therefor the model had to be scaled to the proper size. Digital markers were placed on Gait2392 in the same location as the motion capture palpation sites. *OpenSim* calculates the distance between these sites and the distance between the palpations on the motion capture subject during the static calibration trial. The ratio of these distances is used to compute the scale factor for each body segment.

During the motion capture, it is important to have an idea about which palpations are trusted to be in a position that may be defined on Gati2392. For instance, the knee condyle palpations were completed as close as possible to the joint line, removing the possibility for ambiguity in the position of the knee center. This confirms the length of the tibia and femur are correct.

After scaling each participant, the inverse kinematic analysis tool was used to create a set of joint angles from the marker data. Marker positions were recorded in X,Y,Z coordinates throughout time, and *OpenSim's* inverse kinematics tool aligns the Gait2392's body segments to match these marker positions, minimizing the sum of squares of the error between the model and the motion capture. Large errors in the inverse kinematics tool were found in left greater trochanter, where the range of motion had surpassed

25

normal use of the model. This marker was removed from the process when large errors were observed. A depiction of the inverse kinematics results performed on a single leg jump landing is observed in Figure 12.
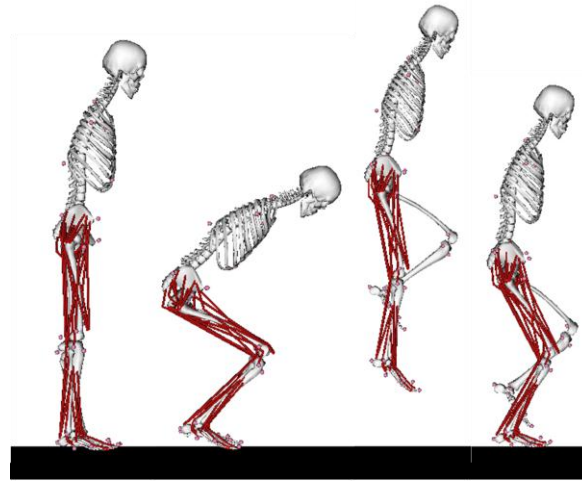
Figure 12 *OpenSim* **Inverse Kinematics of a Single Leg Jump Landing**

Body accelerations simulated by *OpenSim* was compared with the ground reaction forces measured in the motion capture lab, accounting for both sides of the equation Force=Mass*Acceleration. *OpenSim's* Reduced Residual Algorithm (RRA) was used to help minimize the equation imbalance (residuals) by slightly altering the model's kinematics and the torso center of mass (Scott L Delp et al., 2007). By altering these kinematics, RRA changes the accelerations and reduces the residuals. Residuals are primarily caused by incorrect kinematics, soft tissue accelerations and incorrect filtering rates. *OpenSim* uses rigid bodies and cannot account for the wobbling muscle and fat tissue, which change the location and acceleration of the center of mass. Filtering rates are predetermined by the literature and implemented in pre-process code. However, *OpenSim* can change the kinematics, justified by the inherent nature of joint errors accumulated in the inverse kinematics process, which can differ from the actual joint kinematics by 3 degrees or more (Peters, Galna, Sangeux, Morris, & Baker, 2010). Marker cluster movements due to soft tissue accelerations differing from the underlying bone structure are the primarily cause of this error. This presents a difficulty; although RRA can alter the kinematics to reduce the residual, it gives no indication if the simulated kinematics are closer to the experimental kinematics (because they are unknown). For this experiment, RRA was allowed to change the joint kinematics by a maximum of one degree to prevent excessive kinematic drift.

The RRA tool allows for the user to input a tracking weight for each joint and an optimal force for residuals. Increasing the tracking weight decreases the error on the joint, while decreasing optimal force decreases the residual. A balance exists between joint errors and residuals; larger joint errors generally lower the residuals, while smaller joint errors increase the residuals. There are 23 different tracking weights and six optimal forces to balance in the Gait2392 RRA simulations. This leads to a very complex problem, which can take a large number of iterations to reach an optimal solution. Completing this task manually is time consuming. A Matlab code was written to iterate these RRA simulations. The logic used in this MatLab code is shown in Figure 13.
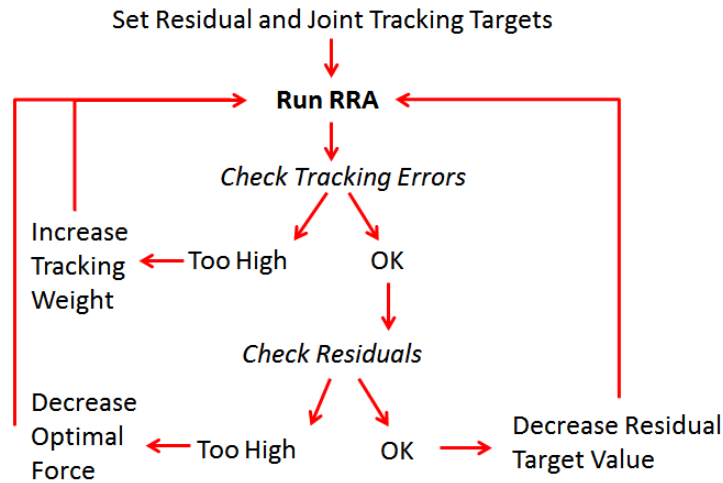
Figure 13 RRA Optimization Code Flow Chart

Computed Muscle Control (CMC) was then used to compute a set of muscle forces that drive the model to perform the SLJL (Scott L Delp et al., 2007). CMC is a combination of forward and inverse dynamics. It calculates a set of muscle forces at an instance in time (inverse dynamics) and applies these forces for a short period of time (forward dynamics). This process is repeated until the total simulation has been completed. Because this model has 23 DOF and 92 muscles, there are more unknown forces then DOF. An optimization routine is required to determine which muscles to activate, by minimizing the sum of activations squared and the sum of the tracking acceleration errors squared.

Due to the inclusion of forward dynamics, CMC solutions accrues kinematic errors with respect to the input RRA kinematics. For this research, CMC was allowed to deviate from the RRA kinematics by

27

1.5 degrees and was run through a similar *Matlab* optimization algorithm as RRA. When the muscle force optimization algorithm was not able to recreate the desired joint torque, reserve torques were applied. Reserve torques keep the simulation from becoming instable and deviating greatly from the desired kinematics. These torques are artificial, not representing applied muscle forces, and should be kept to a minimum.

Between the errors accrued through RRA and CMC, joint angles were tracked within 2.5 degrees, (2 degrees RMS) of the inverse kinematics results. Residuals forces were less than 2% of body weight and moments less than 5%. Peak reserve actuators were less than 5% of body weight and required on only one participant simulation. These error values are similar to those recommended by the guidelines set by *OpenSim*, and are comparable with the findings of similar studies (Hamner & Delp, 2013).

Muscle forces and joint kinematics were extracted from *OpenSim* and used as inputs for the Dynamic Knee Simulator (DKS) (Cassidy et al., 2013). The hamstring force included muscle activations from the semimembranosus, semitendinosus, biceps femoris long-head and biceps femoris short-head. The quadriceps force included activations from the rectus femoris, vatus medialis, vastus lateralis and vastus intermedius. Gastrocnemius forces were a combination of the medial and lateral gastrocnemius muscles. The muscle moment arms about the knee were extracted using the *OpenSim* plot tool and multiplied with muscle force to obtain the net knee moment contribution from each muscle. Ankle and hip kinematics were extracted using *OpenSim's* point analysis tool. The sagittal plane components of the kinematics were separated and used as inputs for the DKS.

4.3 Cadaver knee dissection

Six fresh-frozen cadaver knee specimens, (4 male, 2 female, mean age (SD) 47.5 (3.67) years) were dissected during this study. These specimens were provided through *Science Care* (Pheonix, AZ) and *Innoved Institute* (Rosemont, IL). The cadaver specimens were split from the donor at the hip, and included both the femoral head and the foot. These were not needed for the experiments and were removed. An estimate of the knee joint line was marked, and the limb was cut 27cm proximally on the femur and 29.5cm distally on the tibia. The motion capture participants had femur lengths ranging from 39-44cm and tibia lengths ranging from 37-43cm. The cadaver limb lengths were cut shorter to allow for the application of the adjustable limb length fixtures, discussed in the next section. The cadaver specimens were defrosted overnight and were dissected the next morning.

28

The knee dissections involved many steps and procedures, discussed here in brief. An incision was made vertically along the axis of the tibia and femur, overtop of the patella, as seen in Figure 14-A. The incision cut through the layer of fat until muscle was seen; care was taken to not cut the pattelar tendon. Layers of skin and fat were removed from the muscle by incising through the layer of fascia. Intermediate removal is seen in Figure 14-B and full removal in Figure 14-C. Care was taken around the knee capsule to not damage any ligaments. The hamstring tendons were found and the muscle leading to these tendons were removed. These tendons were superficial and easy to spot, seen in Figure 14-D. The gastrocnemius muscles were separated mid-calf, usually with the hands and with minimal incisions, shown in Figure 14-E. The muscles were followed to the knee capsule and the muscle insertion sites were dissected. This required careful work as the gastrocnemius muscle insertions lie next to the capsule. The soleus was subsequently removed from the tibia and fibula in a similar manor to the gastrocnemius muscle removal, seen in Figure 14-F. Quadriceps muscles were lifted from the femur, Figure 14-G, and separated from the medial and lateral capsule, Figure 14-H,I. The quadriceps tendon was then separated from the muscle tissue. The tendon was scraped clean of flesh with the back side of a surgical tweezers, Figure 14-J. An incision was cut along the medial side of the patella, running from the medial quadriceps tendon down to 5mm away from the patellar tendon, Figure 14-K. With the capsule open, the fat pad obstructing placement of the DVRT was removed Figure 14-L. The completed dissection can be seen in Figure 15.
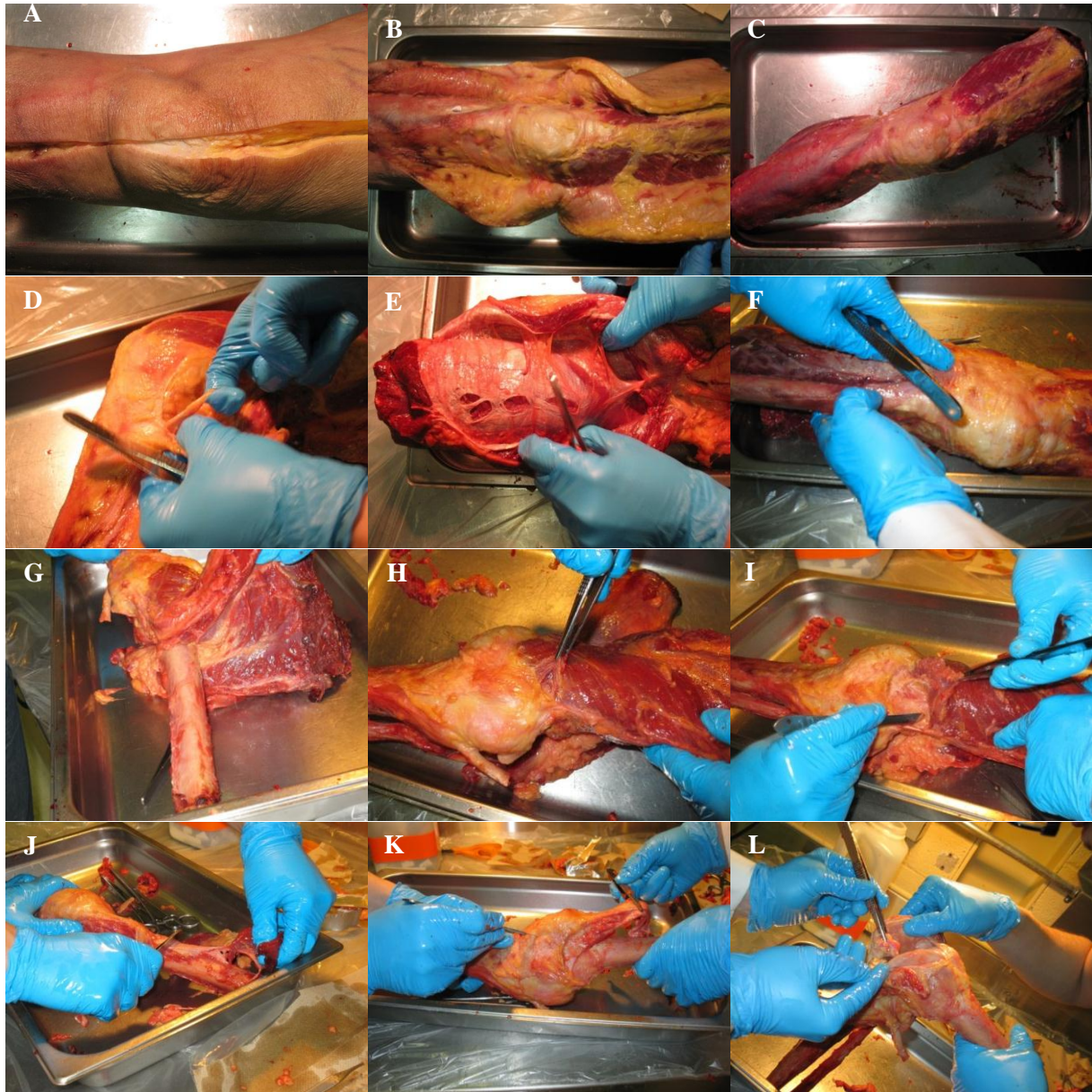
Figure 14 Dissection Photos Showing the Chronological Dissection Progression
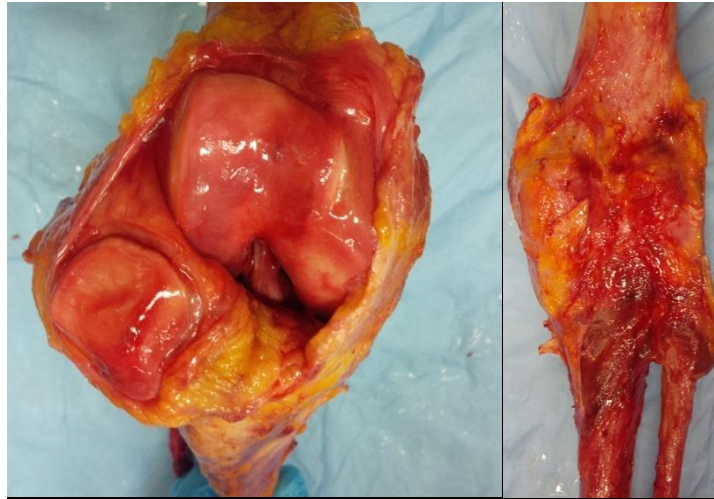
Figure 15 Completed Dissection

Cadaver knee Preperation

After dissection, the specimen was prepared for use on the DKS. The first step was to add limb extension blocks on the ends of the tibia and femur. The tibial and femoral canals were tapped using either a ½" NC tap or a 5/8" NC tap, depending on the canal size. The bone marrow was scraped from the inside of the canal and the bone tapped 70mm deep. The canal was filled with *Elmer's* Ultimate polyeutrothane glue and 100mm length of hardened steel rod was threaded 70mm into the canal.

Square aluminum blocks, 45mmx45mmx30mm, were machined and tapped to be mounted on the threaded rod. The machine interfaced with the tibia and femur by gripping these blocks. Before the *Elmer's* glue had a chance to dry, the blocks were threaded on the rod and fully tightened, creating a bond between the glue and the surface of the tibia and femur. The orientation of these blocks did not matter as the DKS interface can rotate 360 degrees. It was critical to allow the glue to create a strong bond between the block and bone, preventing rotation of the block during simulation. Once a tight fit was achieved the composite stucture was left to dry for two hours. The dissected knee with limb extension blocks is shown in Figure 16.

Figure 16 Dissected Specimen with Limb Extender Blocks

A differential variable reluctance transducer (DVRT, Lord Microstrain, VT) was used in this study to measure the elongation of the ACL of the cadaver knee during simulated landing. A notchplasty was performed using an air grinder with ball tip, to remove femoral notch cartilage, which impinged on the DVRT in extended knee positions. Removing this tissue prevented this issue. The removed tissue was not part of any load bearing surfaces. The DVRT was sutured on the AMB in the direction of the fibers, 5mm from the anterior insertion site of the ACL on the tibia. The gauge length was set to 5mm between the insertion pins, and the voltage was recorded. The DVRT was secured using surgical thread with three sutures; next to the second pin, at the end of the shaft and on the wire at the edge of the capsule. The notch plasty, DVRT insertion and the sutures can be seen in Figure 17.
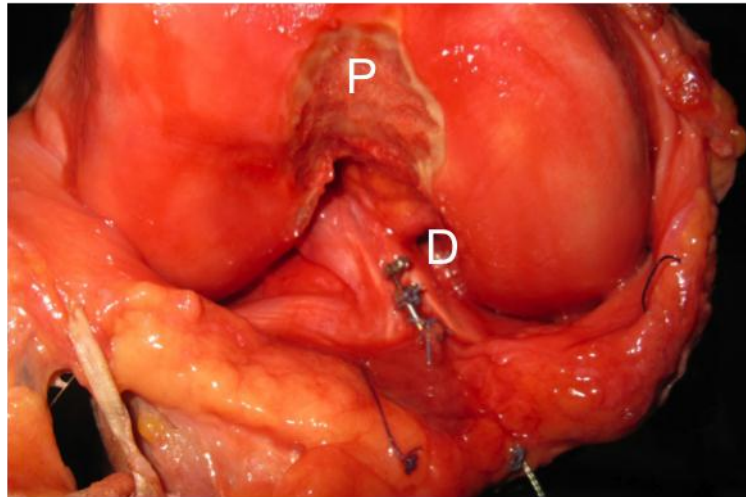
Figure 17 Instrumented ACL with DVRT (D) and Notch Plasty (P)

Steel aircraft cables were connected to the insertion sites of the gastrocnemius muscle (Cassidy et al., 2013). Two holes were drilled on the posterior side of the femur, and the cable was strung from posterior, around a reinforcement plate on the anterior surface and passed through the other hole. The reinforcement plate was used to prevent the cable from pulling through the anterior surface of the bone.

A new cable attachment system was used on the hamstrings. A 1/4" stainless steel tube was mounted on the posterior surface of the tibia, with one end bent to match to tibial plateu curvature near the capsule. The tube was secured using a hose clamp and 3M casting tape. The cable was strung through the pipe, around the tibia and back through the tube. This created a muscle attachment site at the anatomic hamstring positions without causing stress concentrations on the tibia.

A set of freeze clamps, similar to those found in Riemersa (1982), were attached to the quadriceps tendon and frozen using dry ice. This type of clamp is preferable to the techniques used in Cassidy (2013), because it preserves the under surface of the patella.

The muscle moment arms for the quadriceps, hamstrings and gastrocnemius muscles were calculated using the tendon excursion method (S L Delp, Ringwelski, & Carroll, 1994). Moment arms, assuming no work is done, are defined as the differential change in muscle length over the differential knee flexion angle. These moment arms are a function of the knee angle and are continuously changing. The moment arm calculations used were a linear estimation of this change and were represented as single value. Both the muscle length change, measured by a linear variable differential transformer (LVDT), and

33

the knee angle, measure by an angle goniometer, were recorded as the knee was flexed. The experimental setup can be seen in Figure 18–A. The muscle length change was plotted against the knee angle, as seen in Figure 18-B, where the slope of the line defines the moment arm. The figure shows a constant linear slope, indicating a constant moment arm. These moment arms convert the *OpenSim* muscle moments into applied cadaver muscle force, producing an equivalent knee moment on the cadavers (Cassidy et al., 2013).
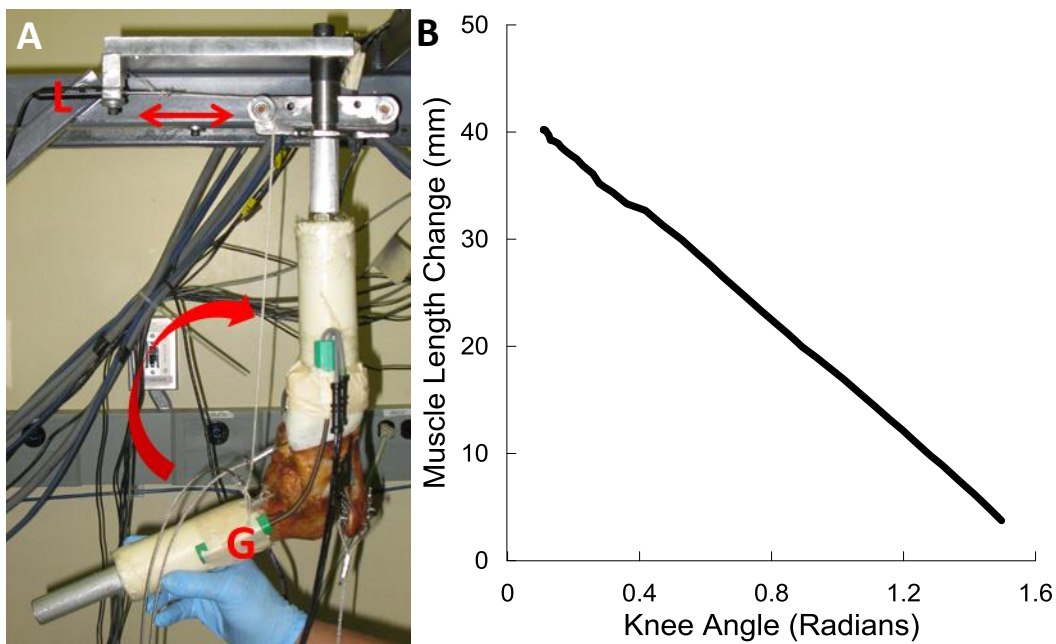
Figure 18 A. Moment-Arm Measurement Setup: LVDT (L) and angle goniometer (G) B.

gastrocnemius muscle length change vs knee angle

The voltage of the DVRT at the zero ACL strain value was found using the Lachman tester. Details on the Lachman tester can be found in previous thesis work by Hangalur G (2014) (Section 4.2). Due to the slow nature of the stepper motor, and difficulty clamping the tibia and femur, ACL zero strain was difficult to find. The zero strain location was found to be dependent on the internal/external rotation of the tibia, which cannot be controlled during the DKS simulation. Therefore, the absolute ACL strain data was not calculated, rather, relative strain was calculated.

4.4 Simulator preparations

The dynamic knee simulator required a number of upgrades, discussed here in brief. Previously, the height of the hip actuator was limited by the quadriceps cable attachments on the hip axis. The attachment was vertical (Figure 19-A), preventing full range of motion of the hip, coming in contact with the top of the DKS. The quadriceps attachment was changed to be at 45 degrees, seen in Figure 19-B. In addition, the 45 degree attachment allowed for a larger change in limb length. As the limb lengths increase, the cable attachment is pulled towards the pulley. The previous attachment setup allowed for one inch of travel, while the new attachment allowed for three inches of travel and was large enough that cable adjustment was not needed during testing.
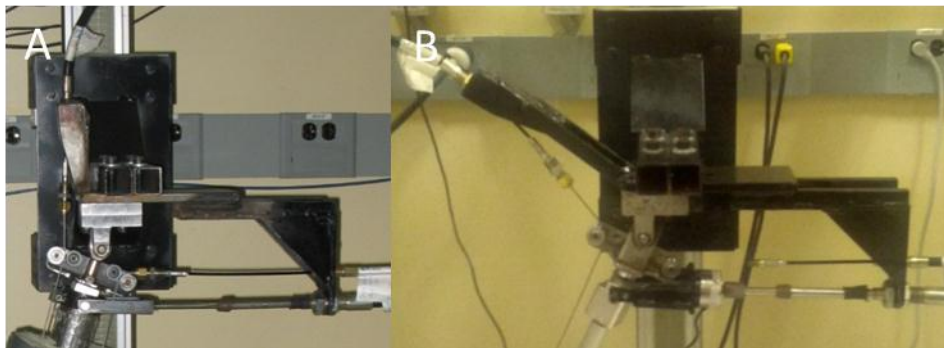
Figure 19 A. Previous Quadriceps Attachment B. 45 Degree New Quadriceps Attachment

Moment arm contributions about the hip, from the quadriceps and hamstring muscles cables, needed to be recalibrated due to this change in configuration. An angle goniometer was attached to the hip joint and a linear transducer to the cable attachment site. The change in length of the muscle cable was measured as the femur was articulated about the hip. Moment arms were calculated with the tendon excursion method explained previously. The results are shown in Figure 20. The quadriceps muscle caused a hip flexion moment, while the hamstring caused hip extension moment. The moment contributions of the quadriceps and hamstring were found to be defined by the following equations:

$$Quad\ Moment\ Arm\ (mm) = -0.718 * HipFlexionAngle + 57.233$$

$$Hamstring\ Moment\ Arm\ (mm) = -0.914 * HipFlexionAngle - 17.33$$

*Angles are in degrees
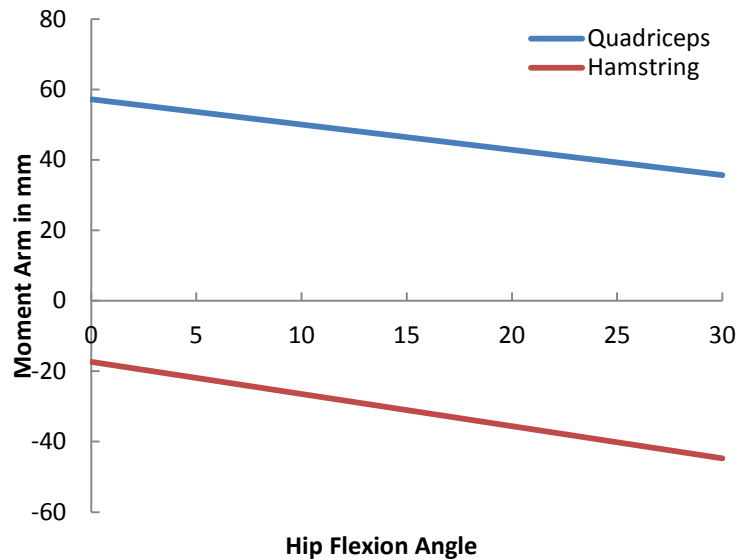
Figure 20 DKS Machine Hip Moment Arms as a Function of Hip Flexion Angle

The hip and ankle attachments between the cadaver specimen and the DKS were also upgraded. In general, the participant's knee geometry and the cadaver's do not match precisely. For instance, the cadaver specimen may have more varus/valgus or a different tibial slope. These mismatches can cause unwanted forces on the cadaver knee by forcing the specimen to perform the exact same kinematics. The DKS allowed for the mismatch of geometry, by allowing the ankle to slide a short distance in the medial-lateral directions, while both the hip and ankle actuators were free to change abduction angles. Unfortunately, during the pilot testing of this study, an excess of movement was observed due to the unrestricted DOF. This created a very large unnatural abduction/adduction moment about the knee, possibly creating an uncontrolled injury mechanism on the simulator. To prevent this unnatural abduction/adduction, the hip DOF was replaced with a single roller bearing, allowing only movement about flexion/extension of the hip, seen in Figure 21-A. The ankle was upgraded to a tight tolerance heim joint, shown in Figure 21-B, which allowed for much smaller angles than its predecessor. The allowable medial/lateral translation was limited to two inches in either direction. Although this upgrade may not prevent all unconstrained movement, it drastically reduced the amount of abduction/adduction moment applied to the knee, while still allowing for the natural movement of the cadaver specimen through flexion/extension.
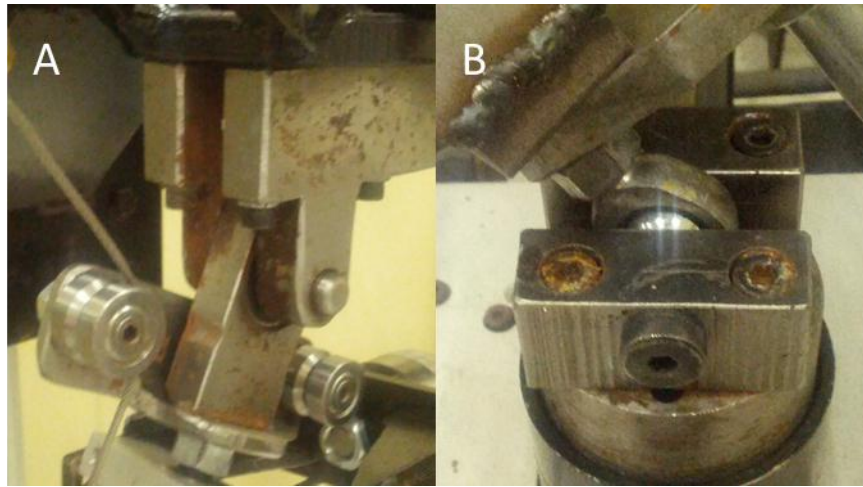
Figure 21 A. Hip attachment roller bearing B. Limited movement ankle attachment

Limb extenders were created to change the length of the tibia and femur for the different participants. It was important to match limb lengths because the kinematics of the ankle center and the hip center were used to control the DKS axes. Improper limb lengths would create knee angle kinematics inconsistent with the motion capture, and may fail the specimen. 2x2" Stainless steel tube was cut 7" long and 14 holes were tapped on each side. Bolts were used to grip onto the aluminum blocks at the end of the tibia and femur by friction. This friction proved more than enough to hold the knee in place despite the dynamic loads. If the limb length needed changing during simulation, the bolts were released and the limb slid in or out of the extender and the bolts were retightened on the block. This setup allowed for quick adjustment between trials of different limb lengths.

The custom *LabView* program designed for the dynamic knee simulator was upgraded for this experiment. The code was upgraded to reduce the time necessary to change between setups of both limb lengths and muscle force profiles. Previously, the program would zero the DKS to the start location with a single file. This would reset the DKS start position for every run to the same position. For this experiment, the start position needed changing for each participant trial. The *LabView* code was upgraded to select a zero position from a file explorer. In addition, the code was upgraded to show both the DVRT strain and goniometer angle as a live value before the simulation began. This information helps give the researcher important information on the state of the DVRT and knee. If the knee had experienced a failure or stretch of the ligament, the program allowed for easy diagnosis without re-running a trial, and thereby avoiding potential further destruction of the knee and DVRT.

Diagnostic Matlab code was also written to assess the quality of the simulation. The code compares DKS trial input against DKS trial output. Twelve graphs were created to show the comparison of the target value (input) with the results (output) of the DKS. An RMS error value is shown to help the user tune the machine. The graphs also show the GRF's developed, angle goniometer data and DVRT voltage. Figure 22, shows the *MATLB* readout.
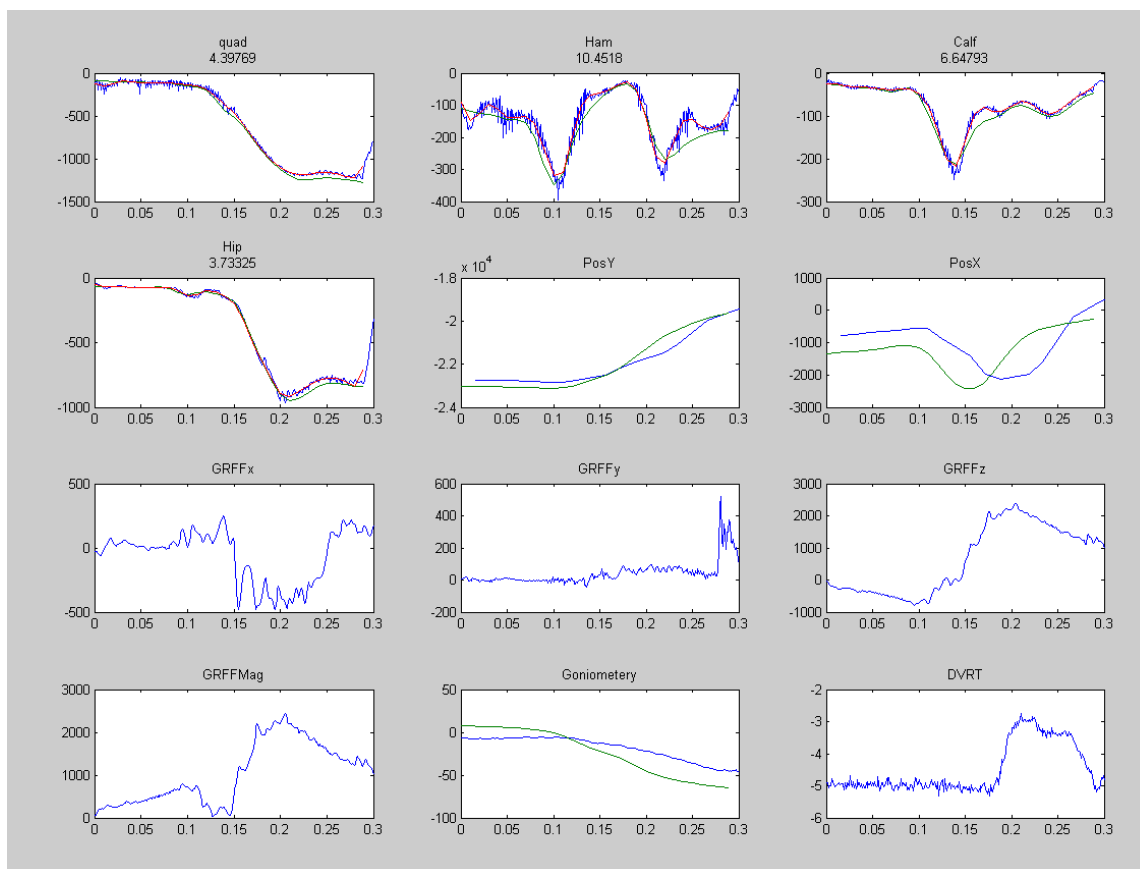
Figure 22 DKS testing display. Green Lines – DKS input, Blue Lines – DKS output, Red Lines – DKS filtered output. Numbers below the figure title show the RMS error values between the filtered DKS output and DKS input. Quadriceps (lbs), Hamstring (lbs), Calf (lbs), and Hip Forces (lbs), X and Y positions (encoders), Ground Reaction Forces (x,y,z directions and magnitude), Goniometer data (Degrees) and DVRT(voltage) are displayed.

38

Testing Procedure

Prior to testing days, specimens were removed from the freezer the night before to allow for the specimen to fully defrost. The next morning, the knee was mounted on the simulator and placed in the initial starting position for the first trial. Limb lengths were fixed to the correct length and muscle cables were attached. The freeze clamps were attached to the quadriceps tendon parallel to their line of action, and dry ice was inserted into the freeze pocket. The clamps were left to freeze the tendon for twenty minutes. The final setup can be viewed in Figure 23.
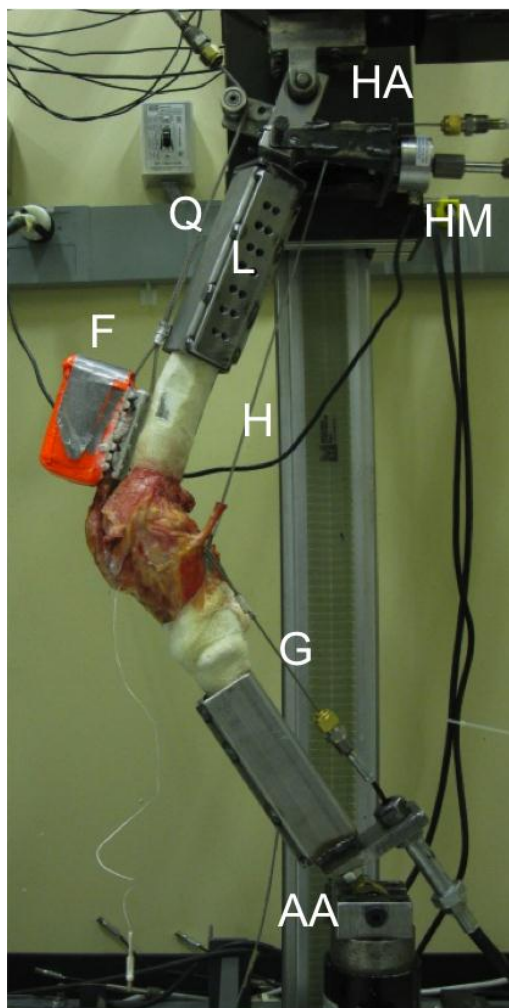
Figure 23 Fully Mounted Knee Specimen: freeze clamps (F), limb extenders (L), quadriceps cable (Q), hamstring cable (H), gastrocnemius cable (G), hip moment actuator (HM), hip actuator (HA), and ankle actuator (AA)

The participant testing order was set to provide the least setup change between participants, starting from smallest limb lengths. Large limb lengths corresponded to taller, heavier subjects, who were considered to be more at risk of injury. Testing in this order was conservative, allowing for more data collection before failure of each specimen. Each specific participant was simulated twice on each knee to test for data repeatability. The specimens were tested in the participant order, shown in Table 1. All simulations were completed from 100ms pre ground contact – 200ms post ground contact. 100ms of pre ground contact simulation allowed for the development of muscle forces present at contact, which, if applied instantaneously, would cause both muscle and strain artifacts.

TABLE 1 Specimen Testing Order and Limb Length

Order	Participant	Femur Length (CM)	Tibia Length (CM)
1	P1	39.9	36.8
2	P5	41.1	38.1
3	P6	41.1	38.1
4	P2	42.2	40.4
5	P7	43.7	40.4
6	P4	42.2	39.1
7	P3	42.9	39.6
8	P8	44.2	42.7
9	P9	42.2	39.1
10	P10	40.4	38.1

After each simulation, the diagnostic code was inspected for simulation adherence and any indication of tissue failure. The resting position of the DVRT was also checked, as large differences in DVRT voltage could indicate an ACL tear not seen in the diagnostic *Matlab* code.

Data Analysis

Prior to DVRT insertion on the ACL, DVRT voltage was recorded when the pins were 5mm apart, to be used in the strain calculations. The DVRT was calibrated using a custom built jig that measures the displacement of the pins and the voltage. The slope of this line was the DVRT calibration and closely matched the manufacturer specifications. The equation $\varepsilon = (l - L')/L'$ was used to calculate ACL strain, where L' is the gauge length at landing and l, as the length at any point in time. Gauge length, L', is defined as

$$Gauge\ Length\ (mm)\ =\ 5mm\ +\ (DVRT\ voltage\ at\ 100ms\ -\ Voltage\ at\ 5mm)\ *\ (\frac{mm}{V}\ cal)$$

The length, l, is defined as:

$$Length\ (mm)\ =\ 5mm\ +\ (DVRT\ voltage\ -\ Voltage\ at\ 5mm)\ *\ (\frac{mm}{V}\ cal)$$

Then the ACL strain is:

$$ACL\ Strain\ =\ (Length\ -\ (Gauge\ Length))/\ (Gauge\ Length)$$

After the strain was calculated for each trial, duplicate trials were averaged, and this average was used in the subsequent analysis. All strain data was filtered with a 50 Hz Butterworth filter. *Minitab* statistical analysis software was used to for all statistical analysis.

The strain values for each knee were normalized within that knee, using the normalization formula, z-transform (Withrow et al., 2006) when population parameters are unknown.

$$\frac{Strain - \overline{Strain_{knee}}}{(SD)_{knee}}$$

Bivariate analysis was performed on the normalized strain with the following sagittal plane parameters, extracted from the *OpenSim* simulations at maximum ground reaction force and maximum values for the entire trial.

- Body Weight

- Ground Reaction Forces

- Sagittal Kinematics and Moments

  - Ankle, Knee, Hip and Trunk

- Muscle Forces Quadriceps, Hamstring and Gastrocnemius

- Knee, Hip, Knee/Hip Range of motion (ROM)

- Knee and Hip Velocity

In addition, bivariate analysis was conducted on the time to peak ACL strain using the same sagittal plane parameters. Time to peak ACL strain was measured by subtracting the landing time (100ms) from the time of peak strain during the simulation.

Regression analysis was performed to create an empirical model to calculate peak ACL strain from sagittal plane parameters. A Box-Cox transformation was used to reduce the variance between max strain values on each knee (Box & Cox, 1964). The Box-Cox transform used $\lambda=0$, defined the transformed strain, as equal to the natural log of the non-transformed strain. The regression equation included a knee anatomic constant, a categorical predictor for each knee. This categorical predictor was a constant for each knee, differencing the max-strain values for each specimen when the equivalent loading conditions were applied. In addition to the knee anatomic factor, the regression equation was created using a combination of factors seen from the bivariate analysis. The best regression equation was considered to be the equation with the highest R-Square value with all factors statistically significant ($P<.05$). Due to the large number of possible equations, best subset regression was used to find high R-Square equations. Best subset regression applies all combinations of the independent variables in the attempt to find the highest R-square equations. This tool did not differentiate statistically significant factors, so the best equations were rechecked with the linear regression tool. A formula for Time to Peak ACL strain was also created using the same methodology as above, but without a Box-Cox transformation.

Chapter 5 Results

The 10 Participants (5 Male, 5 Female) had an average body mass of 67kg, GRF of 1997N and jump height of 316 mm. Details can be found in Table 2. Multiple participants did not have successful repeat jump landing simulations on cadaver knee and are denoted by *. Subsequent graphs and values reported reflect only the seven participants to prevent the reader from drawing conclusions from non-simulated trials.

TABLE 2 Participant Information

Participant	Sex	BM (KG)	GRF (N)	Jump Height (mm)
1	F	59.0	1869	328
2	F	61.0	1705	303
3	M	72.0	2546	380
4	M	79.0	2508	327
5	F	57.5	1885	339
6	F	67.5	1675	264
7	F	66.0	1729	272
8*	M	72.5	2282	311
9*	M	74.0	1857	229
10*	M	65.0	1913	283
Average (SD)	-	67 (7)	1997 (326)	303 (43)

Five cadaver specimens (3 male, 2 female) were used during this study and one specimen used for collecting pilot data. The specimen details can be found in Table 3. The moment arms calculated for each specimen can be found in Table 4.

TABLE 3 Donor Tissue information

Knee #	Sex	Body mass (kg)	Age	Height (cm)	Failure mode
1	M	95	49	175	Tibial Fracture
2	F	113	49	191	Tibial Plateau Failure
3	M	79	49	183	Patellar Tendon Failure
4	M	132	40	185	No Failure
5	F	77	49	170	ACL Rupture
Pilot	M	77	49	170	ACL Rupture

TABLE 4 Cadaver Moment Arm Calculations

Knee	Pilot	1	2	3	4	5
Quadriceps Moment Arm (mm)	61	43	44	50	43	41
Hamstring Moment Arm (mm)	54	34	42	40	43	36
Gastrocnemius Moment Arm (mm)	44	25	22	20	17	16

Results of the *OpenSim* simulations can be found in Figure 24, demonstrating the variability in the kinematics, moments, ground reaction forces and muscle forces experienced by the participants.
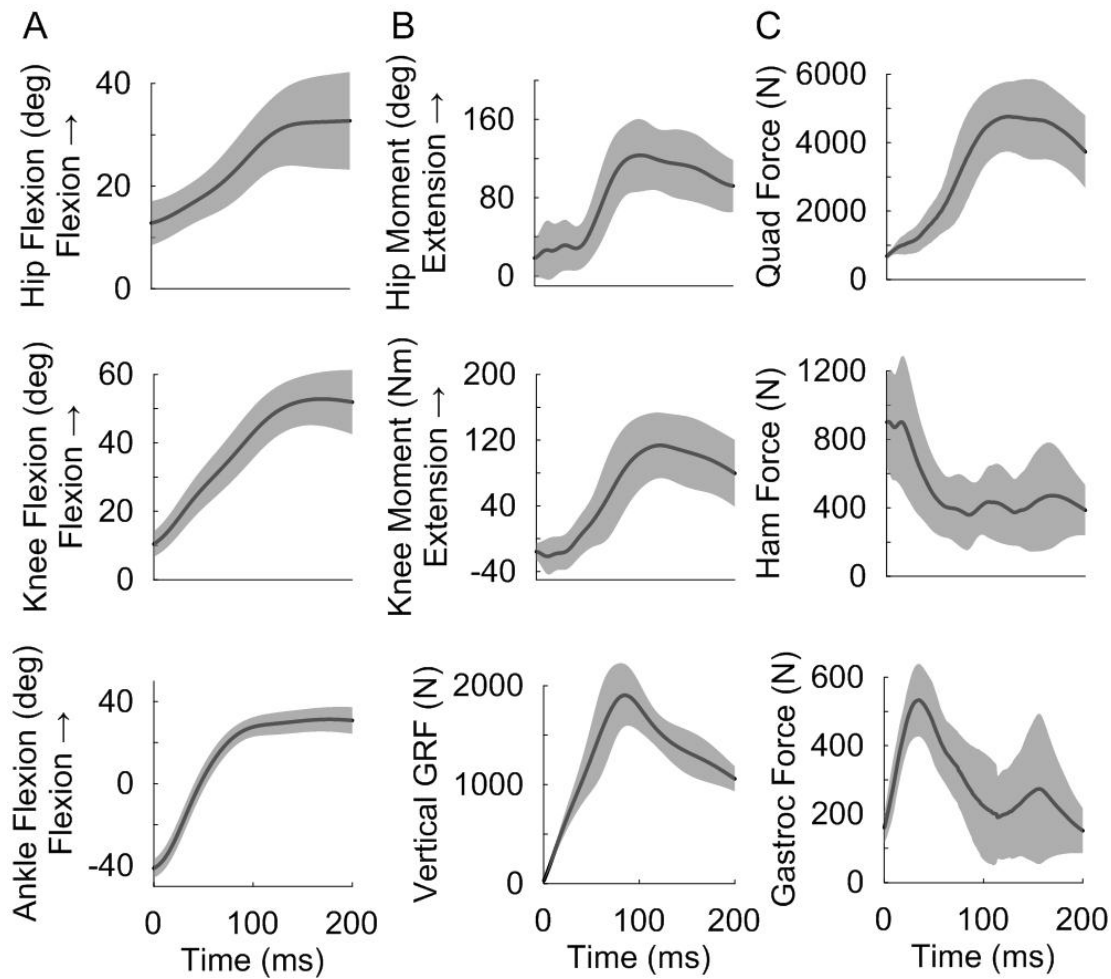
Figure 24 Opensim Sagittal Plane Mechanics: average (black) and ±1 standard deviation (grey) of the following parameters during Opensim Simulation (A) Kinematics of hip, knee, and ankle flexion angles. (B) Hip and knee extension moments and vertical ground reaction force. (C) Quadriceps, hamstring and gastrocnemius muscle group contributions. For all figures t=0 represents time of initial contact

Details Sagittal plane parameters of each of the seven participants based on *OpenSim* simulations are provided in Table 5. Variables are reported at both max for whole trial and at maximum GRF where appropriate. Body mass, ground reaction forces, kinematics, range of motion, joint velocities, joint moments and muscle forces are reported.

TABLE 5 Participant Sagittal Plane Variables

		Participant	1	2	3	4	5	6	7
		Body Mass (Kg)	59	61	72	79	57.5	67.5	66
		GRF (N)	1869	1705	2546	2508	1885	1675	1729
Kinematics	Max Whole Trial	Ankle Flexion (°)	36	36	32	30	25	38	21
		Knee Flexion (°)	60	67	52	53	51	57	38
		Hip Flexion (°)	26	45	22	30	33	48	26
		Trunk Flexion (°)	20	24	24	25	22	2	26
	At Max Ground Reaction Force	Ankle Flexion (°)	30	27	24	21	20	28	16
		Knee Flexion (°)	49	42	36	32	38	37	25
		Hip Flexion (°)	22	29	15	19	24	35	17
		Trunk Flexion (°)	17	14	22	18	18	-4	24
Joint Moments	Max Whole Trial	Knee Extension (Nm)	175	198	148	194	152	141	63
		Hip Extension (Nm)	72	105	142	126	106	59	134
		Trunk Extension (Nm)	97	103	153	184	72	86	152
	At Max Ground Reaction Force	Knee Extension (Nm)	162	129	84	129	92	122	23
		Hip Extension (Nm)	58	73	128	47	90	36	121
		Trunk Extension (Nm)	59	35	149	26	30	34	134
Muscle Forces	Max Whole Trial	Quadriceps (N)	3985	4166	3710	4643	3061	3247	1504
		Hamstrings (N)	1052	1134	1570	1236	1202	1185	1815
		Gastrocnemius (N)	832	699	1632	1033	1025	1071	1174
	At Max Ground Reaction Force	Quadriceps (N)	3575	2574	2082	2806	1803	2675	879
		Hamstrings (N)	245	215	542	462	163	360	440
		Gastrocnemius (N)	570	357	1076	496	791	397	639
		Q/H contraction Ratio	15	12	4	6	11	7	2
Range of Motion	At Max Ground Reaction Force	Knee (°)	35	26	26	21	28	28	21
		Hip (°)	15	11	5	8	9	15	6
		Knee/Hip (°)	2	2	5	3	3	2	3
Joint Velocity	At Max Ground Reaction Force	Knee (°/s)	0.34	0.32	0.25	0.26	0.25	0.23	0.15
		Hip (°/s)	0.08	0.06	0.03	0.05	0.05	0.08	0.03
		Knee/Hip (°/s)	4.21	5.15	8.52	5.27	5.28	2.98	4.45

Strain graphs from of the seven participants on each of the five knees are presented in Figure 25. The time is in milliseconds after landing and strain is in percent. Knee 1 and Knee 2 only successfully simulated the first six participants, Knee 3 and 4 all seven participants and Knee 5 only two of the participants.
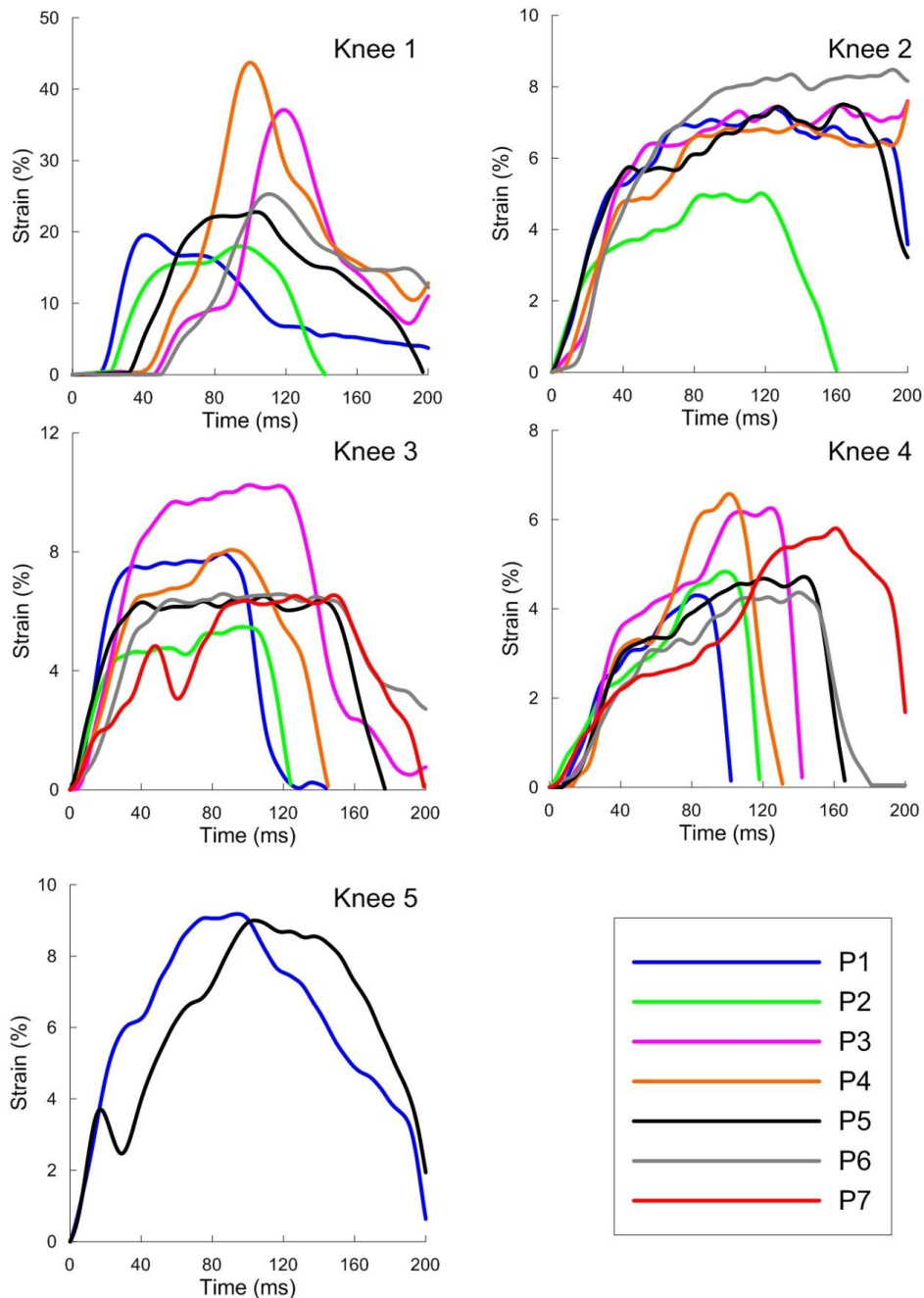
Figure 25. ACL Strain trends of the seven participants on Knees 1,2,3,4,5.

Strain graphs of each participant are presented with each line from a different knee in Figure 26.The time is in milliseconds after landing and strain is in %. Participant 1 and 5 simulations were run on all five knees while Participant 2,3,4, and 6 were simulated on four knees and Participant 7 was simulated on just Knees 3 and 4.
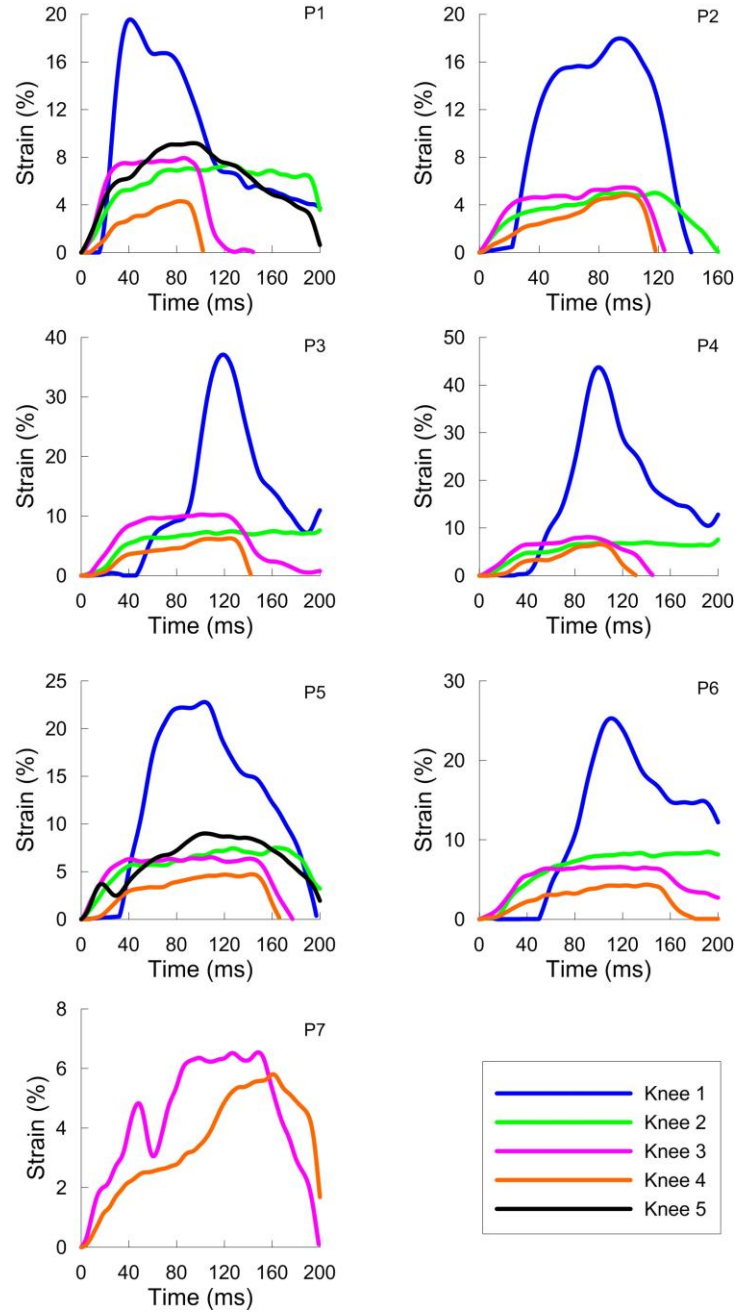
Figure 26 ACL Strain tends for the seven participants on the five cadaver knees

48

The strain value measured for each knee/participant combination is presented in Table 6. The average strain value measured was 10.85%. The time to peak ACL strain in milliseconds is presented in italics next to the strain values.

TABLE 6 Max ACL Strain % Values and Time to Max ACL Strain in ms

| Knee		1		2		3		4		5	
		Max	Tmax	Max	Tmax	Max	Tmax	Max	Tmax	Max	Tmax
Participant	1	19.6	*41*	7.4	*124*	7.9	*86*	4.3	*83*	9.2	*94*
	2	18.0	*94*	5.0	*118*	5.5	*97*	4.8	*99*	-	-
	3	37.1	*119*	7.6	*200*	10.3	*101*	6.3	*124*	-	-
	4	43.7	*100*	7.6	*200*	8.1	*91*	6.6	*101*	-	-
	5	22.8	*103*	7.5	*164*	6.5	*109*	4.7	*143*	9.0	*104*
	6	25.3	*110*	8.5	*192*	6.6	*86*	4.4	*140*	-	-
	7	-	-	-	-	6.5	*148*	5.8	*161*	-	-
	8	-	-	-	-	-	-	6.3*	*109**	-	-
	9	-	-	-	-	-	-	2.8*	*156**	-	-
	10	-	-	-	-	-	-	-	-	-	-
	Average	27.7	95	7.3	166	7.3	95	5.3	115	9.1	99
	SD	10.3	28	1.2	38	1.6	22	0.9	28	0.1	7

Normalized strain values are presented in Table 7. The strain values for each knee were calculated using the formula $\frac{X - \overline{X_{knee}}}{s_{knee}}$, where X is the max strain for the trial and $\overline{X_{knee}}$ is the average max strain value per knee.

TABLE 7 Normalized Max ACL Strain Values

	Knee	1	2	3	4	5
Participant	1	-0.79	0.12	0.38	-1.03	0.71
	2	-0.94	-1.92	-1.19	-0.46	-
	3	0.90	0.29	1.86	1.06	-
	4	1.54	0.25	0.47	1.41	-
	5	-0.48	0.21	-0.53	-0.59	-0.71
	6	-0.24	1.04	-0.48	-0.96	-
	7	-	-	-0.51	0.58	-

Pearson correlations and p-values are shown below for the normalized maximum strain values and the time to maximum strain values with the parameters from Table 7. Significant factors ($P<.05$) are noted with * and highly significant factors ($P<.01$) are noted with **. Results are reported in Table 8.

TABLE 8 Correlation Results between Sagittal Plane Permanents, Max Strain Values and Time to Max Strain

			Max Strain			Time to Max Strain		
			Pearson Correlation	P-Value		Pearson Correlation	P-Value	
		BW	0.619	<0.001	**	0.257	0.187	
		GRF	0.684	<0.001	**	0.495	0.135	
Kinematics	Max Whole Trial	Ankle Flexion (°)	-0.139	0.481		-0.288	0.137	
		Knee Flexion (°)	-0.404	0.033	*	-0.42	0.026	*
		Hip Flexion (°)	-0.494	0.008		-0.024	0.902	
		Trunk Flexion (°)	0.137	0.487		-0.033	0.866	
	At Max Ground Reaction Force	Ankle Flexion (°)	-0.255	0.190		-0.391	0.040	*
		Knee Flexion (°)	-0.327	0.090		-0.499	0.007	**
		Hip Flexion (°)	-0.536	0.003	**	-0.095	0.630	
		Trunk Flexion (°)	0.215	0.272		0.006	0.976	
Joint Moments	Max Whole Trial	Knee Extension (Nm)	-0.096	0.628		-0.382	0.045	*
		Hip Extension (Nm)	0.385	0.043	*	0.273	0.161	
		Trunk Extension (Nm)	0.591	0.001	**	0.185	0.346	
	At Max Ground Reaction Force	Knee Extension (Nm)	-0.144	0.465		-0.47	0.012	*
		Hip Extension (Nm)	0.166	0.399		0.24	0.218	
		Trunk Extension (Nm)	0.384	0.043	*	0.223	0.253	
Muscle Forces	Max Whole Trial	Quadriceps (N)	0.135	0.493		-0.322	0.095	
		Hamstrings (N)	0.38	0.046	*	0.435	0.021	*
		Gastrocnemius (N)	0.587	0.001	**	0.381	0.045	*
	At Max Ground Reaction Force	Quadriceps (N)	-0.019	0.923		-0.445	0.018	*
		Hamstrings (N)	0.664	<0.001	**	0.31	0.109	
		Gastrocnemius (N)	0.409	0.031	*	0.206	0.293	
		Q/H contraction Ratio	-0.511	0.005	**	-0.488	0.008	**
Range of Motion	At Max Ground Reaction Force	Knee (°)	-0.263	0.177		-0.39	0.040	*
		Hip (°)	-0.388	0.041	*	-0.334	0.082	
		Knee/Hip (°)	0.426	0.024	*	0.25	0.199	
Joint Velocity	At Max Ground Reaction Force	Knee (°/s)	-0.214	0.274		-0.458	0.014	*
		Hip (°/s)	-0.382	0.045	*	-0.379	0.047	*
		-	-	-	-	-	-	-

The regression equation created was to calculate actual strain values. The box-cox power transform applied to the max strain values had λ = 0. Therefore the rank preserved transformed max strain values, Strain', is equal to the natural log of the max strain (Box & Cox, 1964). A multivariate linear regression model was developed to estimate the max Strain' values from the variables listed in Table 4. Only those parameters that significantly contributed to the R^2 value of the model were included in the model. The following regression models (Table 9 and 10) were found to give the highest R2 value with each independent variable being significant contributor to the R2 value and having significant p-value. Table 9 shows the P-value of each included variable and the contribution towards explaining the variation in the measured ACL strain in Regression 1.

$$\text{Strain}' = \text{Knee Anatomic Constant} - 0.048 \, (\text{Hip Angle at Maximum GRF}) - 0.026 \, (\text{Trunk Angle at Maximum GRF})$$

TABLE 9 Max ACL Strain Regression 1

R2 = 94.81 %, Degrees of Freedom = 27

Source	Coefficient	P Value	Contribution
Regression		0.000	94.81%
Trunk angle at max GRF	-0.048	0.002	0.04%
Hip angle at max GRF	-0.026	0.000	5.45%
Knee Anatomic Constant		0.000	89.32%
1	4.806		
2	3.507		
3	3.504		
4	3.178		
5	3.798		
Error			5.19%
Total			100.00%

$$\text{Strain}' = \text{Knee Anatomic Constant} + .149 \text{ (Max Knee Flexion Angle)}$$
$$-0.188 \text{ (Knee Flexion Angle at Max GRF)} - 0.235 \text{ (Max Hip Flexion Angle)}$$
$$+0.264 \text{ (Hip Angle at Maximum GRF)}$$

Table 10 shows the P-value of each included variable and the contribution towards explaining the variation in the measured ACL strain in ACL strain Regression 2.

TABLE 10 Max ACL Strain Regression 2

R^2 = 95.76 %, Degrees of Freedom = 27

Source		Coefficient	P Value	Contribution
Regression			0.000	95.76%
Max Knee Flexion Angle		0.149	0.002	0.18%
Knee Flexion at Max GRF		-0.188	0.001	0.92%
Max Hip Flexion Angle		-0.235	0.002	1.36%
Hip Flexion at Max GRF		0.264	0.003	5.63%
Knee Anatomic Constant			0.000	87.66%
	Knee 1	3.886		
	Knee 2	2.587		
	Knee 3	2.586		
	Knee 4	2.259		
	Knee 5	2.916		
Error				4.24%
Total				100.00%

A regression model was created to estimate the time to peak strain values. Each knee has a separate knee parameter. This parameter is intended to separate out all of the effects that are included from the cadaver knee.

$$\text{Time to Peak Strain} = \text{Knee Anatomic Constant} - 162.7 \text{ (knee angular velocity)}$$

TABLE 11 Time to Max ACL Strain Regression

R2 = 79.44 %, Degrees of Freedom = 27

Source	Coefficient	P Value	Contribution
Regression		0.000	79.44%
Knee Angle Velocity	-162.7	0.000	24.74%
Knee Anatomic Constant		0.000	54.70%
Knee 1	193.5		
Knee 2	265.4		
Knee 3	195.2		
Knee 4	214.2		
Knee 5	203.2		
Error			20.56%
Total			100.00%

Dynamic Knee Simulator results are shown in Figure 27 for Participant 1. All measurements recorded by the DKS are shown for each individual run, quadriceps/hamstring/gastrocnemius force, ankle load cell X and Y force, and X and Y positions. Net hip moment is also shown for reference (not measured). All timing is in milliseconds and landing occurs at 100ms. Similar figures for the remaining participants can be found in Appendix B.
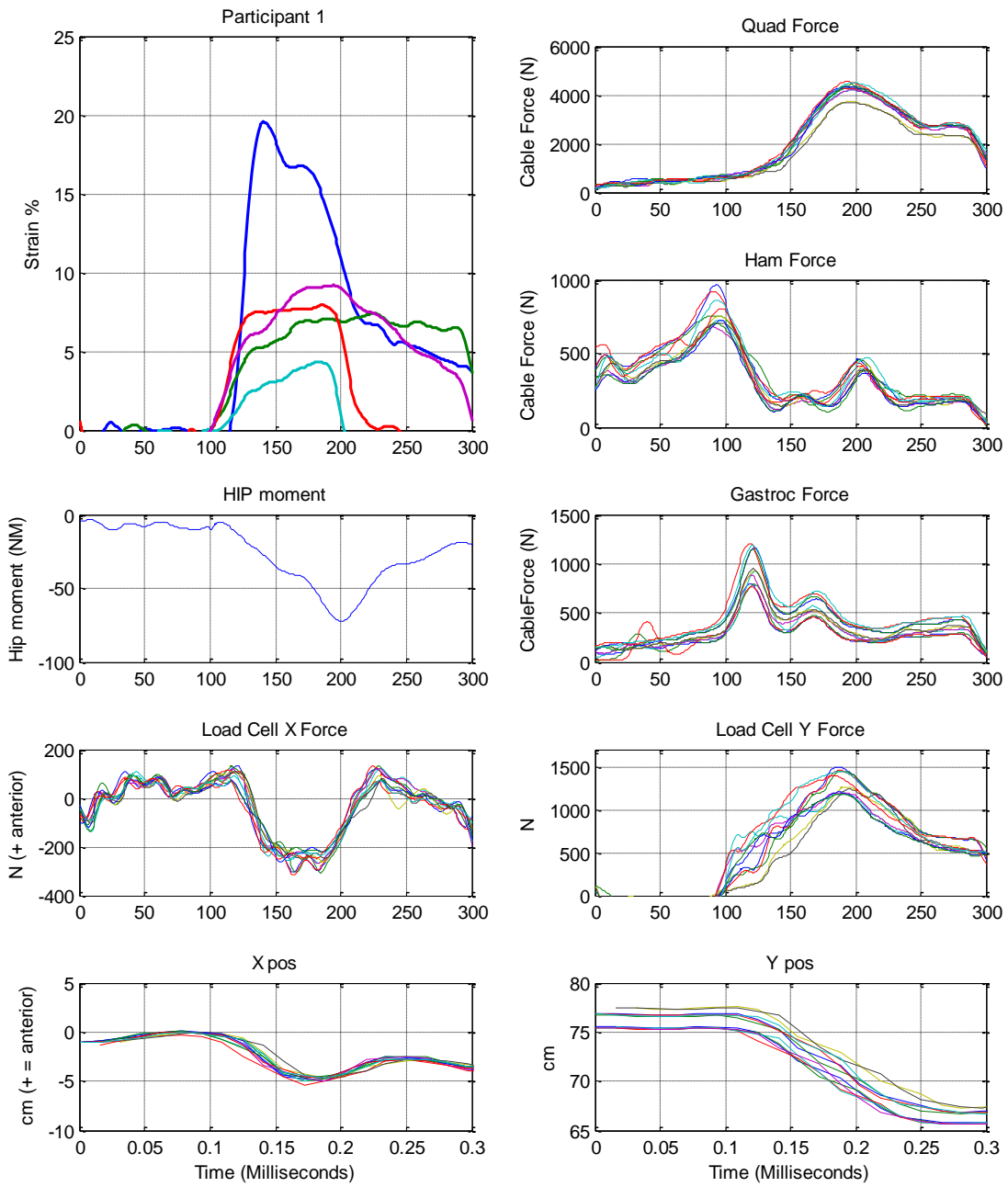
Figure 27 Participant 1 DKS results

Chapter 6

Discussion

The use of the in-vivo/computational/in-vitro approach developed in Cassidy (2013) has helped overcome a number of limitations that exist while studying in-vitro ACL strain. Dynamic movements and muscles forces were replicated using the Dynamic Knee Simulator, reflecting the kinematics and kinetics experienced during single leg jump landing. To our knowledge, this is the first study that incorporated these parameters throughout time.

It is clear from both Figures 25 and 26 that both maximum ACL strain and trend are highly dependent on the knee specimen. For instance, Knee 1 had large strain values with 27% average strain, versus Knee 4 with 5.3% average strain. Both knees experienced the same combination of kinematics and joint torques, but one knee experienced over five times the strain experienced by the other. In addition to max strain values, the trends varied dramatically. Knee 3 experienced a quick rise in strain, followed by a plateau and a quick drop-off to zero. In contrast, Knee 4 did not demonstrate a plateau, but rather a gentle rise followed by an immediate decrease after peak strain was reached. Knee 2 also showed plateau like features, but did not return to zero as quickly as Knee 3, with some plateaus lasting almost the entire trial. These differences reinforce the notion that ACL strain is highly depended on intrinsic variables. Although not investigated, variables such as joint geometry and ligament properties may play a large role in dictating the trend patterns seen during this study. For instance, the max strain values in Knee 2 are very similar across five of the six participants simulated. This uniformity was not seen in any other knee. It is possible that this knee possessed an anatomical "catch" or divot. As the knee experienced anterior tibial translation (ATT) the tibio-femoral joint may have caught this divot and prevented further ATT. The increasing anterior loads seen by the different participants may not have been enough to overcome this mechanical restraint, leading to multiple loading conditions causing the same maximum strain values. Although this is a hypothetical scenario, it demonstrates the importance small anatomical changes may have on ACL strain trends.

The influence participant loading patterns have on the timing of maximum ACL strain is apparent in Figure 26. To contrast, max ACL strain occurred much earlier in Participant 1 when compared to Participant 5. These timing differences are most likely due to the time profiles of the different loading conditions. For instance, Participant 1 has a maximum quadriceps force 90 milliseconds after landing,

while Participant 5 has maximum quadriceps force 150ms after landing. This may explain the difference in timing; the late development of forces may contribute to the late development of ACL strain. Beyond the influence of timing, it is difficult to decipher from Figure 26 and Table 4 the differences in the participant loading parameters. The anatomical differences between knees dominate the effect. The normalization applied to the strain values within each knee was used to remove this effect and results shown previously in Table 7. After normalization, strain values may now be compared with one another.

6.1 Maximum Strain Correlation Analysis

Correlation analysis was conducted between the key sagittal plane mechanics in Table 4 with the normalized ACL strain in Table 7, and results are recorded in Table 8. All statistics, where applicable, were carried out with the maximum variable values for the whole trial and at maximum GRF. Maximum values were chosen due to the large body of literature surrounding max values. Statistics at maximum GRF were carried out because it gave an easily defined time reference in the middle of the trial, and is the time where the applied force is greatest.

There were six highly significant variables ($p<. 01$) that correlated with increasing ACL strain; increasing body weight, increasing jump height, decreasing hip flexion angle at maximum GRF, increasing maximum trunk extension moment, increasing maximum gastrocnemius muscle force, increasing hamstring force at maximum GRF, and decreasing quadriceps/hamstring ratio at maximum ground reaction force. There were additional significant variables ($p<. 05$), decreasing max knee angles, increasing max hip extensor moments, trunk extension moment at maximum GRF, maximum hamstring forces, decreasing hip and hip/knee range of motion were all statistically correlated with increasing max ACL strain.

It is not surprising that increased body weight and GRF were positively correlated with increasing ACL strain. A number of studies that have suggested this importance (Blackburn & Padua, 2008; Laughlin et al., 2011; Norcross, Blackburn, Goerger, & Padua, 2010). Vertical ground reaction forces are the primary external force applied to the body during a non-contact jump landing, and are influenced by a large number of variables. As the participant, with mass m, is falling from a jump, they pick up speed, V, and thus carry momentum mV. When coming in contact with the ground, this momentum change, as the subject comes to rest, is dissipated by the impulse in the ground reaction force. This is an impulse momentum relationship expressed by the equation $\int_{t:\,PreContact}^{t:Rest} GRF \cdot dt = mv_{Rest} - mv_{PreConatact}.$

The mass and the velocities are defined by the participant's body weight and jump height. The impulse on the left-hand side of the equation though, can take a number of different shapes because the integral of this equation is equal to the change in momentum. For example, if a participant lands "stiff", with the leg straight, a large ground reaction force may be seen for a short period of time. Alternatively, if the participant lands "soft" and without a large ground reaction force, the transmittal of force is spread over time. This is a phenomenon known as energy absorption. Increases in GRF have been correlated with decreases in knee and hip flexion angles. This indicates a "stiff" landing and was demonstrated by Blackburn and Padua (2008). In addition, Noyes (2009) was able to decrease the GRF of the subjects while increasing jump height. A probable explanation is a change in energy absorption techniques.

In the current study, the strongest linear relationship with increasing ACL strain was GRF, more than BW or even BW*Jump height. This strong relationship is worth further investigation. BW*Jump height is a factor that relates to the right-hand side of the impulse momentum equation. Increasing jump height will increase the body velocity upon contact with the ground. This correlation is not as strong as with maximum GRF, suggesting that, while it is a driver of increasing GRF, there are other underlying relationships which have effect.

Decreasing hip flexion angles at peak GRF were correlated with increasing ACL strain with high statistical significance. The Pearson correlation coefficient is not as strong as GRF, but is likely a contributing factor to increasing GRF. As reported above, "stiff" landings have been correlated with decreases in hip flexion and increases in GRF, due to the lack of energy dissipation in the joint (Blackburn & Padua, 2008). Blackburn (2008) also suggests the same relationship was found with increasing knee flexion angles. Significant correlation was found with maximum knee flexion angles but no relationship was found at peak GRF.

An interesting relationship is shown between the maximum trunk extension moment and increasing ACL strain. It is not surprising that Participant 3 and 4 experienced the two largest trunk extension moments due to the large GRFs developed. In general, joint moments increase as the ground reaction forces increase. Participant 7 however, developed a large trunk extension moment but experienced an 800N smaller GRF. This is due to a difference in landing style. Participant 7, landed with an extended leg, evident by the smallest ankle and knee flexion angles and second smallest hip flexion angle among all participants. In addition, Participant 7 displayed the largest trunk flexion angles at both max GRF and the entire trial. Due to similar GRF magnitude development as participants 1,2,5 and 6, but different kinematic parameters, Participant 7 displayed a change in landing strategy. Absorbing the

58

ground reaction force energy through trunk extension moment, instead of the knee extension moments. The knee extension moment was 63Nm while the second closest participant was 141Nm. Due to this decrease in knee extension moment, the maximum quadriceps force was less than half of the second closest participant.

Unfortunately, Participant 7 was only simulated on two of the five knees and coincidently, confidence in the results decreases. Nonetheless, the average normalized values from this knee were the third highest of any participant, trailing only Participant 3 and Participant 4. These results suggest the relationship between increasing GRF and trunk extension moment with increasing ACL strain is multifaceted. Increases in GRF and an extended lower limb configuration (which causes the large trunk extension moments) are both antagonistic to the ACL.

In addition to trunk extension moments, increasing maximum hip extension moment is significantly correlated with maximum ACL strain. The body can apply hip extension moments by activating the hamstring and gluteus muscle groups. Extension moments applied by the gluteus muscle group are applied with posterior force on the proximal femur. This posterior force on the femur may be antagonistic of ACL strain; the femur is pulled posteriorly, while no force is applied to the tibia causing the posterior translation of the femur with respect to the tibia. However, the hamstrings are a biarticular muscle group and create a hip extension moment by applying posterior force to the tibia. Due to the knee flexion moment caused by hamstring activation, the quadriceps force would need to increase to produce equivalent knee extension moments. For these reasons, the need for gluteus maximus activation to create hip extension moments have been identified (Alentorn-Geli et al., 2009b), and are antagonistic of ACL strain.

Hamstring forces in isolation have been shown to be ACL protagonist (Withrow et al., 2008). In contrast, this study found hamstring forces at peak GRF to be correlated with increasing ACL strain. The relationship found in this study must be a correlation and not causation do the posterior line of action of the hamstring on the tibia. Trials with the three largest hamstring forces also have the three largest hip extension moments. It is possible that the *OpenSim* model could not produce adequate gluteus maximus activation at these times due to large hip extension moments and joint configurations. Thus, the relationship between hamstring activation and ACL strain may actually be due to the underlying factors contributing to the activation, and not the activation itself.

Quadriceps force has been found in the literature to be both ACL antagonist (Withrow et al., 2006) and protagonist when applied before impact (J. Hashemi et al., 2007). This study found no evidence that quadriceps force is correlated with increasing or decreasing peak ACL strains. Maximum quadriceps force was typically seen at, or post, maximum GRF when the knee flexion angle was between 32 and 49 degrees (except participant seven). As the knee flexes, the anterior line of action of the patellar tendon decreases and even becomes posterior. Studies demonstrating relationships between quadriceps force and increasing strain have typically tested cadaver specimens at 25 degrees flexion, where the quadriceps line of action is more anterior (Herzog & Read, 1993), which may explain the positive relationship. In addition to the anterior pull, increases in quadriceps force increases the joint contact force. Joint contact forces also have suggested to be both protagonist and antagonistic. The posterior tibial slope can redirect a portion of the force in the anterior direction, causing anterior tibial translation, but an increase in contact force also increases the internal frictional forces.

Decreasing quadriceps-hamstring contraction ratio at maximum ground reaction force was found to be significantly correlated with increasing ACL strain. This is also contradictory to other findings suggesting that decreasing the quadriceps hamstring ratio decreases ACL strain (Withrow et al., 2008). Smaller Q/H ratios mean the hamstring applies a large posterior force compared to the anterior component of the patellar tendon. The three smallest Q/H ratios were found on Participants 3, 4 and 7, trials that displayed more upright postures and in the case of Participants 3 and 4, demonstrated the largest GRFs. It is possible that the dangerous positions experienced by these participants outweigh the benefits of having an increase in Q/H ratio.

Maximum gastrocnemius muscle forces were found to be correlated with increasing strain. As an athlete lands from a jump, the first major joint able to absorb energy, is the ankle joint. These ankle extension moments were not simulated on the DKS, and the contribution is to ACL strain is unknown. However, the gastrocnemius muscle group that contributes to the ankle extension moment is simulated. Participants with higher ground reaction forces, require more energy absorption by the ankle joint, increasing the gastrocnemius force. In addition, these muscle forces increase the joint contact forces inside the knee and are subject to the same concerns with increasing contact forces discussed above. Although the gastrocnemius has a very slight posterior line of action on the tibia, it is generally regarded as negligible.

These correlation results show the importance in performing in-vitro testing under these realistic dynamic conditions. A number of findings appear to be contradictory to the literature. For instance, increasing hamstring activation and decreasing Q/H ratio were not correlated with decreasing peak strains. These finding may be due to the nature of the task and not the underlying biomechanical factors in isolation. With the sample size present in this study, it is difficult to detect what affect these parameters would have on an individual subject performing different landing techniques. The two participants with much larger GRFs experienced the largest strains, making it difficult to detect the subtle differences that may be present between landing styles. It is unknown if under different landing conditions, perhaps influenced by the use of training programs, parameters such as hamstring activation and Q/H ratio may be correlated with decreasing strain.

6.2 Maximum Strain Regression Analysis

Due to the dynamic motion of jump landings, the parameters found in Table 5 are interrelated. For instance, given ground reaction forces and joint angles, net joint moments may be calculated. The interrelated nature of the variables on ACL strain is not apparent in correlation analysis. For this reason, multivariate linear regression was performed to develop an empirical relationship between these variables and ACL strain. The empirical models built allow for quick diagnosis of differences in ACL strain, using variables easily calculated in the motion capture lab. Regression analysis was only performed using these variables and thus does not include muscle force estimations, which require the use of *OpenSim* to calculate. The ground reaction forces, kinematics and moments easily calculated in most motion capture labs were potential factors in the model. Including many variables in a regression equation can lead to a highly significant model, but with each parameter insignificant. To avoid this, many multivariate regression models were created, and only significant variables were left in the model. The two models with the highest R-square values and are presented in results.

Due to the differences in anatomic factors, the variance in ACL strain within each knee was different. Knees with larger strains were likely to see a larger range in strain between the maximum and minimum values. This relationship is expected due to the differences in elastic modulus. Linear regression models prohibit the use of independent variables not normally distributed and are the reason for the box cox transformation. The transform, natural log of the strain, corrects this issue.

To assess the quality of the regression analysis, residual plots were created in *Minitab*. Figure 28 shows a normal probability plot of the residuals, residuals versus fit, histogram of the residuals and the observation order versus the residuals for Regression Model 1, while Figure 29 shows residual plots for Regression Model 2. For both models the residual values appear to be normally distributed with a normal probability plot and histogram of the residuals. Residuals versus Fitted Value reveals a gap in the fitted values, but this is expected due to the large strain values from Knee 1. Residual versus order, show no trend as the observation number increases. These residual plots show no issues with the regression analysis.
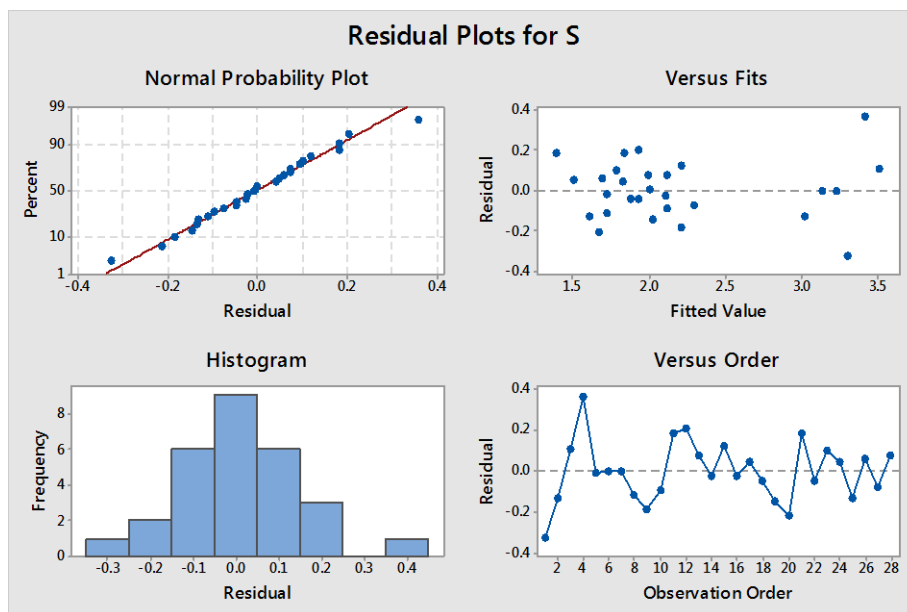

Figure 28 Residual Plots of Regression Equation 1: normal probability plot, histogram, fit, and order graphs are shown from *Minitab*
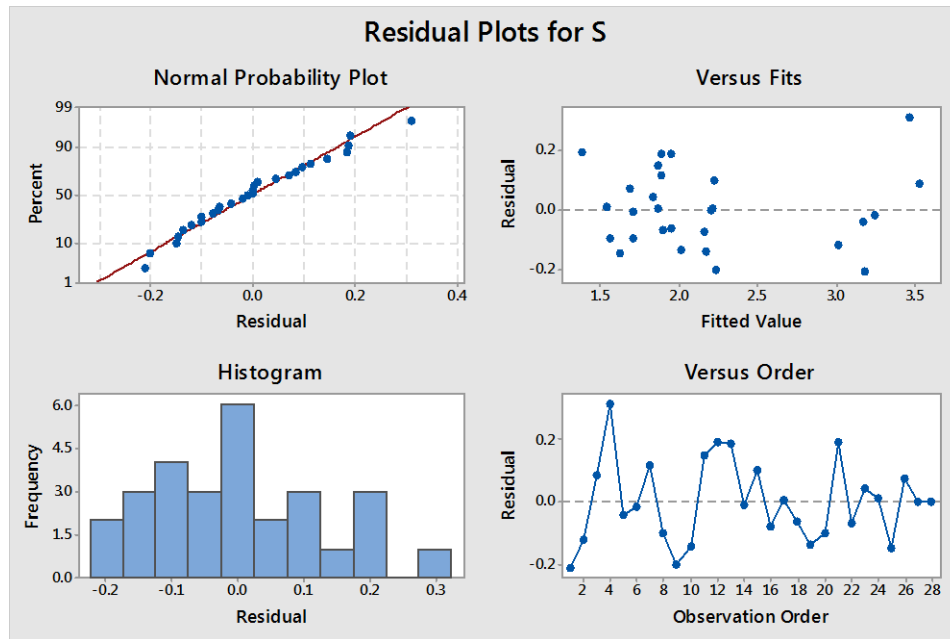
Figure 29 Residual Plots of Regression Equation 2: normal probability plot, histogram, fit, and

order graphs are shown from *Minitab*

It is immediately apparent, based on the models presented in Table 9 and Table 10, that knee anatomic factors are the most critical piece of information when estimating the ACL strain. Over 87% of the variance is carried by this knee anatomic factor (called "Knee Coefficient"), while between 5.5-7% is carried by other factors. This research does not investigate the anatomic factors, but it does stress the importance of further research into understanding them. The anatomic factors leading to larger ACL strain may be important risk factors for injury and may be due to variance in ACL properties, joint geometry and other ligament properties. Preemptive screening for these risk factors may be informative, but ultimately the patient has very little control over these parameters. This may prompt action such as the use of prophylactic bracing, participating in a training program or changing their landing strategy.

In Regression Model 1 the hip and trunk angles at maximum GRF were parameters that best predicted inter-knee variation in ACL strain. Increasing hip and trunk angles at peak GRF, decreases the predicted maximum strain. This relationship is a measure of how "stiff" a landing is. Erect postures during landing increase in the GRF due to the lack of energy absorption. Including GRF did not increase the fidelity of the model, implying that, in addition to the force developed by a stiff landing, the geometric

63

joint relationship also plays an important role. Hashemi et al. (2007) postulated that a "stiff" landing due to incompatible hip and knee velocities may be an ACL antagonist. The regression equation does not use the hip velocity, but it may represent the same phenomenon due to the lack of co-flexion between the hip and knee. In addition, decreasing the hip flexion angle would force the knee into an extended position known to have anatomical drawbacks due to the ACL line of action. Trunk flexion angle has also been shown to be a measure of a flexed landing in previous studies (Blackburn & Padua, 2008). The energy absorbed from this trunk flexion may lead to a decrease in the maximum GRF and reduce the load seen by the knee.

Regression Model 2, shown in Table 10, has four variables, Max Knee Flexion Angle, Knee Flexion at Max GRF, Max Hip Flexion Angle and Hip Flexion at Max GRF in addition to the knee anatomic constant. The model suggests that increasing knee flexion angle at max GRF, but decreasing the max knee angle for the trial, is protective of increasing strain. Decreasing hip flexion at max GRF, but increasing hip flexion for the whole trial, is protective of increasing strain. This means that early trial (from ground contact to max GRF) knee flexion, and late trial (from max GRF to max flexion angle) hip flexion would decrease the ACL strain. Early landing knee flexion may place the knee in a less injury prone position, due to a protective line of action for both the ACL and quadriceps (Herzog & Read, 1993), while the energy is absorbed late landing though hip flexion (Blackburn & Padua, 2009; Shimokochi et al., 2013).

Both regression models are only valid if used within the context of the measured experiments. Single leg jump landing with joint flexion angles experienced during this study: hip (14.7 - 34.6˚) and knee (24.9 – 48.9˚) and trunk (-4.04 - 24.5˚) flexion angles at maximum GRF and maximum hip (22.1 – 47.82˚) and knee (38.3 – 67.4˚) flexion angles.

Extrinsic factors in the regression formulas account for only 51-66% of the variance not explained by the knee anatomic constants. The remaining percentage is due to a combination of errors and unknown contributors. Despite this, the formulas presented demonstrate a large range of predicted strains. For instance, using Regression Model 1 with an average knee coefficient of 3.76, a subject who lands with a hip angle of 25 degrees and trunk angle of 10 degrees at maximum GRF, is estimated to have 9.96% max strain, while the same subject with 30 degrees of hip flexion and 15 degrees at the trunk at maximum GRF is estimated to have 6.88% strain. This is a 27% reduction.

There are concerns about the large strains experienced by Knee 1. Statistical outliers may have a large undesired effect on statistical regression. Upon inspection, this knee did not show any unusual characteristics such as small size or visual tears. Although this is a high strain value, it is not impossible. Chandrashekar et al. (2007) found the average strain at failure to be 30% and the standard deviation to be 6%. This places the strain values from Knee 1 at less than three standard deviations away from the normal maximum tensile strains. To detect the effect Knee 1 may have had on the regression, it was removed from Regression Model 1, and the analysis was repeated. This caused the R-square value to drop from 94% to 80%, due to the leverage these large strain values have over the R-square value. The importance of hip and trunk angles in predicating maximum ACL strain did not change. Results can be found below in Table 12. Similar findings were found from Model 2, in Table 13.

TABLE 12 Max ACL Strain Regression 1 – Without Knee 1

$R^2 = 78.55$ %, Degrees of Freedom = 21

Source	Coefficient	P Value	Contribution
Regression		0.000	78.55%
Trunk Angle at Max GRF	-0.038	0.010	7.71%
Hip Angle at Max GRF	-0.021	0.001	11.99%
Knee Anatomic Constant		0.000	58.85%
Knee 1	-		
Knee 2	3.185		
Knee 3	3.183		
Knee 4	2.857		
Knee 5	3.463		
Error			21.45%
Total			100.00%

TABLE 13 Max ACL Strain Regression 2 –Without Knee 1

$R^2 = 80.74\%$, Degrees of Freedom = 21

Source	Coefficient	P Value	Contribution
Regression		0.000	95.76%
Max Knee Flexion Angle	0.113	0.013	5.27%
Knee Flexion at Max GRF	-0.142	0.010	4.30%
Max Hip Flexion Angle	-0.185	0.010	4.84%
Hip Flexion at Max GRF	0.2085	0.014	11.22%
Knee Anatomic Constant		0.000	55.1%
Knee 1	-		
Knee 2	2.450		
Knee 3	2.452		
Knee 4	2.126		
Knee 5	2.727		
Error			19.26%
Total			100.00%

An additional regression model was created from the full data set, with high R-square values and significant variables. Regression model 3, shown in Table 14, includes the knee anatomic constant and the GRF. This is a useful model because it is the easiest to use, requiring only a force plate to capture. It is easy to understand: reduce the ground reaction forces – reduce ACL strain. However, it does not describe the findings as fully as Regression model 1 or 2.

TABLE 14 Max ACL Strain Regression 3

$R^2 = 94.37\%$, Degrees of Freedom = 27

Source	Coefficient	P Value	Contribution
Regression		0.000	94.37%
Ground Reaction Force	0.00043	0.000	7.47%
Knee Anatomic Constant		0.000	86.9%

Knee 1	2.383	
Knee 2	1.084	
Knee 3	1.108	
Knee 4	0.782	
Knee 5	1.389	
Error		5.63%
Total		100.00%

The three max strain regression models were used on Participant 9 to detect the ability of the regression formulas to predict future trials. Participant 9 was only simulated on Knee 4 and was not included in the statistical correlations and regression analysis due to a lack of repeats on subsequent knees. Participant 8 was also simulated on Knee 4, but post simulation analysis detected errors in the *OpenSim* kinematic solutions and are not valid for comparison. Table 14 compares the measured strain from Participant 9 with the predicted max strain from Regression Models 1, 2 and 3.

TABLE 15 Participant 8 and 9 Strain Regression Prediction

	Measured	Regression 1	Regression 2	Regression 3
Participant 9	2.9%	4.1%	10.1%	4.9%

Although Regression Model 2 appeared to have a very good fit for the original seven participants, the model had the worst prediction of the measured value and is most likely due to over fitting the solution. Over fitting can be caused due to the number of independent variables in the model and therefor does not have good future prediction capabilities. Regression Model 1 outperformed Regression Model 3.

6.3 Timing of Max Strain

In addition to the maximum ACL strain values, ACL strain rate has been identified as a critical factor when determining ACL injury risk. Hashemi et al. (2007) found ACL injuries were more likely to happen under increasing strain rates. In addition, Pioletti et al. (1999) found "supplemental stress" increases with increasing strain rate, reducing the strain at failure of the ligament. An ACL might tear, even though it has not reached its ultimate strain value, when it is loaded faster at the initial phase of

landing. Understanding the factors leading to the quick development of ACL strain may be important for developing a comprehensive understanding of ACL injury risk.

In the current study, knee flexion angles at maximum ACL strain were between 33 and 58 degrees. The time of the two ACL failures was near the beginning of the trials, with small knee flexion angles, 18 and 24 degrees respectively. This supports the notion that although peak loading occurred later in the trial, strain rate and knee position may be critical factors when determining injury risk.

Knee flexion angles and moments were not found to have as strong a relationship with increasing ACL strain as variables associated with other joints, such as the hip and trunk. The timing of peak ACL strain, however, was highly correlated with knee parameters. Larger knee flexion angles at peak GRF were correlated with quicker time to peak ACL strains. Participants who landed with a stiff knee joint have the forces develop in the ACL at a slower rate. In addition, large Q/H ratio at maximum GRF, increases in knee and hip joint velocities, increases in knee flexion ROM and larger knee extension moments were correlated with quicker rise times to peak ACL strain. All of these parameters point to fast movements of the knee developing peak strains faster in the ACL.

The explanation for quicker development of ACL strain may lie in the geometric properties of the ACL insertion sites. Near full extension of the knee, the ACL force required to prevent anterior tibial translation increases due to the vertical line of action. As the knee flexes, the force in the ACL reduces for the same anterior translational force. Forces in the ACL may decrease as the flexion angle increases. Quicker knee flexion places the ACL in line with anterior forces quicker, and forces due to the vertical ACL line of action appear earlier in the trial. In addition, knee angles play a role in the development of muscle forces. For a given GRF, increased knee flexion increases the knee extension torque, due to the increase in moment arm that the external force creates through the tibia about the knee. This increase in knee extension moment will increase the quadriceps force. In this study, quadriceps force was not found to be correlated with increasing strain, but the late development of knee forces due to lagging knee flexion angles may have an effect on the late development of peak ACL strains.

Regression analysis was completed to predict the time to peak ACL strain and the results are found in Table 9. Knee anatomic factors played a major role in the timing development explaining 54.7% of the model. Knee joint geometry, ligament properties and muscle line of actions may be responsible for this dominance of knee anatomic factor. This research does not quantify these variables. Knee angular velocity was found to be the best extrinsic variable accounting for 24.75% of the variance.

The findings from both peak ACL strains and peak ACL strain timing suggest that knee mechanics are correlated with ACL strain rate, while hip and trunk parameters are associated with the ACL strain magnitude. Increases in knee velocity leading to a decrease in the time to peak ACL strain, suggest that a soft landing may lead to the quick development of ACL force and may lead to an increase in strain rate. Strain rate has been suggested to be an critical factor for injury assessment during jump landing (J. Hashemi et al., 2007). Higher strain rates are associated with more ACL tears due to the viscoelastic nature of the ligament. Conversely, as previously described, soft landings were found to reduce the peak ACL strains. It is unknown what the net injury consequence of lower peak strain but increased strain rates may be. Further investigation is required to understand this effect.

The two ACL failures experienced during this study, Knee 5 and a pilot knee, occurred with small knee flexion angles, early in the trials (<50ms) before peak strains and muscle forces were normally developed. These findings are similar to those reported in Koga (2012), where ACL injuries are likely to occur within the first 40ms of landing. These failures are discussed below.

6.4 Failure Analysis

The pilot knee reached its ultimate strain at 50 milliseconds after landing, 2% strain, during the simulation of Participant 5. A 2% strain should not cause an ACL rupture and it is suspected that the ACL was damaged before this trial, although there were no unusual trends in the ACL strain prior to this trial. The rupture occurred at 28 degrees of knee flexion and quadriceps force of 747N, less than one fourth of the maximum quadriceps force. The rupture can be seen in Figure 29-A.

Both the ACL strain patterns and magnitude in the pilot knee were erratic and inconsistent. The starting DVRT voltage indicated between plus or minus 50% strain before each trial. The sutures attaching the DVRT were inspected, but were applied correctly. The ACL was found to have an unusual consistency, with many small bundles, and not a single homogeneous structure. Most likely, the cause for the strain fluctuation was the inability of the ACL to secure the prongs of the DVRT. This erratic nature led to the exclusion of this knee from the analysis.

Knee 5 experienced an ACL tear, 41 milliseconds into testing Participant 6, at 10.9% strain. The knee angle was 21.6 degrees and the quadriceps force was 1528N, less than half of the maximum quadriceps force for the entire trial. The rupture can be seen in Figure 29-B.
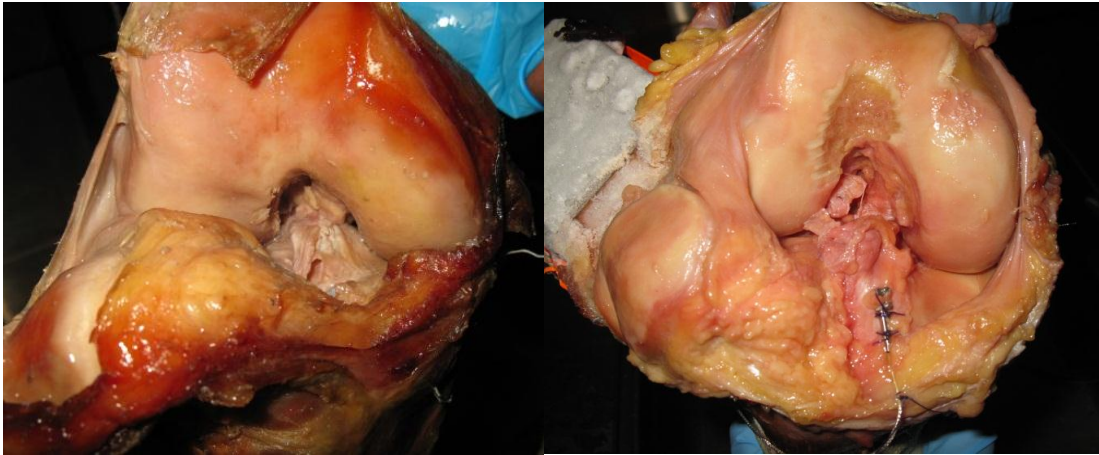
Figure 30 A. Pilot Knee ACL Tear B. Knee 5 ACL Tear

Of the remaining four knees, 1, 2 and 3 experienced failures, while the 4th was able to survive nine rounds of testing. On Knee 1, the hamstring cable was attached by drilling a hole through the tibia and stringing the cable through. During the trial this hole caused a stress concentration and cracked through the anterior portion of the tibia, lifting the tibial tubercle. The crack propagated into the knee cavity and rendered the knee unable to be used for further testing. There was no visible indication of this failure prior to the final trial in the DVRT strain values. Failure occurred in Knee 2 due to the compression and failure of the tibial plateau. Repeated compressive load impacts caused the plateau to cave in. The patellar tendon on Knee 3 failed due to the heavy repeated loading of the quadriceps.

The failure of Knee 1 was due to the mechanical changes needed to mount the knee on the simulator. It is unknown if the failure of Knees 2 and 3 were due to any the specimen preparation, but no defects or irregularities were seen. However, tibial collapse and patellar tendon tears do occur during high impact maneuvers. Both of these failures were due to high force repeated loading, which occurred during these simulations. It is likely that a participant would feel pain prior to these injuries as the damage occurs to the tibial surface or the patellar tendon starts to stretch.

6.5 Limitations

There are a number of limitations that must be addressed with this study.

1. There are known limitations with all computational musculoskeletal modeling. It is unknown if the muscle forces represent the actual muscle forces the participants used during landing. There are no

direct ways to measure muscle forces in human subjects without the surgical implantation of a device. For this reason, great care was taken to simulate the muscle forces and to comply with the standards set forth in the *OpenSim* guidelines and similar studies.

2.   The dynamic knee simulator only replicates sagittal plane mechanics. The controlled contribution of tibial rotation and valgus collapse are absent from these simulations, even if these features were present in the motion capture. The benefit of not simulating these extra DOF is that effects of the sagittal plane mechanics can be studied independently, but the synergistic interaction between the DOF is still unknown. In addition, the muscle forces are lumped sum approximations, which may not represent actual line of action and muscle forces applied throughout the joint. Through the used method however, the net knee and hip joint moments were preserved.

3. Statistical analysis relies on the ability of the simulator to accurately repeat the same loading conditions with minimal error. Figure 27 demonstrates the consistent development of muscle force trends. Variation in muscle force magnitude is expected due to the change in moment arms, but the trends remain consistent. The development of ankle reaction forces were more variable, but still trend consistent, and may be due to differences in bone geometry, incorrect moment arm measurements and positional displacement errors. The variability in ACL strain is far greater than the variability in any of these parameters, and most likely had little effect. In conclusion, repeatability of these tests was satisfactory. However, more investigation should be pursued to increase consistency.

Chapter 7

Future Recommendations

The accuracy, validity and usefulness of cadaveric testing depend on a number of factors. In order to find clinically useful results, the testing must be completed in a manner that best replicates the loading scenario of interest. Recreating the loading scenario is a lengthy process with pitfalls along the way. Errors can accumulate with motion capture, musculoskeletal modeling and the dynamic knee simulations. The following list is a group of recommendations and upgrades, discovered during this study, which could provide higher fidelity simulations in the future.

1. Record electromyography during the task

There are very few tools that allow for a researcher to check the validity of the musculoskeletal model. It is thus imperative that electromyography be taken during motion capture and compared against the activation outputs of the model. This can give the researcher valuable information about muscle firing patterns and can help diagnose problems in their models. If agreement is found between the trends in electromyography and activation, the researcher may have more confidence in the results.

2. Add a seventh actuator to the simulator

The dynamic knee simulator includes a hip torque actuator that applies the net hip moment about the hip joint. This has been included because of the potential link between hip extension moment and peak ACL strain (Javad Hashemi et al., 2011). A number of recent studies have also pointed towards the importance of ankle torque and specifically the muscle groupings around the ankle (Mokhtarzadeh et al., 2013). An ankle plantar flexion torque is thought to be protective of the ACL, just as hip extension moment is antagonistic. The simulator should be upgraded with a seventh axis to address these concerns.

In addition, adding the actuator will help increase the fidelity of the simulations themselves. The ankle force is not fully recreated, and has been confirmed by comparing the ankle force from the dynamic knee simulator to the simulations from *OpenSim*. Adding this actuator will help fix this discrepancy.

3. Remove the need to correct for the quad and hamstring hip torques

With the current configuration, the quadriceps cable is capable of creating up to 300Nm of hip flexion torque, while the hamstrings are capable of 50Nm of hip extension torque. The maximum hip extension torque during the trials is approximately 200Nm. This means the hip torque actuator is required to apply up to 450Nm of torque to correct for the quad force and apply extension torque. The calculations required to correct for this torque is sensitive to a), the geometry of the setup, requiring recalibration for every mechanical change, and b), the machine reproducing the cable forces correctly. If the quadriceps force is recreated within 5% of the maximum force, the hip extension torque may be off by as much as 15Nm. There is no way to correct for this inaccuracy within the dynamic DKS setup.

The solution is to rebuild the hip joint setup and pass both the quadriceps and hamstring cables through the hip joint center. This will create zero torque about the hip, and the hip actuator need only apply force necessary for the extension toque and not correct for the quadriceps and hamstring forces.

Chapter 8

Conclusions

An in-vivo/computational/in-vitro approach was used to measure ACL strain during jump landing. Seven jump landings were successfully simulated on five cadaver specimens, and the results have been reported. Correlation and regression analysis has been conducted between the sagittal plane mechanics and both the max ACL strain values and the time to max ACL strain.

- Maximum strain values were highly correlated with ground reaction force and body weight, in addition to variables defined from the hip and trunk joints, hip angle at maximum GRF and maximum trunk extension moment. Time to max ACL strain was highly correlated with knee variables, knee velocity and knee angle at maximum GRF.

- Anatomic factors dominate the between knee variance of maximum ACL strain and the time to max ACL strain. The Knee Anatomic Constant accounted for more than 87% of the variance found in the max ACL strain regressions and 55% of the time to max ACL strain regression. Although this study did not investigate the individual anatomic factors, it stresses their importance in the development of risk injury models. Further investigation is needed to determine these factors.

- The maximum strain regression formulas presented in this research are easy to use and understand. They provide quantifiable measures that define how stiff a landing is, and the corresponding ACL strain. These formulas could be easily adopted to screen athletes for risk of injury. In addition, they may be used to help design a training program to instruct an athlete how to land more effectively since the equation quantifies ACL strain for different jump landing techniques. The two formulas are presented below:

Max ACL Strain Regression 1

$$\text{Strain}' = \text{Knee Anatomic Constant} - 0.048\,(\text{Hip Angle at Maximum GRF})$$
$$- 0.026\,(\text{Trunk Angle at Maximum GRF})$$

Regression equation 1 bounds:

hip (14.7 - 34.6˚) and trunk (-4.04 - 24.5˚) flexion angles at maximum GRF

Max ACL Strain Regression 2

$$\text{Strain}' = \text{Knee Anatomic Constant} + .149\,(\text{Max Knee Flexion Angle})$$
$$-0.188\,(\text{Knee Flexion Angle at Max GRF}) - 0.235\,(\text{Max Hip Flexion Angle})$$
$$+ 0.264\,(\text{Hip Angle at Maximum GRF})$$

Regression equation 2 bounds:

hip (14.7 - 34.6˚) and knee (24.9 – 48.9˚) flexion angles at maximum GRF maximum

hip (22.1 – 47.82˚) and knee (38.3 – 67.4˚) flexion maximum flexion angles

Bibliography

Alentorn-Geli, E., Myer, G. D., Silvers, H. J., Samitier, G., Romero, D., Lázaro-Haro, C., & Cugat, R. (2009a). Prevention of non-contact anterior cruciate ligament injuries in soccer players. Part 1: Mechanisms of injury and underlying risk factors. *Knee Surgery, Sports Traumatology, Arthroscopy : Official Journal of the ESSKA*, *17*(7), 705–29.

Alentorn-Geli, E., Myer, G. D., Silvers, H. J., Samitier, G., Romero, D., Lázaro-Haro, C., & Cugat, R. (2009b). Prevention of non-contact anterior cruciate ligament injuries in soccer players. Part 1: Mechanisms of injury and underlying risk factors. *Knee Surgery, Sports Traumatology, Arthroscopy : Official Journal of the ESSKA*, *17*(7), 705–29.

Amis, A. a. (2012). The functions of the fibre bundles of the anterior cruciate ligament in anterior drawer, rotational laxity and the pivot shift. *Knee Surgery, Sports Traumatology, Arthroscopy : Official Journal of the ESSKA*, *20*(4), 613–20.

Bennett, D. R., Blackburn, J. T., Boling, M. C., McGrath, M., Walusz, H., & Padua, D. a. (2008). The relationship between anterior tibial shear force during a jump landing task and quadriceps and hamstring strength. *Clinical Biomechanics (Bristol, Avon)*, *23*(9), 1165–71.

Beynnon, B. D., & Fleming, B. C. (1998). Anterior cruciate ligament strain in-vivo: a review of previous work. *Journal of Biomechanics*, *31*(6), 519–25.

Blackburn, J. T., & Padua, D. a. (2008). Influence of trunk flexion on hip and knee joint kinematics during a controlled drop landing. *Clinical Biomechanics (Bristol, Avon)*, *23*(3), 313–9.

Blackburn, J. T., & Padua, D. a. (2009). Sagittal-plane trunk position, landing forces, and quadriceps electromyographic activity. *Journal of Athletic Training*, *44*(2), 174–9.

Boden, B. P., Torg, J. S., Knowles, S. B., & Hewett, T. E. (2009). Video analysis of anterior cruciate ligament injury: abnormalities in hip and ankle kinematics. *The American Journal of Sports Medicine*, *37*(2), 252–9.

Box, A. G. E. P., & Cox, D. R. (1964). An Analysis of Transformations. *Journal of the Royal Statistical Society*, *26*(2), 211–252.

Cassidy, K., Hangalur, G., Sabharwal, P., & Chandrashekar, N. (2013). Combined in vivo/in vitro method to study anteriomedial bundle strain in the anterior cruciate ligament using a dynamic knee simulator. *Journal of Biomechanical Engineering*, *135*(3), 35001.

Chandrashekar, N., Mansouri, H., Slauterbeck, J., & Hashemi, J. (2006). Sex-based differences in the tensile properties of the human anterior cruciate ligament. *Journal of Biomechanics*, *39*(16), 2943–50.

Chappell, J. D., Creighton, R. A., Giuliani, C., Yu, B., & Garrett, W. E. (2007). Kinematics and electromyography of landing preparation in vertical stop-jump: risks for noncontact anterior cruciate ligament injury. *The American Journal of Sports Medicine*, *35*(2), 235–41.

Damsgaard, M., Rasmussen, J., Christensen, S. T., Surma, E., & de Zee, M. (2006). Analysis of musculoskeletal systems in the AnyBody Modeling System. *Simulation Modelling Practice and Theory*, *14*(8), 1100–1111.

Dejour, H., & Bonnin, M. (1994). Tibial translation after anterior cruciate ligament rupture. Two radiological tests compared. *The Journal of Bone and Joint Surgery. British Volume*, *76*(5), 745–9.

Delp, S. L., Anderson, F. C., Arnold, A. S., Loan, P., Habib, A., John, C. T., Thelen, D. G. (2007). OpenSim: open-source software to create and analyze dynamic simulations of movement. *IEEE Transactions on Bio-Medical Engineering*, *54*(11), 1940–50.

Delp, S. L., Loan, J. P., Hoy, M. G., Zajac, F. E., Topp, E. L., & Rosen, J. M. (1990). An interactive graphics-based model of the lower extremity to study orthopaedic surgical procedures. *IEEE Transactions on Bio-Medical Engineering*, *37*(8), 757–67.

Delp, S. L., Ringwelski, D. A., & Carroll, N. C. (1994). Transfer of the rectus femoris: effects of transfer site on moment arms about the knee and hip. *Journal of Biomechanics*, *27*(10), 1201–11.

Duthon, V. B., Barea, C., Abrassart, S., Fasel, J. H., Fritschy, D., & Ménétrey, J. (2006). Anatomy of the anterior cruciate ligament. *Knee Surgery, Sports Traumatology, Arthroscopy : Official Journal of the ESSKA*, *14*(3), 204–13.

Fleming, B. C., Beynnon, B. D., Renstrom, P. a, Johnson, R. J., Nichols, C. E., Peura, G. D., & Uh, B. S. (1998). The strain behavior of the anterior cruciate ligament during Bicycling: an in vivo study. *Arthroscopy : The Journal of Arthroscopic & Related Surgery : Official Publication of the Arthroscopy Association of North America and the International Arthroscopy Association*, *15*(2), 185–91.

Friederich, J. A., & Brand, R. A. (1990). Muscle fiber architecture in the human lower limb. *Journal of Biomechanics*, *23*(1), 91–5.

Gianotti, S. M., Marshall, S. W., Hume, P. a, & Bunt, L. (2009). Incidence of anterior cruciate ligament injury and other knee ligament injuries: a national population-based study. *Journal of Science and Medicine in Sport / Sports Medicine Australia*, *12*(6), 622–7.

Giffin, J. R., Vogrin, T. M., Zantop, T., Woo, S. L. Y., & Harner, C. D. (2004). Effects of increasing tibial slope on the biomechanics of the knee. *The American Journal of Sports Medicine*, *32*(2), 376–82.

Griffin, L. Y., Albohm, M. J., Arendt, E. a, Bahr, R., Beynnon, B. D., Demaio, M., Yu, B. (2006). Understanding and preventing noncontact anterior cruciate ligament injuries: a review of the Hunt Valley II meeting, January 2005. *The American Journal of Sports Medicine*, *34*(9), 1512–32.

Hamner, S. R., & Delp, S. L. (2013). Muscle contributions to fore-aft and vertical body mass center accelerations over a range of running speeds. *Journal of Biomechanics*, *46*(4), 780–7.

Hashemi, J., Breighner, R., Chandrashekar, N., Hardy, D. M., Chaudhari, A. M., Shultz, S. J., Beynnon, B. D. (2011). Hip extension, knee flexion paradox: a new mechanism for non-contact ACL injury. *Journal of Biomechanics*, *44*(4), 577–85.

Hashemi, J., Chandrashekar, N., Jang, T., Karpat, F., Oseto, M., & Ekwaro-Osire, S. (2007). An Alternative Mechanism of Non-contact Anterior Cruciate Ligament Injury During Jump-landing: In-vitro Simulation. *Experimental Mechanics*, *47*(3), 347–354.

Herzog, W., & Read, L. J. (1993). Lines of action and moment arms of the major force-carrying structures crossing the human knee joint. *Journal of Anatomy*, *182 (Pt 2*, 213–30.

Hewett, T. E., Myer, G. D., Ford, K. R., Heidt, R. S., Colosimo, A. J., McLean, S. G., Succop, P. (2005). Biomechanical measures of neuromuscular control and valgus loading of the knee predict anterior cruciate ligament injury risk in female athletes: a prospective study. *The American Journal of Sports Medicine*, *33*(4), 492–501.

Hewett, T. E., Stroupe, A. L., Nance, T. A., & Noyes, F. R. (n.d.). Plyometric training in female athletes. Decreased impact forces and increased hamstring torques. *The American Journal of Sports Medicine*, *24*(6), 765–73.

Ireland, M. L., Ballantyne, B. T., Little, K., & McClay, I. S. (2001). A radiographic analysis of the relationship between the size and shape of the intercondylar notch and anterior cruciate ligament injury. *Knee Surgery, Sports Traumatology, Arthroscopy : Official Journal of the ESSKA*, *9*(4), 200–5.

Kar, J., & Quesada, P. M. (2012). A numerical simulation approach to studying anterior cruciate ligament strains and internal forces among young recreational women performing valgus inducing stop-jump activities. *Annals of Biomedical Engineering*, *40*(8), 1679–91.

Kiapour, A. M., Quatman, C. E., Goel, V. K., Wordeman, S. C., Hewett, T. E., & Demetropoulos, C. K. (2014). Timing sequence of multi-planar knee kinematics revealed by physiologic cadaveric simulation of landing: implications for ACL injury mechanism. *Clinical Biomechanics (Bristol, Avon)*, *29*(1), 75–82.

Kiapour, A. M., Wordeman, S. C., Paterno, M. V, Quatman, C. E., Levine, J. W., Goel, V. K., Hewett, T. E. (2014). Diagnostic value of knee arthrometry in the prediction of anterior cruciate ligament strain during landing. *The American Journal of Sports Medicine*, *42*(2), 312–9.

Koga, H., Nakamae, A., Shima, Y., Iwasa, J., Myklebust, G., Engebretsen, L., Krosshaug, T. (2010). Mechanisms for noncontact anterior cruciate ligament injuries: knee joint kinematics in 10 injury situations from female team handball and basketball. *The American Journal of Sports Medicine*, *38*(11), 2218–25.

Kristianslund, E., Krosshaug, T., & van den Bogert, A. J. (2012). Effect of low pass filtering on joint moments from inverse dynamics: implications for injury prevention. *Journal of Biomechanics*, *45*(4), 666–71.

Krosshaug, T., Nakamae, A., Boden, B. P., Engebretsen, L., Smith, G., Slauterbeck, J. R., … Bahr, R. (2007). Mechanisms of anterior cruciate ligament injury in basketball: video analysis of 39 cases. *The American Journal of Sports Medicine*, *35*(3), 359–67.

Laughlin, W. a, Weinhandl, J. T., Kernozek, T. W., Cobb, S. C., Keenan, K. G., & O'Connor, K. M. (2011). The effects of single-leg landing technique on ACL loading. *Journal of Biomechanics*, *44*(10), 1845–51.

Levine, J. W., Kiapour, A. M., Quatman, C. E., Wordeman, S. C., Goel, V. K., Hewett, T. E., & Demetropoulos, C. K. (2013). Clinically relevant injury patterns after an anterior cruciate ligament injury provide insight into injury mechanisms. *The American Journal of Sports Medicine*, *41*(2), 385–95.

Lipps, D. B., Oh, Y. K., Ashton-Miller, J. a, & Wojtys, E. M. (2014). Effect of increased quadriceps tensile stiffness on peak anterior cruciate ligament strain during a simulated pivot landing. *Journal of Orthopaedic Research : Official Publication of the Orthopaedic Research Society*, *32*(3), 423–30.

Lipps, D. B., Wojtys, E. M., & Ashton-Miller, J. a. (2013). Anterior cruciate ligament fatigue failures in knees subjected to repeated simulated pivot landings. *The American Journal of Sports Medicine*, *41*(5), 1058–66.

Lyon, R. M., Woo, S. L., Hollis, J. M., Marcin, J. P., & Lee, E. B. (1989). A new device to measure the structural properties of the femur-anterior cruciate ligament-tibia complex. *Journal of Biomechanical Engineering*, *111*(4), 350–4.

Mall, N. a, Chalmers, P. N., Moric, M., Tanaka, M. J., Cole, B. J., Bach, B. R., & Paletta, G. a. (2014). Incidence and trends of anterior cruciate ligament reconstruction in the United States. *The American Journal of Sports Medicine*, *42*(10), 2363–70.

Marouane, H., Shirazi-Adl, A., Adouni, M., & Hashemi, J. (2014). Steeper posterior tibial slope markedly increases ACL force in both active gait and passive knee joint under compression. *Journal of Biomechanics*, *47*(6), 1353–9.

Mather, R. C., Koenig, L., Kocher, M. S., Dall, T. M., Gallo, P., Scott, D. J., Spindler, K. P. (2013). Societal and economic impact of anterior cruciate ligament tears. *The Journal of Bone and Joint Surgery. American Volume*, *95*(19), 1751–9.

McLean, S. G., Oh, Y. K., Palmer, M. L., Lucey, S. M., Lucarelli, D. G., Ashton-Miller, J. a, & Wojtys, E. M. (2011). The relationship between anterior tibial acceleration, tibial slope, and ACL strain during a simulated jump landing task. *The Journal of Bone and Joint Surgery. American Volume*, *93*(14), 1310–7.

Mokhtarzadeh, H., Yeow, C. H., Hong Goh, J. C., Oetomo, D., Malekipour, F., & Lee, P. V.-S. (2013). Contributions of the soleus and gastrocnemius muscles to the anterior cruciate ligament loading during single-leg landing. *Journal of Biomechanics*, *46*(11), 1913–20.

Moore Keith L, Dalley Arthur F, *Clinical Oriented Anatomy*, Fourth Edition 1999, published by: Lippincott Williams and Wilkins

Myers, C. a, Torry, M. R., Shelburne, K. B., Giphart, J. E., LaPrade, R. F., Woo, S. L.-Y., & Steadman, J. R. (2012). In vivo tibiofemoral kinematics during 4 functional tasks of increasing demand using biplane fluoroscopy. *The American Journal of Sports Medicine*, *40*(1), 170–8.

Neufeld, A. H., & Liu, B. (2003). Glaucomatous optic neuropathy: when glia misbehave. *The Neuroscientist : A Review Journal Bringing Neurobiology, Neurology and Psychiatry*, *9*(6), 485–95.

Norcross, M. F., Blackburn, J. T., Goerger, B. M., & Padua, D. a. (2010). The association between lower extremity energy absorption and biomechanical factors related to anterior cruciate ligament injury. *Clinical Biomechanics (Bristol, Avon)*, *25*(10), 1031–6.

Noyes, F. R. (2009). The function of the human anterior cruciate ligament and analysis of single- and double-bundle graft reconstructions. *Sports Health*, *1*(1), 66–75.

Oh, Y. K., Lipps, D. B., Ashton-Miller, J. a, & Wojtys, E. M. (2012). What strains the anterior cruciate ligament during a pivot landing? *The American Journal of Sports Medicine*, *40*(3), 574–83.

Peters, A., Galna, B., Sangeux, M., Morris, M., & Baker, R. (2010). Quantification of soft tissue artifact in lower limb human motion analysis: a systematic review. *Gait & Posture*, *31*(1), 1–8.

Pioletti, D. P., Rakotomanana, L. R., & Leyvraz, P. F. (1999). Strain rate effect on the mechanical behavior of the anterior cruciate ligament-bone complex. *Medical Engineering & Physics*, *21*(2), 95–100.

Podraza, J. T., & White, S. C. (2010). Effect of knee flexion angle on ground reaction forces, knee moments and muscle co-contraction during an impact-like deceleration landing: implications for the non-contact mechanism of ACL injury. *The Knee*, *17*(4), 291–5.

Quatman, C. E., Kiapour, A. M., Demetropoulos, C. K., Kiapour, A., Wordeman, S. C., Levine, J. W., … Hewett, T. E. (2014). Preferential loading of the ACL compared with the MCL during landing: a novel in sim approach yields the multiplanar mechanism of dynamic valgus during ACL injuries. *The American Journal of Sports Medicine*, *42*(1), 177–86.

Riemersa, D. J., & Schamhardt, H. C. (1982). The cryo-jaw, a clamp designed for in vitro rheology studies of horse digital flexor tendons. *Journal of Biomechanics*, *15*(8), 619–20.

Shimokochi, Y., Ambegaonkar, J. P., Meyer, E. G., Lee, S. Y., & Shultz, S. J. (2013). Changing sagittal plane body position during single-leg landings influences the risk of non-contact anterior cruciate

ligament injury. *Knee Surgery, Sports Traumatology, Arthroscopy : Official Journal of the ESSKA*, *21*(4), 888–97.

Shultz, S. J., Schmitz, R. J., Benjaminse, A., Chaudhari, A. M., Collins, M., & Padua, D. a. (2012). ACL Research Retreat VI: an update on ACL injury risk and prevention. *Journal of Athletic Training*, *47*(5), 591–603.

Winter, D. A. (2009). *Biomechanics and Motor Control of Human Movement* (4th ed.). John Wiley & Sons.

Withrow, T. J., Huston, L. J., Wojtys, E. M., & Ashton-Miller, J. a. (2006). The relationship between quadriceps muscle force, knee flexion, and anterior cruciate ligament strain in an in vitro simulated jump landing. *The American Journal of Sports Medicine*, *34*(2), 269–74.

Withrow, T. J., Huston, L. J., Wojtys, E. M., & Ashton-Miller, J. a. (2008). Effect of varying hamstring tension on anterior cruciate ligament strain during in vitro impulsive knee flexion and compression loading. *The Journal of Bone and Joint Surgery. American Volume*, *90*(4), 815–23.

Yu, B., McClure, S. B., Onate, J. a, Guskiewicz, K. M., Kirkendall, D. T., & Garrett, W. E. (2005). Age and gender effects on lower extremity kinematics of youth soccer players in a stop-jump task. *The American Journal of Sports Medicine*, *33*(9), 1356–64.
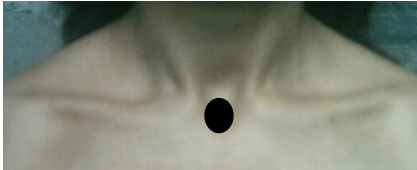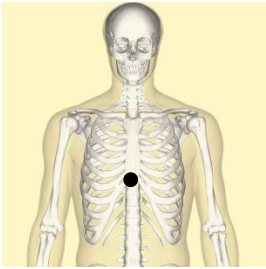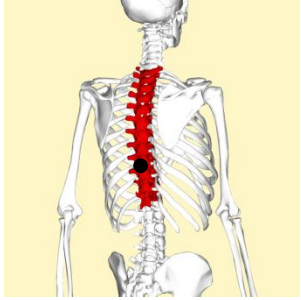
Figure References
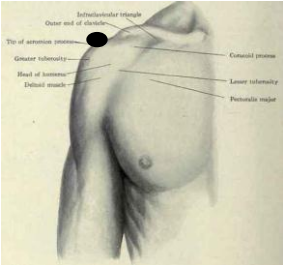
Figure 1 retrieved from website: http://quizlet.com/9862474/ap-168-lab-terms-sectional-anatomy-flash-cards/ and http://yourpathpersonaltraining.com/holiday-challenge-weeks-3-4/

Figure 2 retrieved from website: http://www.turkcebilgi.com/Fibula
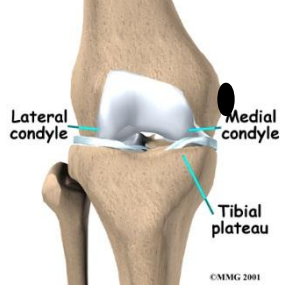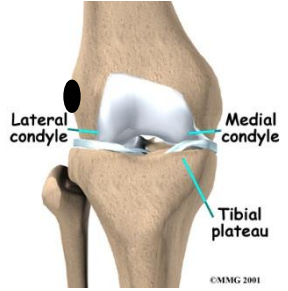
Figure 3 retrieved from website: http://www.healthhype.com/thigh-muscles-diagram-pictures-list-of-actions.html

Appendix A: Anatomic Landmarks
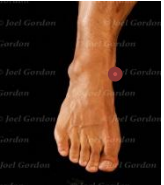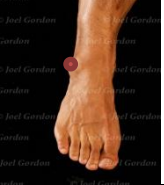
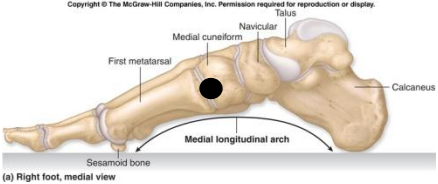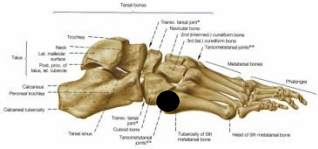| Upper Back Cluster			
Landmark	Marker	Techniques for Palpation	Picture
Suprasternal Notch	SS	• Locate the space between the medial ends of the clavicles • Place the end of the probe in this notch	
Xiphoid Process (note: this is a very sensitive area which should NOT be harshly palpated)	XP	• Locate the bottom of the ribcage on either side (12th rib) • Follow the ribcage medially until your fingers meet in the middle	
T10	T10	• Find the inferior angle (IA) of the scapula on one side • The spinous process immediately medial to the IA is approximately T8 • Palpate 2 spinous processes inferiorly	

C7	C7	• Ask the participant to look toward the floor • Examine the spinous process that projects from the posterior aspect of the neck (C7) • Place the probe on this spinous process	
Acromion (left and right)	RAC/LAC	• Palpate the clavicle laterally until you reach the acromioclavicular joint • The acromion is just lateral to the joint capsule and feels like a 'shelf'	

Low Back Cluster

Landmark	Marker	Techniques for Palpation	Picture
Anterior superior iliac spine	RASIS/ LASIS	• From the anterior side of the participant, use the hands to locate the tops of the iliac crests • With the medial sides of the index fingers on top of the crests, allow the thumbs to run along the crests and down to the protuberance of the ASIS	
Posterior superior iliac spine (note: will be helpful to palpate this before the application of the low back cluster)	RPSIS/ LPSIS	• From the posterior side of the participant, use the medial sides of the index fingers to locate the top of the iliac crest • Find where the sacrum meets the pelvis (sacroilio joint; 'Dimples of Venus') • Follow the sacrum posteriorly to the protuberances of the PSIS	
Greater trochanter (note: make sure you palpate the bone and not the muscle)	RGT/ LGT	• Ask the participant to pretend like they're 'squashing a bug' with their toe • Feel for the head of the femur (i.e., greater tubercle of the trochanter) turn under the skin	

Thigh Cluster

Landmark	Marker	Palpation Technique	Picture
Greater trochanter	RGT/ LGT	See Lower Back Cluster	See Lower Back Cluster
Medial Femoral Condyle	RFMC/ LFMC	- Feel for the tibial tuberosity on the anterior surface of the proximal tibia - Guide your fingers medially along the joint line - Ask the participant to bend the knee - Move the fingers proximally above the joint line to the medial bony landmark of the medial condyle	
Lateral Femoral Condyle	RFLC/ LFLC	- Feel for the tibial tuberosity on the anterior surface of the proximal tibia - Guide your fingers laterally along the joint line - Ask the participant to bend the knee forward - Move the fingers proximally above the joint line to the lateral bony landmark of the lateral condyle	

Shank Cluster

Landmark	Marker	Palpation Technique	Picture
Medial Tibial Condyle	RMTC/ LMTC	• Feel for the tibial tuberosity on the anterior surface of the proximal tibia • Guide your fingers medially along the joint line • Ask the participant to bend the knee • Ensure to place the probe below the joint line along the condyle	
Lateral Femoral Condyle	RFLC/ LFLC	• Feel for the tibial tuberosity on the anterior surface of the proximal tibia • Guide your fingers laterally along the joint line • Ask the participant to bend the knee forward • Feel for the head of the fibula • Place the probe above the head of the fibula and below the joint line	
Tibial Tuberosity	RTIB/ LTIB	• Find the sharp protuberance located on the anterior surface of the proximal tibia, just below the patella	

Medial Malleolus	RMM/ LMM	• Locate the bony protuberance on the medial side of the distal tibia • 'Ankle bone'	
Lateral Malleolus	RLM/ LLM	• Locate the bony protuberance on the lateral side of the distal tibia • 'Ankle bone'	

Foot Cluster

Landmark	Marker	Palpation Technique	Picture
Medial Malleolus	RMM/ LMM	See Shank Cluster	
Lateral Malleolus	RLM/ LLM	See Shank Cluster	
Superior Midfoot	RSMF/ LSMF	• Start with your fingers on the medial malleolus • Move longitudinally down the foot to the first protuberance (talus) • Continue past the next protuberance (navicular) and find the third protuberance (cuniform)	
Lateral Midfoot	RLMF/ LLMF	• Locate the proximal protuberance of the fifth metatarsal where it junctions with the cuboid bone	
Heel	RHEEL/ LHEEL	• Place the probe at the most posterior aspect of the calcaneous	

87

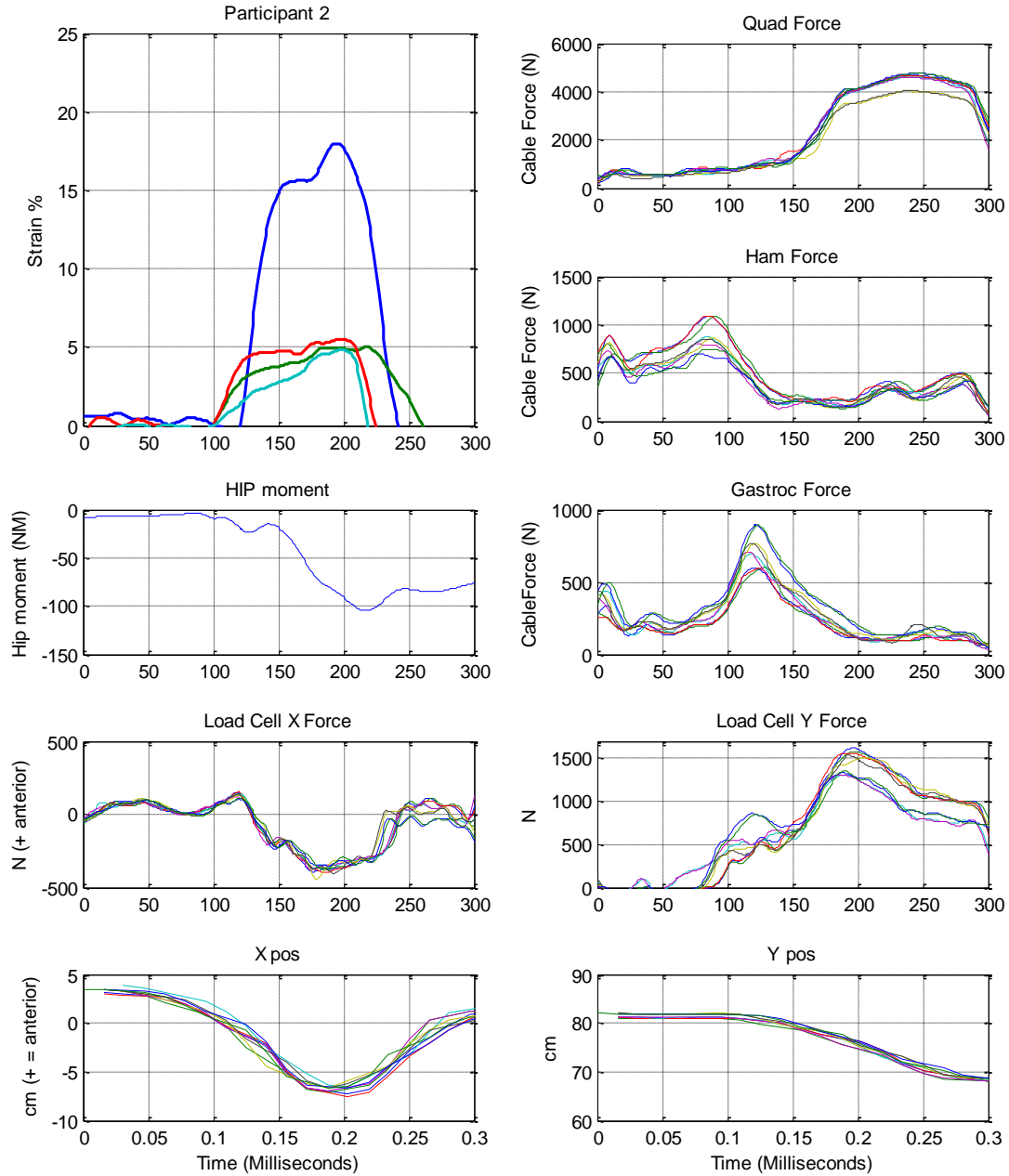| First Metatarsal	RMT1/ LMT1	• Locate the head of the first metatarsal • Base of the 'big toe'	
First Toe	RTOE/ LTOE	• Place the marker (for the right foot) and the probe (for the left foot) on top of the big toe	
Fifth Metatarsal	RMT5/ LMT5	• Locate the head of the fifth metatarsal • Base of the 'baby toe'	

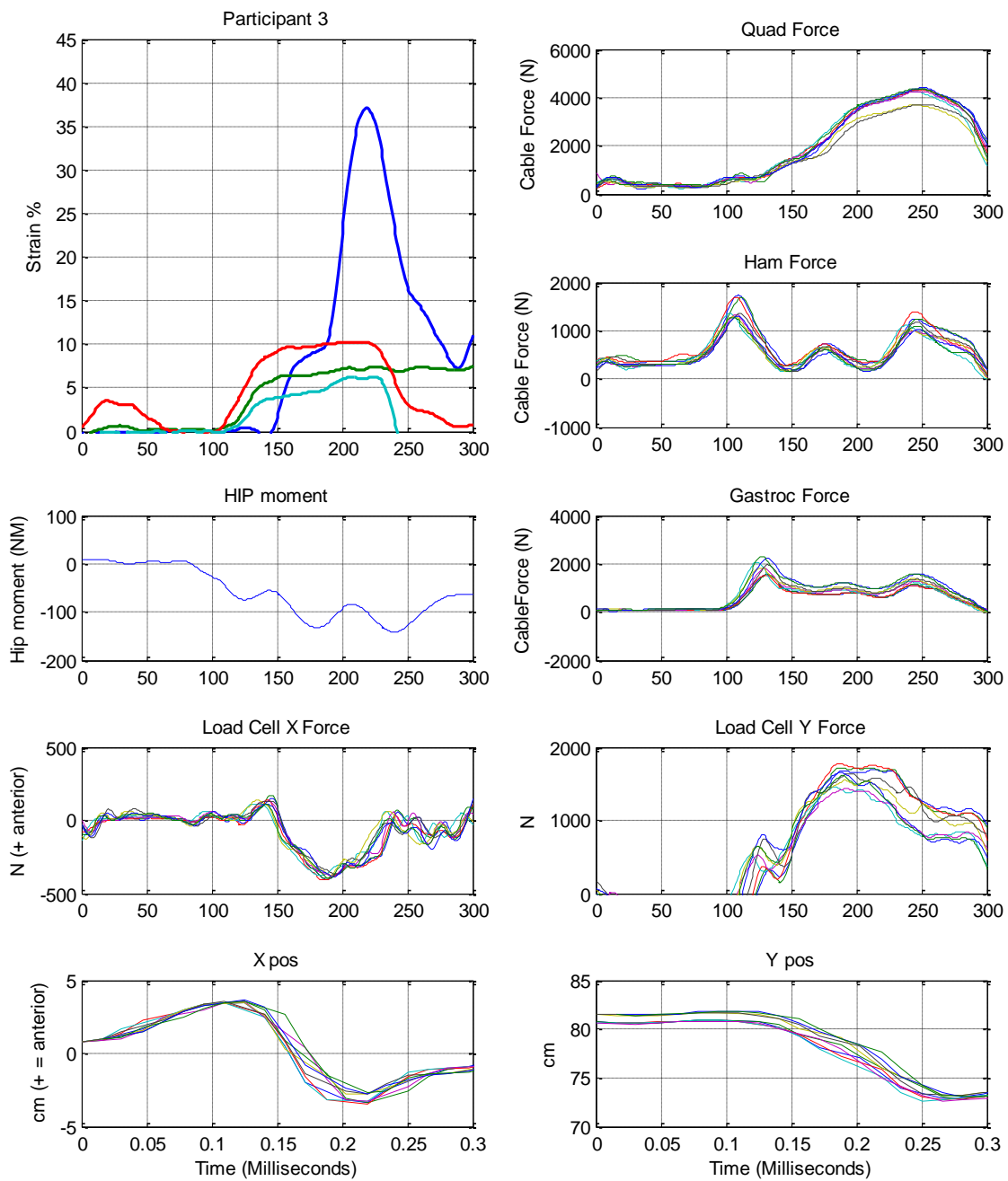# Appendix B: Participant DKS Results

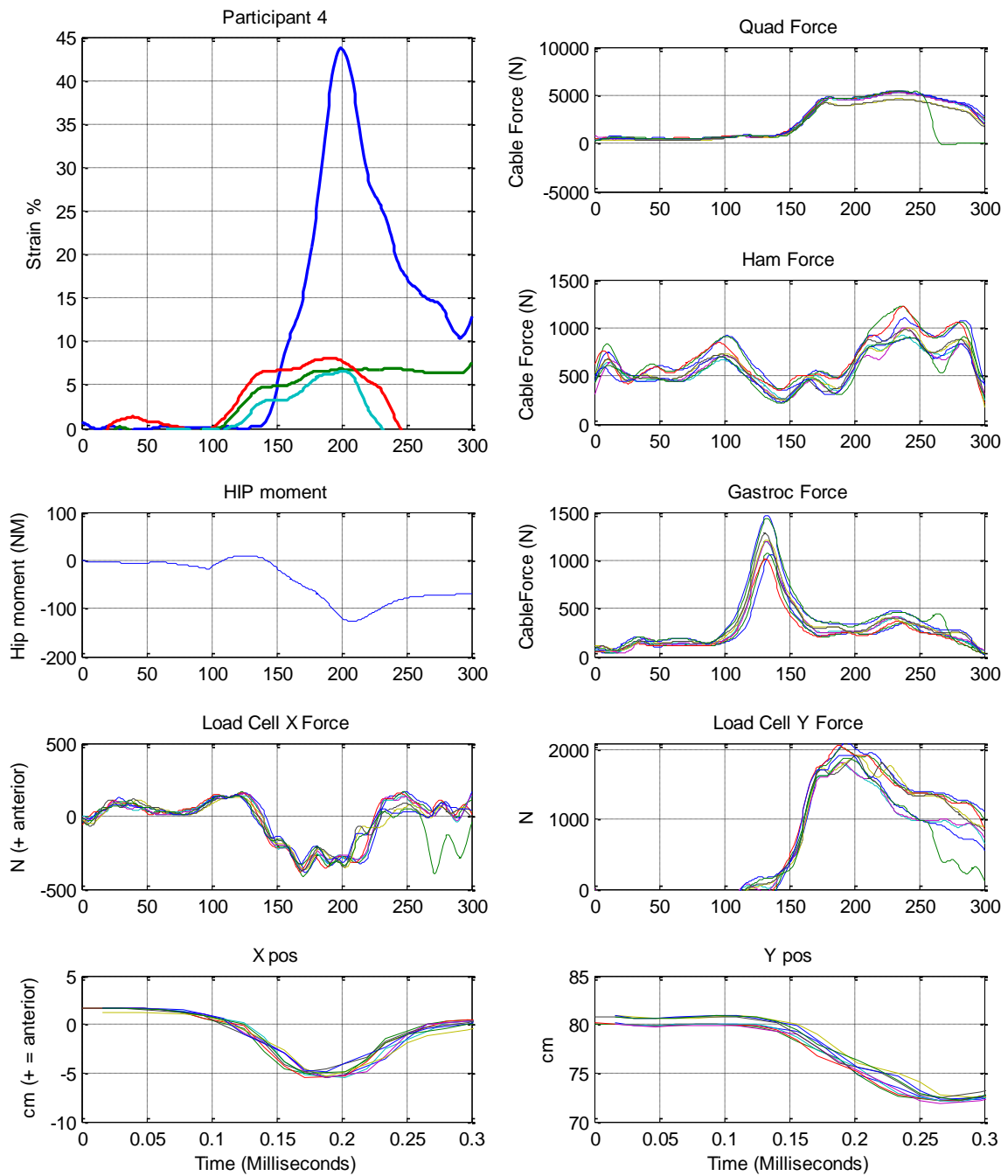**Figure 31 Participant 2 DKS results**

Figure 32 Participant 3 DKS results

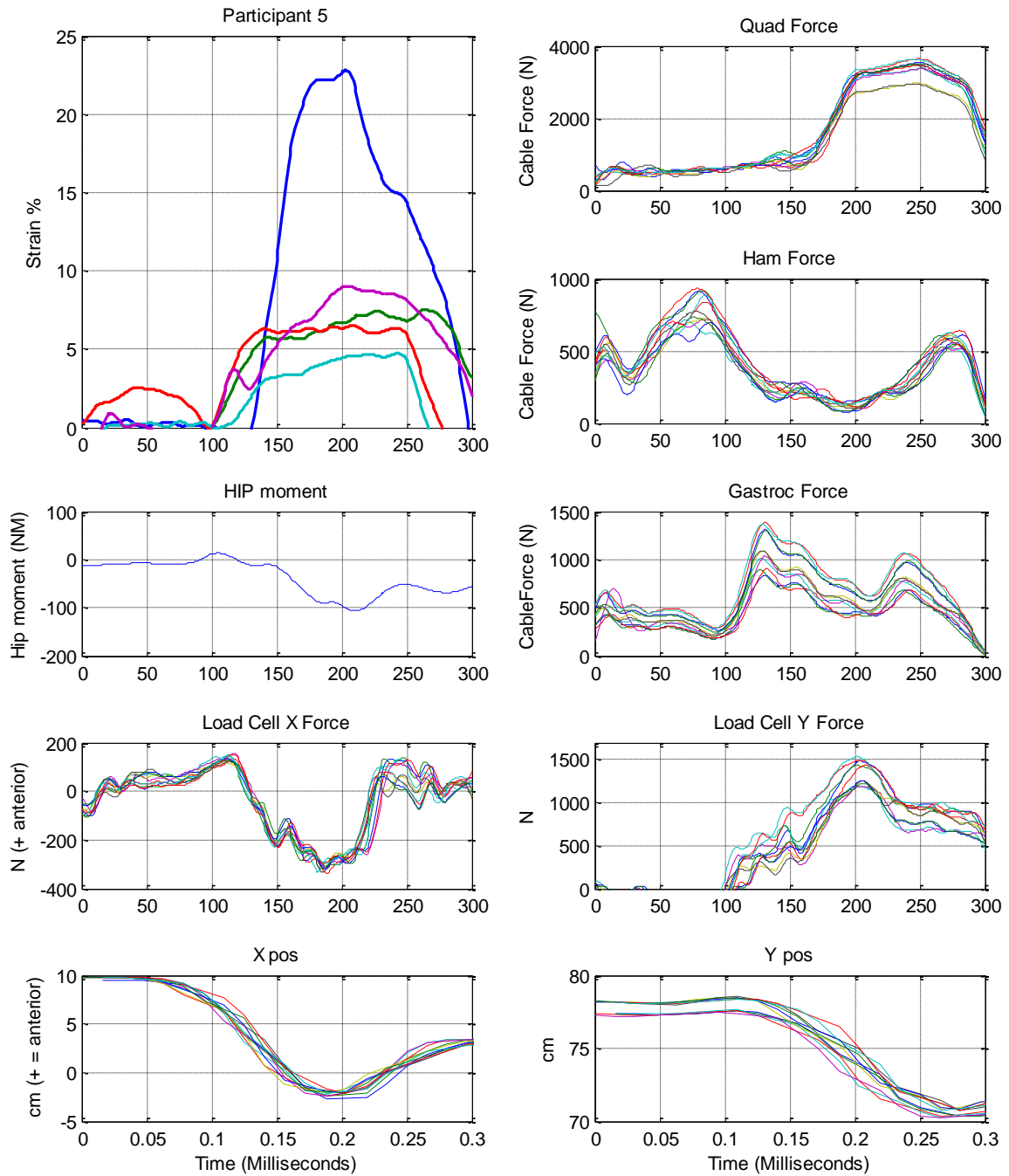**Figure 33 Participant 4 DKS results**

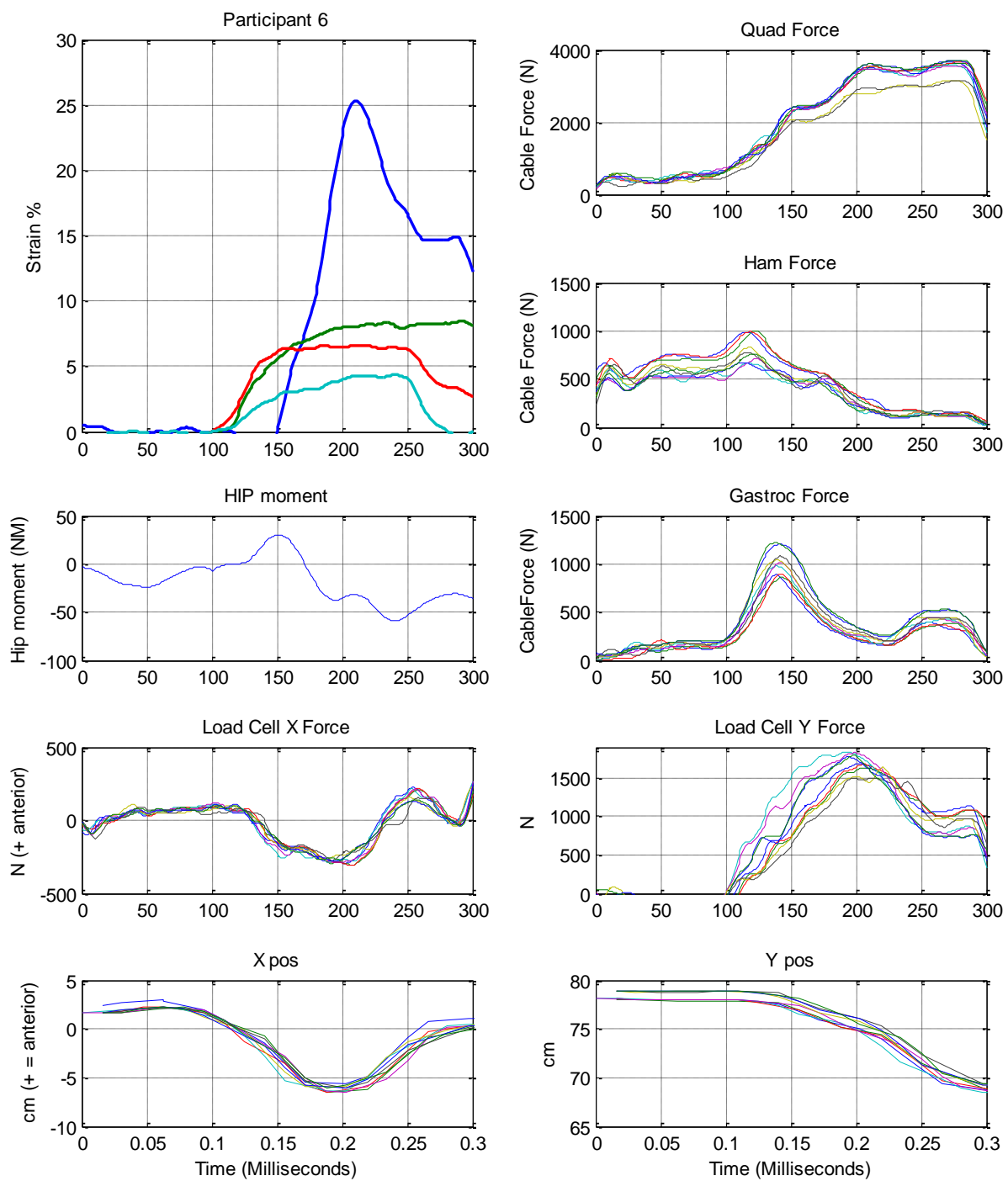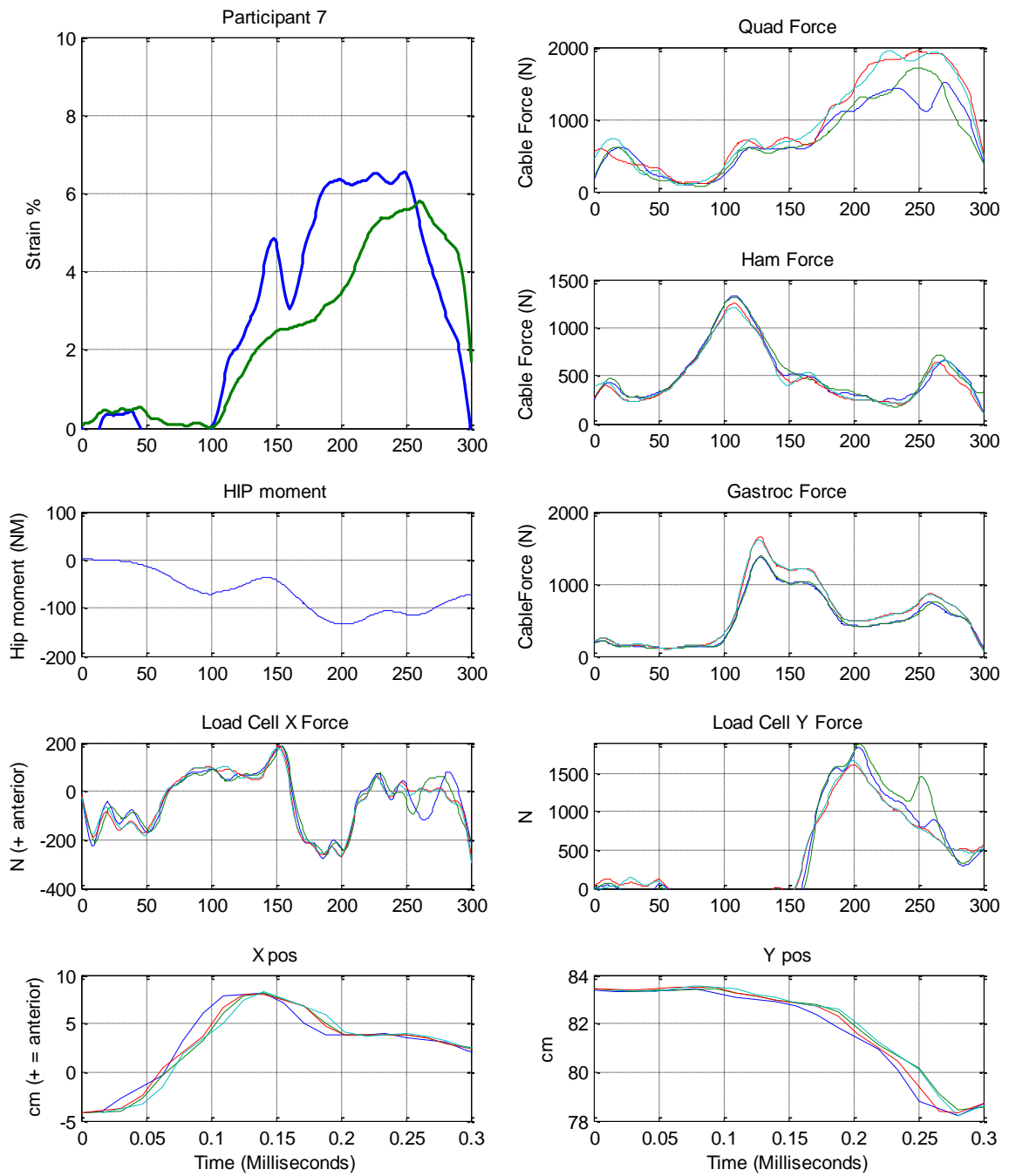**Figure 34 Participant 5 DKS results**

Figure 35 Participant 6 DKS results

93

Figure 36 Participant 7 DKS results